Doctoral Dissertation

Preparation and permeation performance of zeolite membranes for ethanol dehydration, CO_2/CH_4 separation and H_2 purification

（エタノール脱水, CO_2/CH_4 分離と H_2 精製のための ゼオライト膜の作製と透過物性）

March, 2016

QIU LINGFANG

邱 灵芳

Graduate School of Science and Engineering

Yamaguchi University

Abstract

The rapid developing global economy makes energy requirements becoming more and more urgent. On the one hand, the need for alternative gasoline and diesel fuels is becoming more urgent. Anhydrous ethanol is being used by mixing with gasoline as a better clean fuel. However, there is a minimum-boiling azeotrope during ethanol/water distillation. Thus, it is necessary to remove water from ethanol by special processes to obtain anhydrous ethanol. On the other hand, fossil fuels are the mainly demanded energy today. To reduce greenhouse effect mainly caused by a combustion product CO_2, CO_2 separation is necessary. Moreover, to avoid producing CO_2 and using other kinds of fuels, H_2 is a proper energy to be used because it is clean and high efficient. Therefore, it is an urgent task to realize H_2 purification and separation with cost effective and efficient means.

Due to the controllable hydrophilicity and pore size, zeolite membrane is a good candidate for ethanol dewatering, CO_2 separation and H_2 separation. For zeolite membranes, many parameters play a very important role in membrane crystallization, such as seed crystal size, orientation of zeolite crystals in membranes, membrane morphology, crystal component and crystal structure.

In this respect, we focused to optimize synthesis conditions and permeation measurement conditions of zeolite membranes. This dissertation is composed of seven chapters.

The first chapter is the introduction of zeolite membranes.

The second chapter of this dissertation is mainly on sodalite crystal preparation. Higher synthesis temperature as 200 ^{o}C induced uniform sodalite crystals with particle size of (100-200) nm. Pure sodalite can be obtained under a wide $n(Na_2O/SiO_2)$ and $n(Al_2O_3/SiO_2)$ ranges. The crystal size was as small as 50 nm under high $n(Na_2O)/n(SiO_2)$ of 2.0, but it was not uniform. Effect of n (Al_2O_3/SiO_2) on crystallite size was obvious and the crystal size became smaller with lower Si^{4+} concentration. In addition, high water concentration can not induce pure sodalite

crystals. Specific surface areas of silica sources affected crystallite size but had no effect on crystallinity. Finally, crystals prepared at 200 ^{o}C for 24 induced a pure sodalite membrane successfully.

The third section is about sodalite membranes. Effects of composition of synthesis solution, synthesis temperature and crystallization time on the formation of sodalite membranes were studied. Ethanol/water and iso-propanol/water mixtures with different concentrations were used and PV was carried out at 75 ^{o}C. Under the same crystallization condition, thinner and more compact sodalite membrane layer was obtained with water concentration in precursor of $n(H_2O)/n(SiO_2)$ = 50, When synthesis time was 6 h and 12 h, gap between crystals was smaller. Lower operation temperature facilitated water adsorption.

In the fourth section, a thin and well-intergrown zeolite T membrane with high CO_2 permeability and selectivity was prepared by the two-step varying-temperature hydrothermal synthesis process. The influence of synthesis parameters such as synthesis temperature and crystallization time during the two-step durations on crystals growth and separation performance was investigated systematically. Compared with the conventional hydrothermal synthesis at a constant temperature, the two-step method was more effective to synthesize a thin and continuous zeolite membrane layer in short time. It was found that a lower crystallization temperature favored nucleation, while a higher temperature promoted crystallization during the two-step method, thus improving zeolite T crystal growth and membrane separation properties. Under the optimized conditions, CO_2 permeance and CO_2/ CH_4 selectivity of the membrane reached 6.2×10^{-8} mol·m^{-2}·s $^{-1}$·Pa^{-1} and 80 for the CO_2/CH_4 mixture (50/50) at 35 °C, respectively.

The fifth section is about characterization and single gas permeation performances of silicalite-1 membranes prepared in fluoride mediate. Synthesis parameters such as synthesis time, synthesis temperature, silica source, seed crystal size and supports were discussed. Silicalite-1 membrane prepared using TEOS was thinner. The H_2 permeance and permselectivity of this membrane was 9.99×10^{-7} mol·m^{-2}·s^{-1}·Pa^{-1} and 50.0, respectively. Silicalite-1 membranes prepared at higher temperatures were favor

of high H_2 permeance. When larger seed crystals were used, the crystals were (101) oriented. When smaller seed crystals were used, c-axis orientation becomes stronger and the random oriented membranes had higher H_2 permeance. Membranes formed on mullite and NS-1 supports showed high H_2 permenace. H_2 and SF_6 permeation performance in this work was comparable to data in papers. Finally, the silicalite-1 membrane on mullite prepared at 185 ^oC for 14 h showed a good H_2 permeatino stability within 203 days.

The sixth section in this dissertation is to modify silicalite-1 membrane surface with 3-aminopropyltriethoxysilane (APTES). After modification, the membrane surface was covered with an amorphous layer of APTES. The effective pore size of silicalite-1 membrane was reduced significantly. Single gas permeation mechanism was changed to some extent due to the smaller pore size. Permselectivity of H_2 and SF_6 increased from 26.9 to 647, and H_2 permeance kept a comparable value of 2.50×10^{-7} $mol\cdot m^{-2}\cdot s^{-1}\cdot Pa^{-1}$. Moreover, the modified silicalite-1 membrane showed permselectivities of H_2/N_2, H_2/CH_4, CO_2/CH_4, and CO_2/N_2 increased to higher than Knudsen diffusion factors. It is noted that the modified silicalite-1 membrane also showed stable H_2 and SF_6 permeability for 120 hours.

Finally, the senventh chapter summarized the main contents of this dissertation.

要旨

急速な世界経済の発展に伴い、エネルギー需要は著しく増加してきている。そこで、ガソリンやディーゼル燃料に代わる新しい燃料の必要性が高まっている。無水エタノールはガソリンに代わる優れたクリーン燃料である。しかし、エタノール/水の蒸留では共沸が生じる。そのため、無水エタノールを製造する際に残存している水を取り除く特別なプロセスが必要である。

一方、化石燃料は今日の主な需要エネルギーである。化石燃料を燃焼すると、CO_2が発生し、温室効果が上がる。そのため、CO_2分離回収が必要不可欠である。さらに、CO_2が発生し、資源量にも限りがある化石燃料の依存を減らすために、エネルギー効率がよくクリーンで再生可能な水素の適用が検討されているが、そのためには安価で効率的な手段での水素精製、水素分離を実現する必要がある。

制御可能な親・疎水性と孔径により、ゼオライト膜はエタノール水溶液の脱水とCO_2分離と水素精製へ適用の1つの良い候補である。本研究ではこれらの分離に適用するためのゼオライト膜について検討した。ゼオライト膜の微細構造は性能に大きな影響を及ぼす。ゼオライト膜では、結晶の大きさ、結晶の配向性、表面形態、組成や種結晶の特性が膜形成に影響を与える。本研究ではゼオライト膜の合成条件の最適化に焦点を当て、気体透過と浸透気化分離に性能について検討した。

本論文は7つの章から構成されている。第1章はゼオライト膜について紹介した。

第2章では主にソーダライト結晶を調製した。合成温度、合成時間、モル組成、シリカ源などの合成パラメーターの影響について議論した。200℃の高い合成温度にすることで、粒径100~200nmの均一なソーダライト結晶を得た。純粋なソーダライトは広い$n(Na_2O/SiO_2)$,$n(Al_2O_3/SiO_2)$の範囲のもとで得られた。高い$n(Na_2O/SiO_2)$の組成で得られた結晶径は50nmであったが、均一ではなかった。結晶径に与える$n(Al_2O_3/SiO_2)$の影響は明らかであり、Si^{4+}濃度が低くなると結晶径はより小さくなった。さらに、水の濃度が高くなると、純粋なソー

ダライト結晶は得られなかった。ケイ素源の特有な表面積が結晶径に影響を与えるが、結晶性には影響を与えなかった。ソーダライト結晶を 200℃24 時間で合成することで、純粋なソーダライト膜を得ることができた。

第 3 章では、ソーダライト膜について議論した。ソーダライト膜が形成する際の合成液組成、合成温度、結晶化時間の影響を検討した。異なる濃度のエタノール/水、イソプロパノール/水の供給液を用いて、75℃大気中で浸透気化分離実験を行った。50(H_2O/SiO_2)の前駆体濃度で合成したソーダライト膜の膜層は他の膜よりも薄く、緻密であった。合成時間を 6 時間と 12 時間にすると、結晶間隙はより小さかった。また、低温での操作が水の吸着を促進した。

第 4 章では、高い CO_2 透過速度と選択性を有する薄くて、良く相互成長した T 型ゼオライト膜を水熱合成プロセスの温度を変える 2 段階法で製膜した。合成温度、結晶成長における 2 段階間での結晶化時間、分離性能を順番に検討した。一定温度での従来の水熱合成と比較すると、2 段階法が短い時間で薄くて欠陥のないゼオライト膜製膜により効果的であった。高い結晶化温度が結晶化を促進させ、低温が核発生を起こしやすいことが分かり、T 型の結晶成長と膜分離性能を向上させた。最適化された条件下で合成した膜の 35℃、CO_2/CH_4 (50/50) 混合気体における CO_2 透過速度は 6.2×10^{-8}[mol/m^{2}sPa]、CO_2/CH_4 選択性は 80 を示した。

第 5 章では、フッ素を用いて製膜した silicalite-1 膜の特性評価と単成分気体透過性能について議論した。合成時間、合成温度、ケイ素源、種結晶、支持体などの合成パラメーターについて検討した。TEOS を用いて製膜した silicalite-1 膜は薄い膜であった。H_2 透過速度は 9.99×10^{-7}[mol/m^{2}sPa]、H_2/SF_6 理想分離係数は 50.0 であった。高温で製膜した silicalite-1 膜は高い H_2 透過速度を示した。大きな種結晶を用いると、結晶は(101)配向であった。小さな種結晶を用いると、XRD パターンと SEM 観察から膜表面は c 軸配向が強くなるが、ランダム配向であった。また、膜の H_2 透過速度は高くなった。合成時間を長くすることで、ピンホールが少なく、低い H_2 透過速度の膜が得られた。ムライト支持体と NS-1 支持体上に製膜した膜は高い H_2 透過速度を示した。本研究の H_2、SF_6 の透過性能は文献に匹敵する性能であった。ムライト支持体上

に 185℃、14 時間で製膜した silicalite-1 膜の H_2 透過性は 203 日間安定していた。

第 6 章では 3-アミノプロピルエトキシシラン(APTES)を用いた silicalite-1 膜表面の修飾を行った。修飾後、膜表面は APTES のアモルファス層で覆われていた。Silicalite-1 膜の効果的な孔径は顕著に減少した。より小さな孔径となるため、単成分気体透過性能は変化し、H_2/SF_6 選択性は 26.9 から 647 と増加し、H_2 透過速度は 2.50×10^{-7}[mol/m^2sPa]の良い値を保っていた。さらに、修飾した silicalite-1 膜の H_2/N_2、H_2/CH_4、CO_2/CH_4、CO_2/N_2 選択性は増加し、クヌッセン拡散機構から分子ふるい機構へと変化した。修飾した silicalite-1 膜も 120 時間安定した H_2、SF_6 透過性を示した。

第 7 章には本研究の結論をまとめた。

Contents

List of figures

List of tables

Chapter 1 Introduction

1.1 Zeolite membranes

Membrane techniques have many advantages over other traditional ways, such as low energy consumption (A. Alklaibi et al.) [1], cost-efficient, low operating efficiency cost (H. Strathmann et al.) [2], compact and low weight equipment (R. Klaassen et al.) [3], less floor space and maintenance (B. Atkinson et al.) [4], simple to operate (M.T. Ho et al.) [5], simple equipment (Y. Shimizu et al.) [6] and no pollution (M. Elimelech et al.) [7]. Therefore, membrane separation is widely used in chemical industry (S.P. Nunes et al.) [8], pulp and paper industry (A. S. Jönsson et al.) [9], textile industry (G. Ciardelli et al.) [10], pharmaceutical, food and biotechnological applications (A. K. Pabby et al.) [11]. Moreover, among the applications, gasification-based system is even expected to constitute the energy plants for the 21st century (G. J. Stiegel et al.) [12].

As one kind of membranes, zeolite membranes have been investigated for decades, and they are becoming a research hotspot in many fields. Zeolite membranes have many advantages, such as uniform pore size (M. Choi et al.) [13], good shape selectivity (M.B. Sayed et al.) [14], and good continuous long-term stability with inherent mechanical stability, thermal stability and chemical stability (Y. Morigami et al., K.S. Park et al. and A. Galarneau et al.) [15-17]. Moreover, zeolite membranes have high fluxes, and it is a very promising porous material for membrane catalytic reactor (J. Coronas et al.) [18]. Many other applications will be described subsequently.

1.1.1 Preparation of zeolite membranes

Supported and self-supported zeolite membranes are studied widely. Supported membranes are prepared by forming crystals on porous mechanism stable supports (porous ceramic, porous metal or porous glass), and separation process is carried out

through the zeolite layer. Self-supported zeolite membranes only contain zeolite crystals and the crystals build a membrane. Nowadays, many groups have made supported zeolite membranes. For example, MFI membranes can be prepared on porous supports such as stainless steel (E.R. Geus et al.) [19], anodic alumina (Y. Chiou et al.) [20], α-alumina (K. Kusakabe et al.) [21], γ-alumina (J.C. Poshusta et al.) [22], and glass (M.C. Lovallo et al.) [23]. The membrane layer thickness can be controlled from a few hundred to a few micrometers by varying synthesis conditions (L. Gora et al.) [24]. Although supports can influence supported membranes obviously, supported zeolite membranes are still prior to self-supported zeolite membranes in the views of good mechanism properties and reproducibility.

So far, a lot of zeolite membranes have been discovered, such as T (X.L. Zhang et al.) [25], LTA (Y. Morigami et al.) [26], SAPO-34 (M.A. Carreon et al.) [27], , X (S. Li et al.) [28], and MFI (J. Hedlund et al.) [29]. The main preparation techniques can be summarized as follows:

(1) In-situ hydrothermal synthesis

In-situ hydrothermal synthesis can be considered as the most common way to prepare zeolite and zeolite membranes. Supports are not pretreated before crystallization. However, the crystallization time by this way is always too long so that it is not easy to control crystallization conditions. The process is simply shown in **Figure 1-1 (a)**.

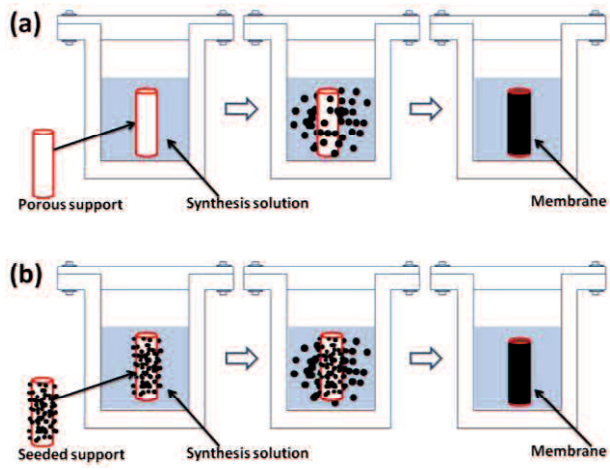

Figure 1-1 Crystallization processes by (a) in-situ hydrothermal synthesis and (b) secondary hydrothermal synthesis.

(2) Secondary growth

Nowadays, secondary growth method is becoming a popular method to obtain more continuous zeolite membranes and reduce the synthesis time. As **Figrue 1-1 (b)** shows, before crystallization, a thin layer of seed crystals is often deposited on the surface of supports, and then seeded supports are put into the synthesis solution. The most two popular ways of seeding are dip-coating and rub-coating. Secondary growth has many prioroties, such as easy operation, and better reproducibility (H. Jiang et al.) [30].

(3) Microwave-assisted method

Microwave-assisted method is a novel method recently developed. It is easier to prepare perfecet zeolite membranes within shorter time. Moreover, membranes prepared by microwave heating technique often have narrow particle size distribution and small crystals, which has been described by X.C. Xu et al. [31]. Up to date, many zeolite membranes have been prepared to this technique, such as SOD (X. Xu et al.) [31], MFI (J. Motuzas et al.) [32], A (Y. Han et al.) [33] and SAPOs (T.G. Tsai et al.) [34].

(4) Two-step temperature varying method

"It was said that the nucleation stage at higher temperatures led to an acceleration of nucleation followed by the crystallization stage at a lower temperature for the control of crystallite size and size distribution." (S.D. Kim et al. and M. Mehdipourghazi et al.) [35, 36] Two-step temperature varying method has been used to prepare dense zeolite membranes by changing synthesis temperature during the crystallization. "It involves a rapid change in tempearature at some point during the crystallization process." (X.L. Zhang et al.) [37] So far, T type (X.L. Zhang et al.) [37] and MFI type (C. Kong et al.) [38] zeolite membranes have been prepared by this method and applied to gas permeation.

(5) Vapor phase transport (VPT) technique

W. Xu et al. first found that "a dry aluminosilicate gel could be transformed to MFI zeolite by contactwith vapors of ethylenediamine (EDA), triethylamine (Et_3N) and water" (W. Xu et al.) [39]. Then this technique is useful for synthesizing various

types of zeolites. M.H. Kim et al. called this method vapor phase transport (VPT) (M.H. Kim et al.) [40]. So far, only a few types of zeolite membranes such as NaA (Z.L. Cheng et al.) [41], FAU (Z. Cheng et al.) [42], LTA (Y. Ma et al.) [43] and MFI (T. Matsufuji et al.) [44] types have been prepared by VPT method successfully. It is not difficult to estimate that VPT technique is difficult to operate although it can result in high permeation performance.

(6) Others

Other synthesis techniques such as heteroepitaxial growth (T. Wakihara et al.) [45], ulsed laser ablation (K.J. Balkus et al.) [46], and embedding method (J.E. Lewis et al.) [47] applied to zeolite membrane preparations are also reported.

1.1.2 Application of zeolite membranes

(1) Pervaporation

Pervaporation can be regarded as one of the most meaningful applications of zeolite membranes. In pervaporation, one liquid mixture is placed in a bottle or a module to contact one side of a membrane and the permeated product will be removed by lower vapor pressure produced by vacuuming from the other side of membrane.

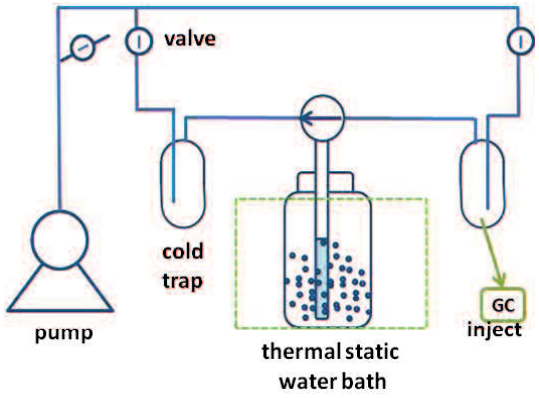

Figure 1-2 Schematic diagram of the pervaporation process

Figure 1-2 shows a schematic of the pervaporation process. A vacuum cold trap is used to condense the permeate vapor and gas chromatography is used to analyze the composition of melted permeate. The driving force for the mass transport is the chemical potential gradient usually prodced by vacuuming across the membrane layer.

So far, many zeolite membranes have been used in pevaporation or another pervaporation process, vapor permeation process (**Figure 1-3**), such as NaA (Y. Morigami et al.) [48], T (R. Zhou et al.) [49], FAU (F. Zhang et al.) [50], CHA (R. Zhou et al.) [51], MOR (X. Lin et al.) [52], and SOD (X. Xu et al.) [31]. Besides, NaA type zeolite membranes have been commercialized in ethanol purification (S.G. Sorenson et al.) [53].

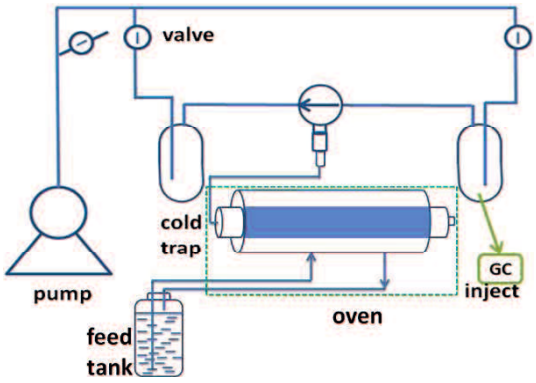

Figure 1-3 A schematic illustration of vapor permeation

The pervaporation performance is characterized by parameters calculated by equations as follows:

$$J = Q/At \qquad (1\text{-}1)$$

where J is permeation flux, Q is the mass of permeate (g) collected during a period of t (h) and A is the effective membrane area in contact with the feed (m^2).

$$\alpha = (y_i/y_j)/(x_i/x_j) \qquad (1\text{-}2)$$

where y_i and y_j stand for the weight percentages of water and alcohols in the permeate, and x_i and x_j represent stand for the weight percentages of water and organics in the feed, respectively.

$$P_{i(j)} = (10^3 \times Q)/(3600 \times M\Delta P) \qquad (1\text{-}3)$$

where $P_{i(j)}$ is the permeance ($mol \cdot m^{-2} \cdot s^{-1} \cdot Pa^{-1}$) of component of i or j. Q is the same parameter in Eq. (1). M is the molar mass ($g \cdot mol^{-1}$) of the correspondence component. ΔP is the pressure difference (Pa) across the membrane.

(2) Gas separation

Gas separation has become an important application of membrane technology. T.

Graham et al. started studying gas permeation performance of zeolite membranes systematically [54]. Both of porous and dense membranes can be used to separate gas mixtures, and the mechanism of gas permeation for porous membranes is shown in **Figure 1-4**.

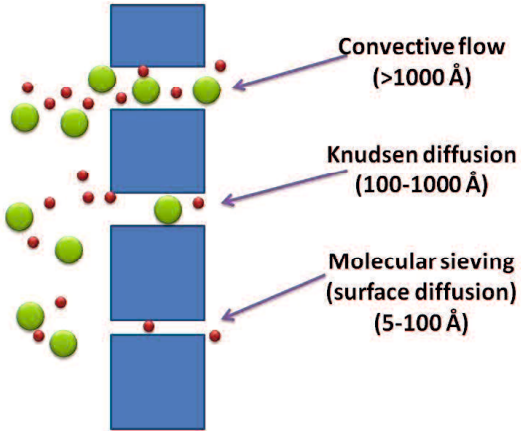

Figure 1-4 Mechanisms for permeation of gases through porous membranes [55].

Zeolite membranes always separate mixtures by molecular sieving. However, when the membranes are not compact and the pore size is larger (100 Å-1000 Å), convective flow and Knudsen diffusion dominate the gas permeation process.

The gas transport process through a zeolite membrane can be summariezed into five steps described as follows. "(1) adsorption from the bulk phase to the zeolite external surface, (2) diffusion from the surface to the inside of the zeolite channels; (3) diffusion inside the zeolite channels; (4) diffusion from the zeolite channel to the external surface and (5) desorption from the external surface to the gas phase" (N.W. Ockwig et al.) [56]. The separation selectivity (α) of gas mixtures is calculated as this equation:

$$\alpha = (y_1/y_2)/(x_1/x_2) \quad (1\text{-}4)$$

where y_1 and y_2 are the mole fractions of components 1 and 2 in permeate side, respectively. And x_1 and x_2 are the mole fractions of components 1 and 2 in feed side, respectively. For single gas permeation, ideal selectivity α is the ratio of permeances of components 1 and 2. It is worth noting that there is no relationship between the permselectivity and the separation factor when strongly adsorbing components are

involved.

Many zeolite membranes for gas separation are topics of research interest, and popular gas separation aims contain CO_2 capture from N_2 and CH_4 (DDR (S. Himeno et al.) [57], MFI (M. Bernal et al.) [58], FAU (Y. Hasegawa et al.) [59] and SAPO-34 (M.A. Carreon et al.) [60] types), H_2 purification from N_2, CO_2, CH_4 and He (NaA (X. Xu et al.) [61], Y (K. Kusakabe et al.) [62], MFI (Z. Hong et al.) [63] sand SAPO-34 (M. Hong et al.) [64], and sodalite (M.J. Vaezi et al.) [65] types). Moreover, isomers separation such as butane isomers (T. Matsufuji et al.) [44], xylene isomers (G. Xomeritakis et al.) [66] and hexane isomers (G.J. Gump et al.) [67] are also carried out through zeolite membranes.

(3) Ion Exchange

For a mixed component system, permselectivity is not only dependent on pore size, but also the interaction between permeate and channel. As reported by K. Kusakabe et al., "if a zeolite is ion-exchanged with cations which possess different interactions with permeates, this could improve the permselectivities of the membrane" [68]. For example, CO_2/N_2 separation performance of NaY-type membranes became more stable after ion-exchange [68]. In addition, ZSM-5 zeolite membranes became more stable after exchanged with H^+, Cs^+ and so on (K. Aoki et al.) [69]. Moreover, pore size of LTA-type zeolite membranes was adjusted to much smaller of 0.30 nm by ion exchange. The corresponding gas permeation was affected significantly by using different solutions (S. Shirazian et al.) [70].

(4) Membrane reactors

By the early 1980s, membrane technology developed a lot so that many research groups started to consider using this technology to control the products during chemical reactions. Among the large amouont of membranes, zeolite membrane technology also has been used widely. Membranes are usually used as contactor or membrane reactor in the application.

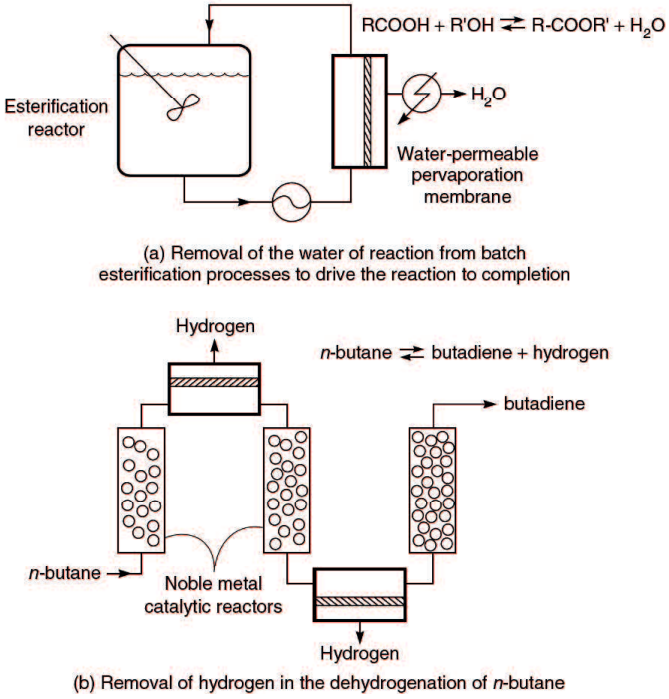

Figure 1-5 Examples of membrane reactors used to change the products of chemical reaction in which the membrane separation step is physically separated from the chemical reaction step. (a) Removal of the water of reaction from batch esterification processes to drive the reaction to completion and (b) removal of hydrogen in the dehydrogenation of n-butane. [55]

Figure 1-5 (a) shows the process when using membranes as contactors. A pervaporation membrane is used to shift the equilibrium of the de-esterification reaction described by Ó. de la Iglesia et al. [71]. In the esterification reactor mixture, there is a catalyst, enzymes, or a cell culture, a membrane is used to separate the reaction medium in another chamber from the reaction tank. Bioreactor should be the most significant one process to use membrane as a contactor. Recently, common chemical separations are becoming hotlights to apply membranes. As a reactor, a membrane can preferentially remove one of the components in the reaction so that it can realize converting the equilibrium of a chemical reaction. As **Figure 1-5 (b)** shows, a membrane is used to shift the equilibrium of the n-butane dehydrogenation reaction described by R.W. Baker et al. [55].

What's more, other innovative applications using zeolite are also becoming more popular such as micro-membrane reactor (X. Tan et al.) [72], functional films (S.G.

Kim et al.) [73], matrix-mixed-membranes (C. Xue et al.) [74].

1.1.3 Modifications of zeolite membranes

Many methods are being discovered gradually so that zeolite membranes can be more perfect. The majority of the techniques are post-treatment methods, such as chemical vapor deposition (CVD) [21], catalytic cracking of silane (CCS) [75], atomic layer deposition (ALD) [76], coking [77], or ion-exchange [69]. They can decrease pore size or fill non-zeolite pores. For example, NaA zeolite membranes on modified substrates showed good dyhydration selectivity of 26 in water/methane mixture. But after ion-exchange, the permselectivity increased to 37 as described by S. Shirazian et al. [78].

Masuda T. et al have reported a novel way to modify the pore size of zeoltie, which can be regarded as the first time to report a modification on zeolite [75]. In that study, to improve H_2 purification performance, MFI zeolite was treated by methyldiethoxysilane (MDES). After catalytically cracking, coke containing Si atoms on the active sites was left and the pore size is reduced effectively. SAPO-34 zeolite membranes are also modified by this method for H_2 separation (M. Hong et al.) [64]. A.S. Huang et al. have modified LTA type membranes on functionalized tubes [79]. To provide heterogeneous sites for the growth of NaA zeolites on the support surface, they used 3-aminopropyltrithoxysilane (APTES) to modify Al_2O_3 particles deposited coarse macroporous tubes. Herein, APTES acts as a cross linker. This method is expected to prepare other zeolite membranes on that kind of supports. Moreover, A. Huang et al. reported that FAU membranes were also formed on APTES functionalized supports without seeding [80]. Such FAU membranes show better H_2 separation performance compared to FAU membranes on unmodified supports.

1.2 Objectives

A major big challenge of the 21st century is to convert our major energy sources by environmental friendly ways. In 2013, the total ethanol production in world was as

high as 88.70×10^9 L [81]. As shown in **Figure 1-6**, A.W. Bhutto et al. have reported the ethanol production in the world and main producing countries between 2007 and 2013 [81]. Anhydrous ethanol is renewable energy. Compared to gasoline, it is has a lot of advantages as a clean-burning fuel. However, as K. Santosh et al. reported, "ethanol-water solution forms a minimum-boiling azeotrope of composition of 89.4 mol% ethanol and 10.6 mol% water at 78.2 ^oC and standard atmospheric pressure" [82]. Therefore, it is valuable to produce anhydrous ethanol more efficiently.

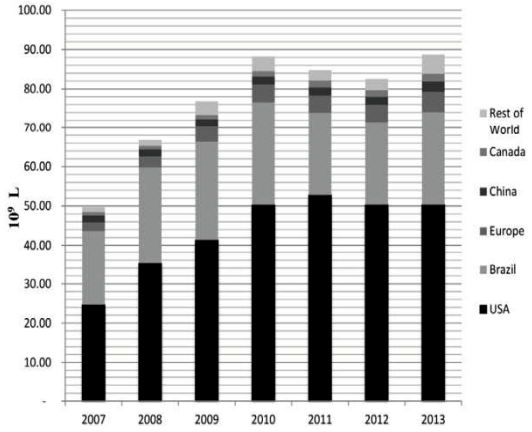

Figure 1-6 World ethanol production. [81]

It is predicted that as global energy consumption increases, hydrogen is a clean and efficient energy and expected to be a potential solution [56]. Besides, as described by X.L. Zhang et al., separate CO_2 from products of fossil combustion is also effective to weaken some environmental problems such as greenhouse effect [37].

The unique properties of zeolite membranes are well-ordered pore structures, molecular sieving effect, and preferential adsorption. Therefore, zeolite membranes have great potential to help solve some environmental issues. In this dissertation, three kinds of zeolite membranes, sodalite, T type and MFI zeolite membranes, have been prepared and applied to three fields mentioned above.

1.2.1 Sodalite and sodalite (SOD) membranes

In this dissertation, both of sodalite crystals and sodalite membranes were investigated. To prepare sodalite membranes with promising performance, sodalite

seed properties should be discussed firstly. Therefore, synthesis conditions of sodalite were investigated in detail. The sodalite crystals with proper morphology and induction ability were used to treat supports by rub-coating. Meanwhile, as J. Jiang et al. reported, sodalite has good ion exchange capacity. Thus, sodalite is considered to be used in many fields such as optical material [83], hydrogen storage [84], hydrogen separation, and catalyst support [85, 86]. Moreover, due to the good hydrophilicity of sodalite with a low Si/Al of 1.0, sodalite membranes were prepared and characterized to realize the dehydration of ethanol to produce anhydrous ethanol.

B. Beagley et al. reported that the pore structure of SOD crystals is shown in **Figure 1-7** [87]. The small structure formed by 4-rings and 6-rings make sodalite membranes (0.28 nm) only can let small molecules (He, H_2O or H_2) to permeate, which was demonstrated by S. Münzer et al. and X. Xu et al. [31, 88].

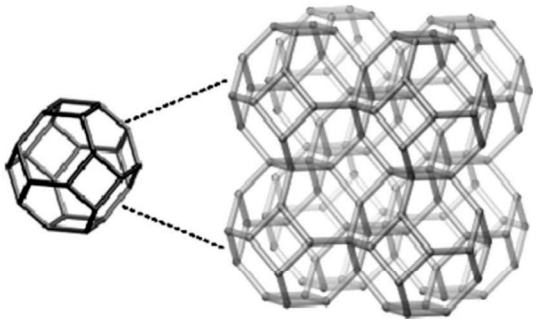

Figure 1-7 Sodalite cage (left) and sodalite framework (right). [89]

To date, several groups (i.e., S. Khajavi et al.) prepared SOD membranes on surface-polished disks without seeding and applied to dehydration process [90]. However, polished flat surface may facilitate a formation of oriented zeoltie membranes, which may enhance the intergrowth of crystals so that membranes will be less compact. The main goal is to use seeding method to prepare SOD membranes. The effects of synthesis temperature and synthesis time on morphology and performance of SOD membranes are also studied.

1.2.2 T-type zeolite membranes

The Si/Al ratio of zeolite T is 3-4. It shows proper hydrophilic and acid resistant

abilities as reported by S. Yang et al. and M. Mirfendereski [91, 92].

In frameworks of T zeoliote, offeretite and erionite are contained. The corresponding structure and pore size are indicated in **Figure 1-8 (a)**, which have been reported by J. Bengoa et al. [93]. Zeolite T is made of framework formed by the stacking of offretite phase and a small amount of erionite sheets. Y. Cui et al. reported that T zeolite framework has proper Al ratio so that zeolite membranes have promising CO_2 preferential adsorption ability [94].

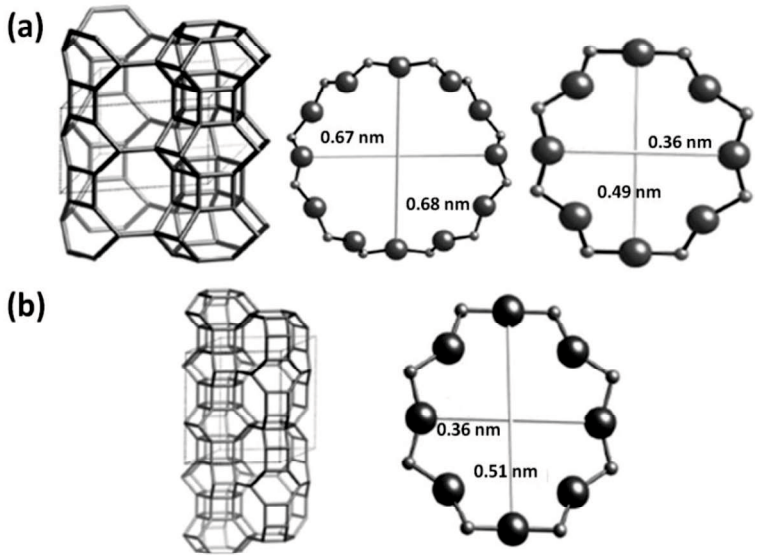

Figure 1-8 Frameworks of (a) offretite and (b) erionite. [95]

The main goal of this part is to prepare dence zeolite T membranes and apply them to CO_2 separation process. A series of synthesis conditions are discussed. For example, the synthesis temperature and synthesis time on both of the first step and the second step. The results are also compared with results in papers.

1.2.3 Silicalite-1 (Al free MFI) zeolite membranes

As we know, MFI zeolite has advantages like simple synthesis and the promising seperation performance of light hydrocarbons.

Figure 1-9 shows the structure of MFI zeolites [96]. The straight channel along b-axis has an approximate pore diameter of 0.56 nm×0.54 nm, and another channel

along a-axis has an estimated pore diameter of 0.51 nm×0.55 nm. During the transportation, H_2 is always fixed in aromatic hydrocarbons by hydrogenation. When H_2 is used, by-productions such as toluene and methylcyclohexane will appeared. Thus, the proper pore size of silicalite-1(Al-free MFI) is favor of H_2 permeation. Moreover, modification is a good way to increase the compactness of silicalite-1 membranes. And H_2 separation factor from other gases with an acceptable H_2 permeance lose can be achieved.

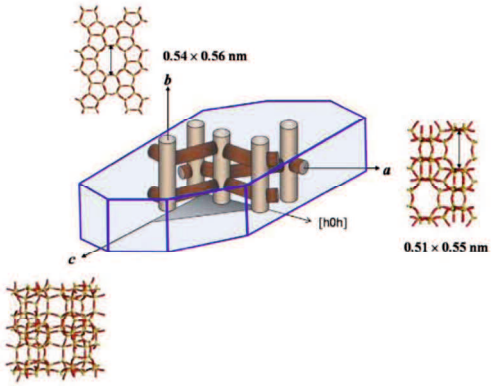

Figure 1-9 The framework structure of MFI zeolite. [96]

The overarching theme of this part is to optimize the synthesis conditions of silicalite-1 membranes by discussing synthesis conditions. Focus is placed on the effects of crystallization conditions, gel components, seed crystal size and substrates. In terms of modifying silicalite-1 membranes, gas permeation performance of different single gas pairs were compared and analyzed in detail.

1.3 Outlines

(1) Chapter 1

It introduces the critical background about the subjects dealt in this dissertation. The main purposes of all researches are also discussed. Moreover, **Chapter 1** also provides the overview of membrane technology. Current synthesis methods, classifications, applications, separation mechanisms of liquid and gas molecules in zeolite membranes and modifications are reviewed.

(2) Chapter 2

Sodalite powders are prepared. Synthesis parameters have obvious effects of morphology of sodalite crystals.

(3) Chapter 3

By using the sodalite crystals prepared in **Chapter 2**, sodalite membranes are prepared. Sodalite membranes are applied to dehydration process in ethanol (EtOH)/water and iso-propanol (IPA)/water mixtures. Effects of temperature and feed concentration for pervaporation, synthesis time and synthesis temperature are discussed.

(4) Chapter 4

T-type zeolite membranes are prepared by two-step varying-temperature hydrothermal synthesis process. The effects of synthesis parameters for the two steps on gas separation performance of T zeolite membranes were studied in detail.

(5) Chapter 5

Silicalite-1 zeolite membranes are prepared in fluoride mediate. Effects of synthesis conditions such as crystallization time and temperature, silica source, seed crystal size and supports are investigated. In addition, effects of gas permeation temperature and pressure difference on single gas permeation performance of silicalite-1 membranes also have been described. The H_2 permeation performance of this work is compared with data in papers.

(6) Chapter 6

3-aminopropyltriethoxysilane (APTES) was used to modify silicalite-1 membranes. All single gas permeation performances of membrane before and after modification are compared. For different single gas pairs, the effects of measurement temperature and pressure difference are compared and discussed.

(7) Chapter 7

A summary of this dissertation and future work are also proposed.

References

[1] A. Alklaibi, N. Lior, Membrane-distillation desalination: status and potential, Desalination, 171 (2005) 111-131.

[2] H. Strathmann, Membrane separation processes: current relevance and future opportunities, AIChE Journal, 47 (2001) 1077-1087.

[3] R. Klaassen, Achieving flue gas desulphurization with membrane gas absorption, Filtration & Separation, 40 (2003) 26-28.

[4] B. Atkinson, F. Bux, H. Kasan, Considerations for application of biosorption technology to remediate metal-contaminated industrial effluents, Water S. A., 24 (1998) 129-135.

[5] M.T. Ho, G.W. Allinson, D.E. Wiley, Reducing the cost of CO_2 capture from flue gases using membrane technology, Industrial and Engineering Chemistry Research, 47 (2008) 1562-1568.

[6] Y. Shimizu, Y. Okuno, K. Uryu, S. Ohtsubo, A. Watanabe, Filtration characteristics of hollow fiber microfiltration membranes used in membrane bioreactor for domestic wastewater treatment, Water Research, 30 (1996) 2385-2392.

[7] M. Elimelech, W.A. Phillip, The future of seawater desalination: energy, technology, and the environment, Science, 333 (2011) 712-717.

[8] S.P. Nunes, K. Peinemann, Membrane technology: in the chemical industry, John Wiley & Sons, 2006.

[9] A. Jönsson, R. Wimmerstedt, The application of membrane technology in the pulp and paper industry, Desalination, 53 (1985) 181-196.

[10] G. Ciardelli, L. Corsi, M. Marcucci, Membrane separation for wastewater reuse in the textile industry, Resources, conservation and recycling, 31 (2001) 189-197.

[11] A.K. Pabby, S.S. Rizvi, A.M.S. Requena, Handbook of membrane separations: chemical, pharmaceutical, food, and biotechnological applications, CRC press, 2015.

[12] G.J. Stiegel, R.C. Maxwell, Gasification technologies: the path to clean, affordable energy in the 21st century, Fuel Processing Technology, 71 (2001) 79-97.

[13] M. Choi, K. Na, J. Kim, Y. Sakamoto, O. Terasaki, R. Ryoo, Stable

single-unit-cell nanosheets of zeolite MFI as active and long-lived catalysts, Nature, 461 (2009) 246-249.

[14] M.B. Sayed, A. Auroux, J.C. Védrine, The effect of boron on ZSM-5 zeolite shape selectivity and activity: II. Coincorporation of aluminium and boron in the zeolite lattice, Journal of Catalysis, 116 (1989) 1-10.

[15] K.S. Park, Z. Ni, A.P. Côté, J.Y. Choi, R. Huang, F.J. UribeRomo, H.K. Chae, M. O'Keeffe, O.M. Yaghi, Exceptional chemical and thermal stability of zeolitic imidazolate frameworks, Proceedings of the National Academy of Sciences, 103 (2006) 10186-10191.

[16] Y. Morigami, M. Kondo, J. Abe, H. Kita, K. Okamoto, The first large-scale pervaporation plant using tubular-type module with zeolite NaA membrane, Industrial and Engineering Chemistry Research, 25 (2001) 251-260.

[17] A. Galarneau, D. DesplantierGiscard, F. Di Renzo, F. Fajula, Thermal and mechanical stability of micelle-templated silica supports for catalysis, Catalysis Today, 68 (2001) 191-200.

[18] J. Coronas, J. Santamarıa, Catalytic reactors based on porous ceramic membranes, Catalysis Today, 51 (1999) 377-389.

[19] E.R. Geus, H. van Bekkum, W.J. Bakker, J.A. Moulijn, High-temperature stainless steel supported zeolite (MFI) membranes: preparation, module construction, and permeation experiments, Microporous Materials, 1 (1993) 131-147.

[20] Y. Chiou, T. Tsai, S. Sung, H. Shih, C. Wu, K. Chao, Synthesis and characterization of zeolite (MFI) membrane on anodic alumina, Journal of the Chemical Society, Faraday Transactions, 92 (1996) 1061-1066.

[21] K. Kusakabe, S. Yoneshige, A. Murata, S. Morooka, Morphology and gas permeance of ZSM-5-type zeolite membrane formed on a porous α-alumina support tube, Journal of Membrane Science, 116 (1996) 39-46.

[22] J.C. Poshusta, R.D. Noble, J.L. Falconer, Temperature and pressure effects on CO_2 and CH_4 permeation through MFI zeolite membranes, Journal of Membrane Science, 160 (1999) 115-125.

[23] M.C. Lovallo, A. Gouzinis, M. Tsapatsis, Synthesis and characterization of

oriented MFI membranes prepared by secondary growth, American Institute of Chemical Engineers. AIChE Journal, 44 (1998) 1903.

[24] L. Gora, J.C. Jansen, T. Maschmeyer, Controlling the performance of silicalite-1 membranes, Chemistry-A European Journal, 6 (2000) 2537-2543.

[25] X.L. Zhang, L.F. Qiu, M.Z. Ding, N. Hu, F. Zhang, R.F. Zhou, X.S. Chen, H. Kita, Preparation of Zeolite T Membranes by a Two-Step Temperature Process for CO_2 Separation, Industrial and Engineering Chemistry Research, 52 (2013) 16364-16374.

[26] Y. Morigami, M. Kondo, J. Abe, H. Kita, K. Okamoto, The first large-scale pervaporation plant using tubular-type module with zeolite NaA membrane, Separation and Purification Technology, 25 (2001) 251-260.

[27] A.M. Hillock, S.J. Miller, W.J. Koros, Crosslinked mixed matrix membranes for the purification of natural gas: effects of sieve surface modification, Journal of Membrane Science, 314 (2008) 193-199.

[28] S. Li, V.A. Tuan, J.L. Falconer, R.D. Noble, X-type zeolite membranes: preparation, characterization, and pervaporation performance, Microporous and Mesoporous Materials, 53 (2002) 59-70.

[29] J. Hedlund, J. Sterte, M. Anthonis, A. Bons, B. Carstensen, N. Corcoran, D. Cox, H. Deckman, W. De Gijnst, P. de Moor, High-flux MFI membranes, Microporous and Mesoporous Materials, 52 (2002) 179-189.

[30] H. Jiang, B. Zhang, Y. Lin, Y. Li, Synthesis of zeolite membranes, Chinese Science Bulletin, 49 (2004) 2547-2554.

[31] X. Xu, Y. Bao, C. Song, W. Yang, J. Liu, L. Lin, Microwave-assisted hydrothermal synthesis of hydroxy-sodalite zeolite membrane, Microporous and Mesoporous Materials, 75 (2004) 173-181.

[32] J. Motuzas, S. Heng, P.Z. Lau, K. Yeung, Z. Beresnevicius, A. Julbe, Ultra-rapid production of MFI membranes by coupling microwave-assisted synthesis with either ozone or calcination treatment, Microporous and Mesoporous Materials, 99 (2007) 197-205.

[33] Y. Han, H. Ma, S. Qiu, F. Xiao, Preparation of zeolite A membranes by

microwave heating, Microporous and Mesoporous Materials, 30 (1999) 321-326.

[34] T. Tsai, H. Shih, S. Liao, K. Chao, Well-aligned SAPO-5 membrane: preparation and characterization, Microporous and Mesoporous Materials, 22 (1998) 333-341.

[35] S.D. Kim, S.H. Noh, J.W. Park, W.J. Kim, Organic-free synthesis of ZSM-5 with narrow crystal size distribution using two-step temperature process, Microporous and Mesoporous Materials, 92 (2006) 181-188.

[36] M. Mehdipourghazi, A. Moheb, H. Kazemian, Incorporation of boron into nano-size MFI zeolite structure using a novel microwave-assisted two-stage varying temperatures hydrothermal synthesis, Microporous and Mesoporous Materials, 136 (2010) 18-24.

[37] X. Zhang, L. Qiu, M. Ding, N. Hu, F. Zhang, R. Zhou, X. Chen, H. Kita, Preparation of Zeolite T Membranes by a Two-Step Temperature Process for CO_2 Separation, Industrial and Engineering Chemistry Research, 52 (2013) 16364-16374.

[38] C. Kong, J. Lu, J. Yang, J. Wang, Preparation of silicalite-1 membranes on stainless steel supports by a two-stage varying-temperature in situ synthesis, Journal of Membrane Science, 285 (2006) 258-264.

[39] W. Xu, J. Dong, J. Li, J. Li, F. Wu, A novel method for the preparation of zeolite ZSM-5, Journal of the Chemical Society, Chemical Communications, (1990) 755-756.

[40] M. Kim, H. Li, M.E. Davis, Synthesis of zeolites by water-organic vapor-phase transport, Microporous Materials, 1 (1993) 191-200.

[41] Z. Cheng, Z. Chao, H. Wan, Preparation of NaA zeolite membrane with high permeability by using a modified VPT method, Chemistry Letters, 35 (2006) 1056-1057.

[42] Z. Cheng, E. Gao, H. Wan, Novel synthesis of FAU-type zeolite membrane with high performance, Chemical Communications, (2004) 1718-1719.

[43] Y. Ma, J. Li, Z. Xuan, R. Liu, Synthesis, characterization and antitumor activity of some arylantimony triphenylgermanylpropionates and crystal structures of $Ph_3GeCH(Ph)CH_2CO_2SbPh_4$ and $[Ph_3GeCH_2CH(CH_3)CO_2]_2Sb(4\text{-}ClC_6H_4)_3$, Journal of Organometallic Chemistry, 620 (2001) 235-242.

[44] T. Matsufuji, N. Nishiyama, M. Matsukata, K. Ueyama, Separation of butane and

xylene isomers with MFI-type zeolitic membrane synthesized by a vapor-phase transport method, Journal of Membrane Science, 178 (2000) 25-34.

[45] T. Wakihara, S. Yamakita, K. Iezumi, T. Okubo, Heteroepitaxial growth of a zeolite film with a patterned surface-texture, Journal of the American Chemical Society, 125 (2003) 12388-12389.

[46] K.J. Balkus, T. Muñoz, M.E. GimonKinsel, Preparation of zeolite UTD-1 films by pulsed laser ablation: Evidence for oriented crystal growth, Chemistry of Materials, 10 (1998) 464-466.

[47] J.E. Lewis, G.R. Gavalas, M.E. Davis, Permeation studies on oriented single-crystal ferrierite membranes, AIChE Journal, 43 (1997) 83-90.

[48] Y. Morigami, M. Kondo, J. Abe, H. Kita, K. Okamoto, The first large-scale pervaporation plant using tubular-type module with zeolite NaA membrane, Separation and purification technology, 25 (2001) 251-260.

[49] R. Zhou, F. Zhang, N. Hu, X. Chen, H. Kita, Fast preparation of high-performance zeolite T membranes in fluoride media, Chemistry Letters, 40 (2011) 1383-1385.

[50] F. Zhang, L. Xu, N. Hu, N. Bu, R. Zhou, X. Chen, Preparation of NaY zeolite membranes in fluoride media and their application in dehydration of bio-alcohols, Separation and Purification Technology, 129 (2014) 9-17.

[51] R. Zhou, Y. Li, B. Liu, N. Hu, X. Chen, H. Kita, Preparation of chabazite membranes by secondary growth using zeolite-T-directed chabazite seeds, Microporous and Mesoporous Materials, 179 (2013) 128-135.

[52] X. Lin, E. Kikuchi, M. Matsukata, Preparation of mordenite membranes on α-alumina tubular supports for pervaporation of water–isopropyl alcohol mixtures, Chemical Communications, (2000) 957-958.

[53] S.G. Sorenson, E.A. Payzant, W.T. Gibbons, B. Soydas, H. Kita, R.D. Noble, J.L. Falconer, Influence of zeolite crystal expansion/contraction on NaA zeolite membrane separations, Journal of Membrane Science, 366 (2011) 413-420.

[54] T. Graham, On the absorption and dialytic separation of gases by colloid septa, Philosophical transactions of the Royal Society of London, 156 (1866) 399-439.

[55] R.W. Baker, Membrane technology and applications, 3rd Edition, WILEY, 2012.

[56] N.W. Ockwig, T.M. Nenoff, Membranes for hydrogen separation, Chemical Reviews, 107 (2007) 4078-4110.

[57] S. Himeno, T. Tomita, K. Suzuki, K. Nakayama, K. Yajima, S. Yoshida, Synthesis and permeation properties of a DDR-type zeolite membrane for separation of CO_2/CH_4 gaseous mixtures, Industrial and Engineering Chemistry Research, 46 (2007) 6989-6997.

[58] M. Bernal, J. Coronas, M. Menendez, J. Santamaria, Separation of CO_2/N_2 mixtures using MFI-type zeolite membranes, AIChE Journal, 50 (2004) 127-135.

[59] Y. Hasegawa, T. Tanaka, K. Watanabe, B.-H. Jeong, K. Kusakabe, S. Morooka, Separation of CO_2/CH_4 and CO_2/N_2 systems using ion-exchanged FAU-type zeolite membranes with different Si/Al ratios, Korean Journal of Chemical Engineering, 19 (2002) 309-313.

[60] M.A. Carreon, S. Li, J.L. Falconer, R.D. Noble, Alumina-supported SAPO-34 membranes for CO_2/CH_4 separation, Journal of the American Chemical Society, 130 (2008) 5412-5413.

[61] X. Xu, W. Yang, J. Liu, L. Lin, Synthesis of a high-permeance NaA zeolite membrane by microwave heating, Advanced Materials, 12 (2000) 195-198.

[62] K. Kusakabe, T. Kuroda, A. Murata, S. Morooka, Formation of a Y-type zeolite membrane on a porous α-alumina tube for gas separation, Industrial and Engineering Chemistry Research, 36 (1997) 649-655.

[63] Z. Hong, F. Sun, D. Chen, C. Zhang, X. Gu, N. Xu, Improvement of hydrogen-separating performance by on-stream catalytic cracking of silane over hollow fiber MFI zeolite membrane, International Journal of Hydrogen Energy, 38 (2013) 8409-8414.

[64] M. Hong, J.L. Falconer, R.D. Noble, Modification of zeolite membranes for H_2 separation by catalytic cracking of methyldiethoxysilane, Industrial and Engineering Chemistry Research, 44 (2005) 4035-4041.

[65] M.J. Vaezi, A.A. Babaluo, Effect of dehydration temperature on the H_2 separation potential of hydroxy sodalite zeolite membranes, Iranian Journal of Hydrogen & Fuel

Cell, 1 (2015) 209-214.

[66] G. Xomeritakis, Z. Lai, M. Tsapatsis, Separation of xylene isomer vapors with oriented MFI membranes made by seeded growth, Industrial and Engineering Chemistry Research, 40 (2001) 544-552.

[67] C.J. Gump, R.D. Noble, J.L. Falconer, Separation of hexane isomers through nonzeolite pores in ZSM-5 zeolite membranes, Industrial and Engineering Chemistry Research, 38 (1999) 2775-2781.

[68] K. Kusakabe, T. Kuroda, S. Morooka, Separation of carbon dioxide from nitrogen using ion-exchanged faujasite-type zeolite membranes formed on porous support tubes, Journal of Membrane Science, 148 (1998) 13-23.

[69] K. Aoki, V.A. Tuan, J.L. Falconer, R.D. Noble, Gas permeation properties of ion-exchanged ZSM-5 zeolite membranes, Microporous and Mesoporous Materials, 39 (2000) 485-492.

[70] S. Shirazian, S.N. Ashrafizadeh, LTA and ion-exchanged LTA zeolite membranes for dehydration of natural gas, Journal of Industrial and Engineering Chemistry, 22 (2015) 132-137.

[71] Ó. de la Iglesia, R. Mallada, M. Menéndez, J. Coronas, Continuous zeolite membrane reactor for esterification of ethanol and acetic acid, Chemical Engineering Journal, 131 (2007) 35-39.

[72] X. Tan, K. Li, Membrane microreactors for catalytic reactions, Journal of Chemical Technology and Biotechnology, 88 (2013) 1771-1779.

[73] S.G. Kim, D.H. Hyeon, J.H. Chun, B. Chun, S.H. Kim, Nanocomposite poly (arylene ether sulfone) reverse osmosis membrane containing functional zeolite nanoparticles for seawater desalination, Journal of Membrane Science, 443 (2013) 10-18.

[74] C. Xue, D. Yang, G. Du, L. Chen, J. Ren, F. Bai, Evaluation of hydrophobic micro-zeolite-mixed matrix membrane and integrated with acetone-butanol-ethanol fermentation for enhanced butanol production, Biotechnology for biofuels, 8 (2015) 1-9.

[75] T. Masuda, N. Fukumoto, M. Kitamura, S.R. Mukai, K. Hashimoto, T. Tanaka, T.

Funabiki, Modification of pore size of MFI-type zeolite by catalytic cracking of silane and application to preparation of H_2-separating zeolite membrane, Microporous and Mesoporous Materials, 48 (2001) 239-245.

[76] J.L. Falconer, S.M. George, A.W. Ott, J.W. Klaus, R.D. Noble, H.H. Funke, Modification of zeolite or molecular sieve membranes using atomic layer controlled chemical vapor deposition, in, Google Patents, 2000.

[77] Y. Yan, M.E. Davis, G.R. Gavalas, Preparation of highly selective zeolite ZSM-5 membranes by a post-synthetic coking treatment, Journal of Membrane Science, 123 (1997) 95-103.

[78] S. Shirazian, S.N. Ashrafizadeh, Synthesis of substrate-modified LTA zeolite membranes for dehydration of natural gas, Fuel, 148 (2015) 112-119.

[79] A. Huang, F. Liang, F. Steinbach, J. Caro, Preparation and separation properties of LTA membranes by using 3-aminopropyltriethoxysilane as covalent linker, Journal of Membrane Science, 350 (2010) 5-9.

[80] A. Huang, N. Wang, J. Caro, Seeding-free synthesis of dense zeolite FAU membranes on 3-aminopropyltriethoxysilane-functionalized alumina supports, Journal of Membrane Science, 389 (2012) 272-279.

[81] A.W. Bhutto, K. Harijan, K. Qureshi, A.A. Bazmi, A. Bahadori, Perspectives for the production of ethanol from lignocellulosic feedstock-A case study, Journal of Cleaner Production, 95 (2015) 184-193.

[82] S. Kumar, N. Singh, R. Prasad, Anhydrous ethanol: A renewable source of energy, Renewable and Sustainable Energy Reviews, 14 (2010) 1830-1844.

[83] N.P. Blake, V.I. Srdanov, G.D. Stucky, H. Metiu, An investigation of the electronic and optical properties of dehydrated sodalite fully doped with Na, The Journal of chemical physics, 104 (1996) 8721-8729.

[84] J. Weitkamp, M. Fritz, S. Ernst, Zeolites as media for hydrogen storage, International Journal of Hydrogen Energy, 20 (1995) 967-970.

[85] J. Jiang, X. Gu, L. Feng, C. Duanmu, Y. Jin, T. Hu, J. Wu, Controllable synthesis of sodalite submicron crystals and microspheres from palygorskite clay using a two-step approach, Powder Technology, 217 (2012) 298-303.

[86] M.S. Nabavi, T. Mohammadi, M. Kazemimoghadam, Hydrothermal synthesis of hydroxy sodalite zeolite membrane: Separation of H_2/CH_4, Ceramics International, 40 (2014) 5889-5896.

[87] B. Beagley, J.O. Titiloye, Modeling the similarities and differences between the sodalite cages (β-cages) in the generic materials, Structural Chemistry, 3 (1992) 429-448.

[88] S. Münzer, J. Caro, P. Behrens, Preparation and characterization of sodium-free nanocrystalline sodalite, Microporous and Mesoporous Materials, 110 (2008) 3-10.

[89] S. Khajavi, J.C. Jansen, F. Kapteijn, Application of hydroxy sodalite films as novel water selective membranes, Journal of Membrance Science, 326 (2009) 153-160.

[90] S. Khajavi, F. Kapteijn, J.C. Jansen, Synthesis of thin defect-free hydroxy sodalite membranes: New candidate for activated water permeation, Journal of Membrance Science, 299 (2007) 63-72.

[91] M. Mirfendereski, M. Sadrzadeh, T. Mohammadi, Effect of synthesis parameters on single gas permeation through T-type zeolite membranes, International Journal of Greenhouse Gas Control, 2 (2008) 531-538.

[92] S. Yang, N. Evmiridis, Synthesis and characterization of an offretite/erionite type zeolite, Microporous Materials, 6 (1996) 19-26.

[93] J. Bengoa, S. Marchetti, N. Gallegos, A. Alvarez, M. Cagnoli, A. Yeramian, Stacking faults effects on shape selectivity of offretite, Industrial and Engineering Chemistry Research, 36 (1997) 83-87.

[94] Y. Cui, H. Kita, K. Okamoto, Preparation and gas separation performance of zeolite T membrane, Journal of Materials Chemistry, 14 (2004) 924-932.

[95] C. Baerlocher, L.B. McCusker, D.H. Olson, Atlas of zeolite framework types, Elsevier, 2007.

[96] I.H. Lee, Synthesis and characterization of nanoporous materials and their films with controlled microstructure, in, Texas A&M University, 2010.

Chapter 2 Preparation and characterization of sodalite

2.1 Introduction

Zeolites are hydrated aluminosilicate minerals. The group has a limitless three-dimensional anion network. And the chemistry of zeolites is based on the tetrahedron (TO_4), where T = Si, Al or P. Sometimes other heteroatom (such as B, Ca and Be) may appear. Zeolites have unique pore structures, large specific surface area and tunable pore size [1]. As catalyst, adsorbent, separating agent and ion-exchange agent [2-6], zeolites have been applied extensively to petrochemical industry, soil improvement, wastewater treatment, metallurgy and pharmaceuticals industry [7-11]. Sodalite has a framework consisting of β-cages [12]. Sodalite has an effective pore size of 0.28 nm, which allows small molecules (H_2 or H_2O) pass through channels of sodalite. Due to the unique structure and properties, sodalite has attracted many attentions. Moreover, Berg et al found that sodalite can even be considered as a H_2 storage material because of its high H_2 adsorption ability [13]. Therefore, exploring the synthesis of sodalite is great significance.

In this work, sodalite was obtained by hydrothermal synthesis. The effects of different synthesis parameters, including synthesis time, synthesis temperature, n (Na_2O/SiO_2), n (H_2O/SiO_2), n (Al_2O_3/ SiO_2) and silica source, have been investigated. The effect of seeds on sodalite membrane preparation also has been discussed.

2.2 Experimental

2.2.1 Chemicals

Alumina sources were alumina hydroxide ($Al(OH)_3$, 100%, Wako) and sodium alumina (n (Al/NaOH) = 0.8, Wako). Sodium source was sodium hydroxide (NaOH, 97%, Wako), Cl^- was provided by sodium chloride (NaCl, 99.99%, Wako), silica sources were colloidal silica (Ludox HS-40, Ludox AS-40, Ludox TM-40, 40 w.t.%, Aldrich), fumed silica dioxide (98%, Aerosil) and water.

2.2.2 Synthesis

All the sodalite crystals with different features were prepared by hydrothermal synthesis method which has been applied to zeolite preparation widely [14, 15]. The following molar compositions were used: 1.0 SiO_2: (0.10-0.60) Al_2O_3: (0.60-2.00) Na_2O: (0-0.95) NaCl: (15-35) H_2O. The synthesis process was different from the typical preparation procedure of sodalite membranes [16-18]. The alkali source was prepared by dissolving sodium hydroxide in a turbid solution of alumina hydroxide and some water. Then keep heating and stirring the solution until clear. After the clear alkali source cooled to ambient temperature, the rest water was supplemented. Finally, sodium chloride and silica source were added to the alkali source in sequence while stirring and stirred 1 h at room temperature. Then the resulting gel was removed into a PTFE-lined autoclave. The hydrothermal synthesis was carried out at 383-473 K for 0.5-168 h. The products was isolated by centrifugation and washed with water for several times until neutral. The powders were dried and saved in an oven at 353 K for later experiments.

2.2.3 Characterization

All the powder samples were measured by X-ray diffraction (XRD, SHIMADZU XRD-6100) with Cu-Kα radiation. The spectra were scanned in the range of 2θ = 5^o-45^o at a scanning rate of 4^o/min. Scanning electron microscopy (FE-SEM, JEOL JSM 6335F) was used to investigate the morphology and particle size of the powders.

The crystallite size was obtained from Scherrer's equation:

$$D = k\lambda/\beta cos\theta \qquad (1)$$

Where D is the average crystallite size of the crystals, k is the Scherrer's constant (0.89), λ is the wavelength of the X-ray beam used (0.154056 nm). β is extra width of the diffraction peak, it can be calculated as equation (2):

$$\beta = \sqrt{B^2 - b^2} \qquad (2)$$

For a diffraction peak, the full width at half maximum is regarded B. And b is the width of the instrument, which can be obtained from Jade software. And θ is the

diffraction angle [19].

2.3 Results and discussion

2.3.1 Effect of synthesis temperature

To investigate the effect of crystallization temperature, powders were crystallized for 24 h at different temperatures. **Figure 2-1** shows the XRD patterns of powders prepared at 383 K, 403 K, 423 K and 473 K. The results indicate that pure sodalite can be prepared successfully in a large arrange of crystallization temperature. The patterns show sharp diffractions at around 2θ = 14.21°, 24.27° and 43.33°. These typical peaks are originated from the (110), (211) and (411) plane of sodalite [20].

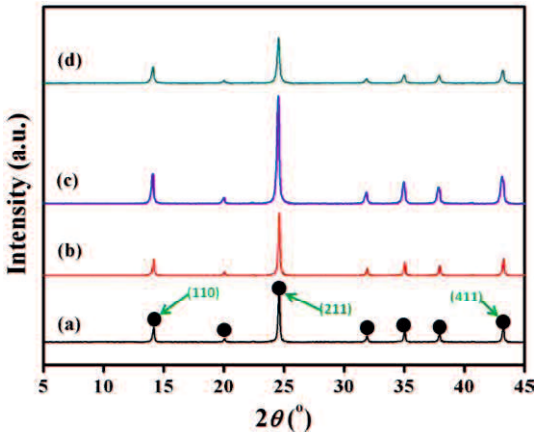

Figure 2-1 X-ray diffraction patterns of powders prepared at (a) 383 K, (b) 403 K, (c) 423 K and (d) 473 K for 24 h (roundness indicates the typical peaks of sodalite)

On the other hand, SEM analysis confirmed the morphologies of as-synthesized sodalite and **Figure 2-2** gives the corresponding SEM images. It is obviously that the sodalite crystals have different morphologies and crystal sizes as the synthesis temperature changed. All of the four sodalite samples have a certain amount of small particles with a visual size of about 100-200 nm. However, the uniformity was quite different. When the synthesis temperature was lower, larger particles always arise. For the powder prepared at 423 K (**Figure 1-1(c)**), even particles with a size about 700 nm appeared and the particles have sharp edges. It is because low temperature can

inhibit the evaporation of a solvent, the environment encourage the growth of larger and purer crystals. However, a solvent will evaporate faster at higher temperature. Crystals will form quickly than at a low temperature because it removes solvent from the solution, forcing the crystals to form quickly. Thus, small crystals can be easily formed.

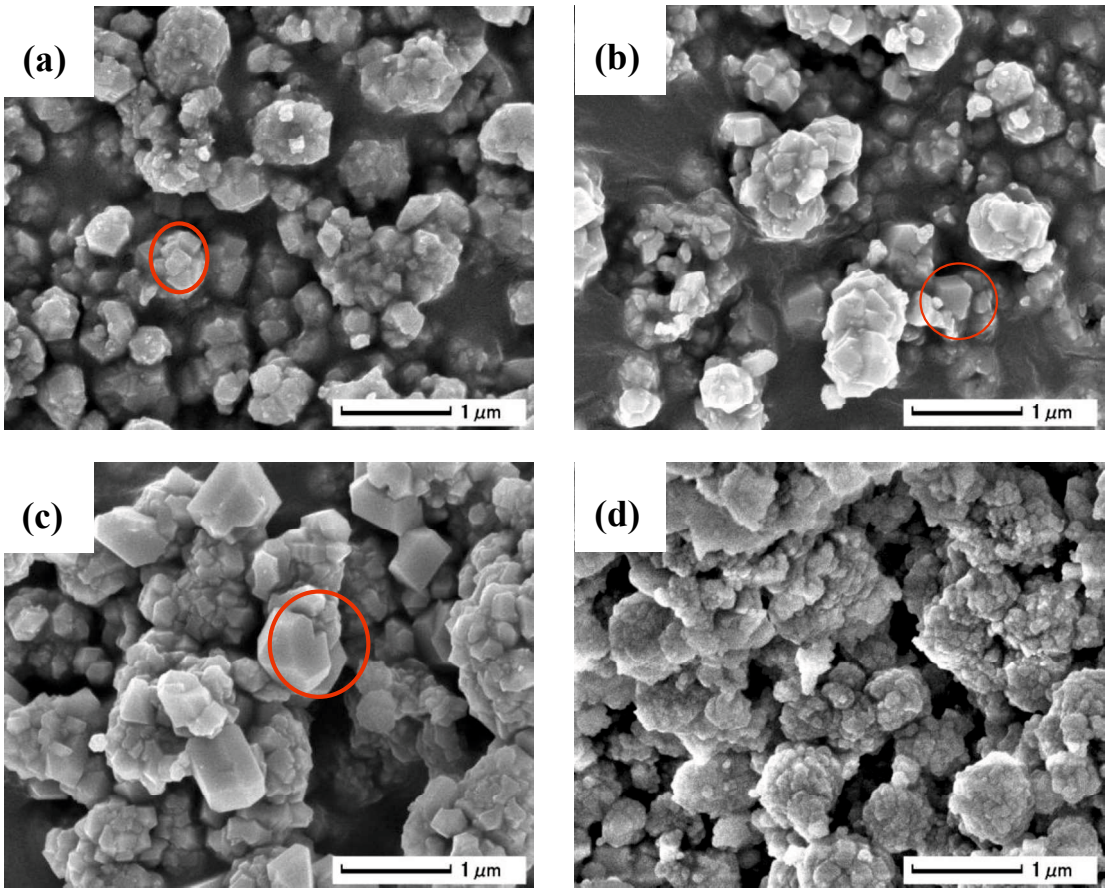

Figure 2-2 The representative SEM images of powders prepared at different temperatures: (a) 383 K, (b) 403 K, (c) 423 K and (d) 473 K for 24 h.

The results here confirmed such explanations well. **Figure 1-1(d)** shows that sodalite obtained at 473 K was more uniform than others, and accompanied particle aggregation. The higher temperature of 473 K was in favor of producing uniform nanometer sized sodalite. Small sodalite was also prepared from meta-kaolin by Lin et al. at high temperature, which can further proof our results [21].

2.3.2 Effect of crystallization time

Figure 2-3 shows the XRD patterns of powders synthesized for 0.5-168 h at 423 K. The patterns indicated that pure sodalite can be prepared for longer than 8 h. To begin with, A type and FAU type (X and Y) crystals also occurred. **Figure 2-4** showed the SEM images of powders prepared at 423 K for 0.5 h, 2 h, 18 h and 144 h, respectively.

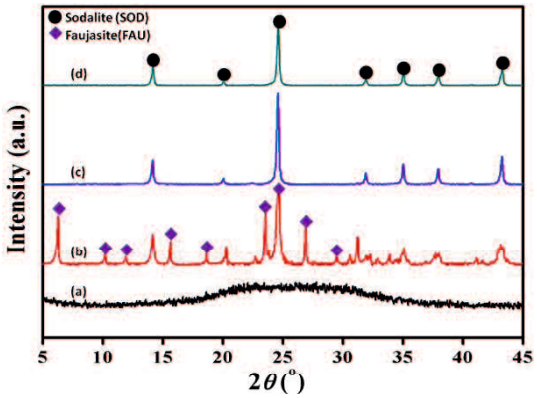

Figure 2-3 X-ray diffraction patterns of powders prepared at 423 K for (a) 0.5 h, (b) 2 h, (c) 18 h and (d) 144 h

As the synthesis time increased, the powders changed from amorphous to nanometer sized sodalite crystals. **Figure 2-4(b)** also exhibited the intergrowth of sodalite and FAU crystals clearly. Combining with related researches [16, 22], it is noted that A type and FAU type crystals are common impurity in the synthesis of sodalite crystals and sodalite membranes.

Figure 2-5 shows the curves of the crystallinity as a function of the synthesis time at different temperature of 383 K, 403 K, 423 K and 473 K, respectively. It is noteworthy that sodalite with 100% crystallinity can be obtained at all four temperatures. As can be expected, when the temperature was 473 K, shorter time was needed to reach the maximum crystallinity. Compared to the figure on right in **Figure 2-5**, the period of pure sodalite crystal growth was relatively longer when the crystallization time was 423 K. Therefore, it is more suitable for the following analysis.

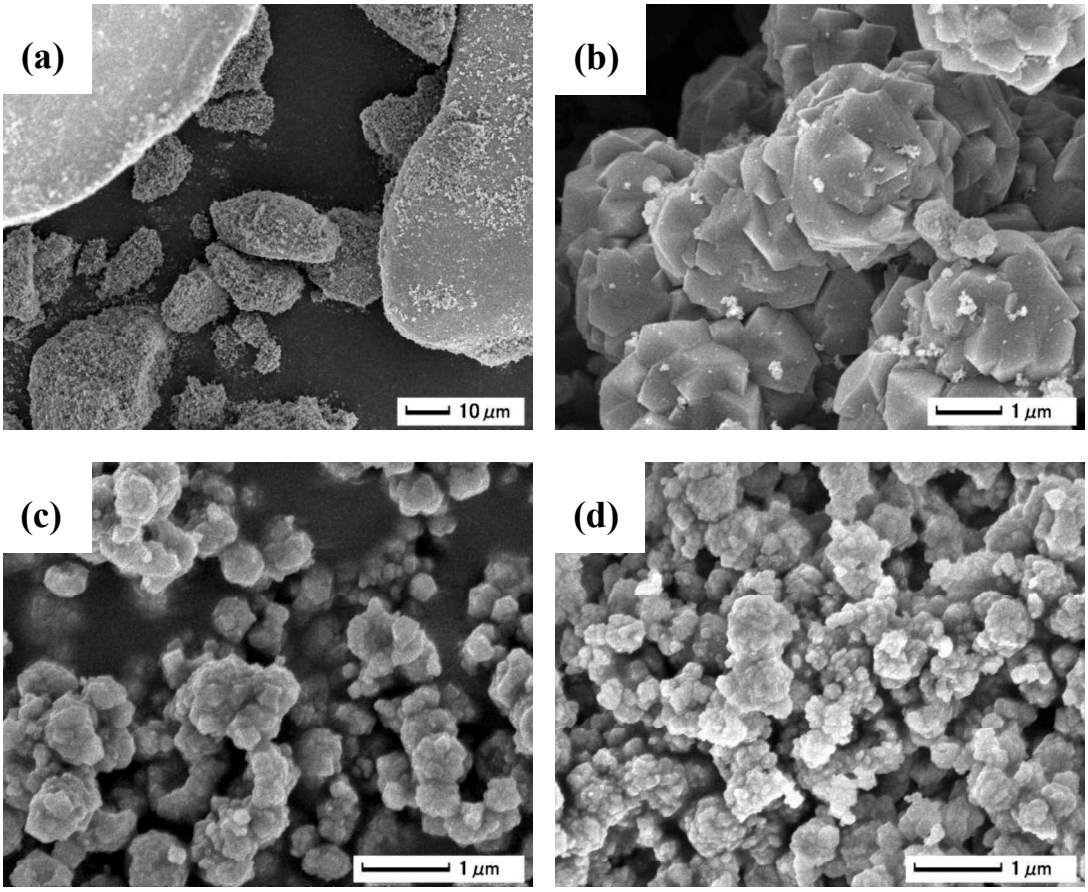

Figure 2-4 SEM images of powders prepared at 423 K for (a) 0.5 h, (b) 2 h, (c) 18 h and (d) 144 h

Crystal growth is caused by crystal surface growth through transport process and surface processes of atoms or molecules. Both of layer growth and multi-nucleation multilayer growth were mentioned by Pablo et al. [23] Thus, we can consider crystal particles contain a mount of smaller crystallites. The trend line of crystallite size of many samples as a function of synthesis time was shown in **Figure 2-5(left)**. It can be seen that nucleation takes place after an induction time, which is corresponding to teeny crystallite with a size of 0.8 nm. The crystallite size increased rapidly until the crystallinity reached 100% for a longer time. After that, even the synthesis time was prolonged to 168 h, the crystallite size hardly changed.

In consideration of the significant contribution that uniform crystals with high crystallinity can make to the applications of uniform defect free sodalite membrane preparation, we prepared powders at 473 K for 24 h when other factors were

investigated.

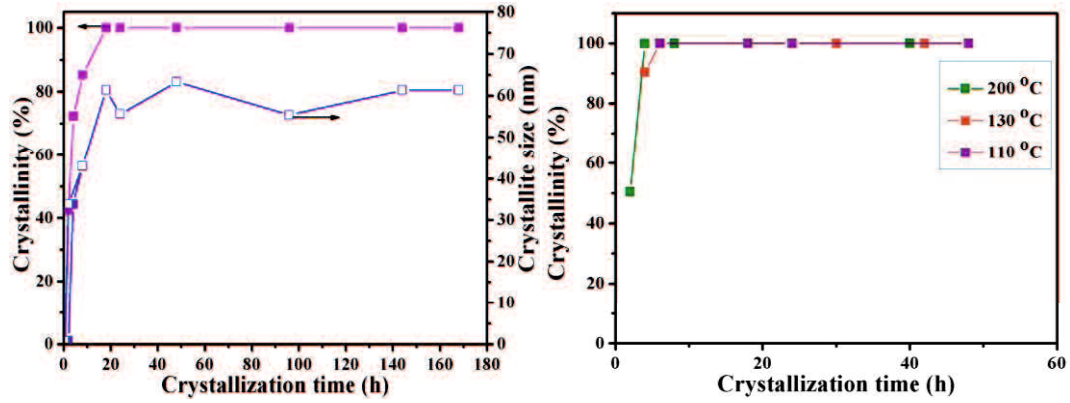

Figure 2-5 Crystallinity and crystallite size of powders prepared at 423 K as a function of crystallization time (Figure on left side). And crystallinity of powders prepared at 383 K, 403 K and 473 K as a function of crystallization time (Figure on right side).

2.3.3 Effect of n (Na_2O/SiO_2)

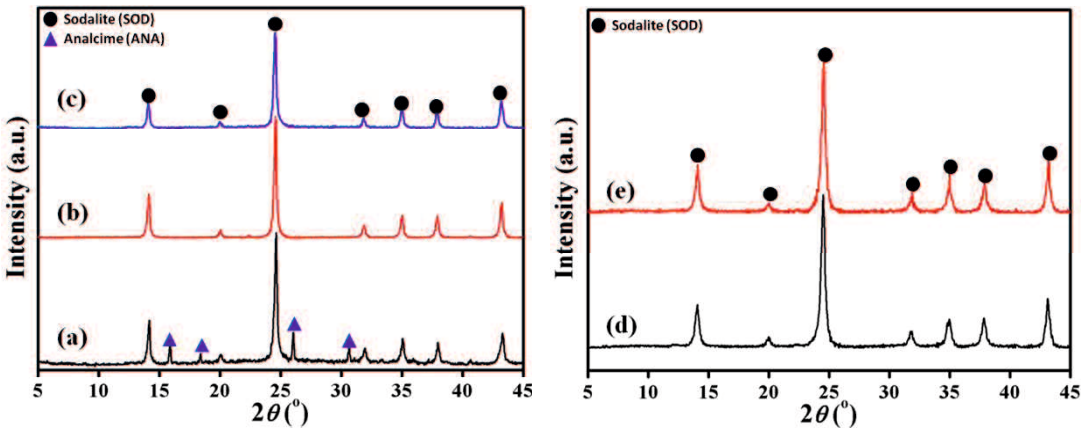

Figure 2-6 X-ray diffraction patterns of powders obtained with (a) n (Na_2O/SiO_2) = 0.8, (b) n (Na_2O/SiO_2) = 0.96, (c) n (Na_2O/SiO_2) = 1.2, (d) n (Na_2O/SiO_2) = 1.4, (e) n (Na_2O/SiO_2) = 2.0

The value of n (Na_2O/SiO_2) was considered as a critical factor influencing on crystal growth behavior. In this part, different amount of sodium hydroxide was dissolved in the solutions. The gel composition was 1.0 SiO_2: 0.5 Al_2O_3: (0.8-2.0) Na_2O: 0.65 NaCl: 20.5 H_2O.

Figure 2-6 shows the XRD diffraction patterns of the solids obtained after

hydrothermal synthesis at 473 K for 24 h. When n (Na_2O/SiO_2) was 0.8, sodalite appeared. However, analcime with typical peaks focusing on15.8°, 18.28°, 25.95° and 30.5° also appeared. When n (Na_2O/SiO_2) increased, pure sodalite crystals can be obtained easily. Moreover, the crystallinity reached to the maximum (**Figure 2-7**).

On the other hand, the changing curve of crystallite size as a function of n (Na_2O/SiO_2) behaved differently from **Figure 2-5**. A peak of the crystallite size arised when n (Na_2O/SiO_2) was 1.2 as shown in **Figure 2-7**. It is because that increasing nucleation and crystal growth rate increased the alkalinity increased, which facilitates the growth of crystallite. However, when the alkalinity was much higher, the solubility of colloid SiO_2 and aluminum hydroxide increased rapidly, large amount of nuclei were formed in gels.

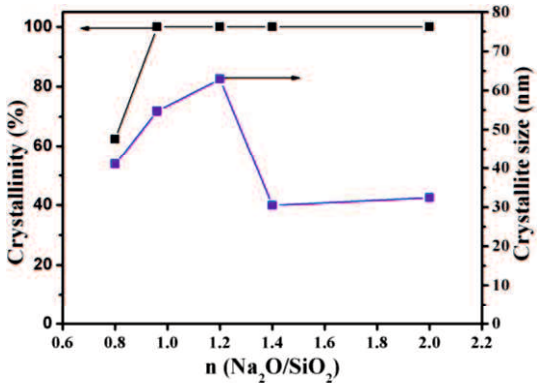

Figure 2-7 Crystallinity and crystallite size of powders prepared at 473 K for 24 h as a function of n (Na_2O/SiO_2).

Figure 2-8 shows the SEM images of powders prepared different n (Na_2O/SiO_2) varied from 0.8 to 2.0. The rhombic crystals as large as 800 nm marked by a red circle indicted the existence of ANA zeolite, which was in accordance with the Figure 2-6(a). When the n (Na_2O/SiO_2) increased to 0.96 and 1.2, the sodalite particles were about 100 nm and the crystals prepared with n (Na_2O/SiO_2) of 0.96 still showed edges. As the n (Na_2O/SiO_2) increased to 1.4 and 2.0, the crystals became ball-like particles and the particle size was about 50 nm, which demonstrated the variation crystallite size showed in **Figure 2-7**. However crystals obtained under high n (Na_2O/SiO_2) of 2.0 were not uniform as showed in **Figure 2-8(e)**.

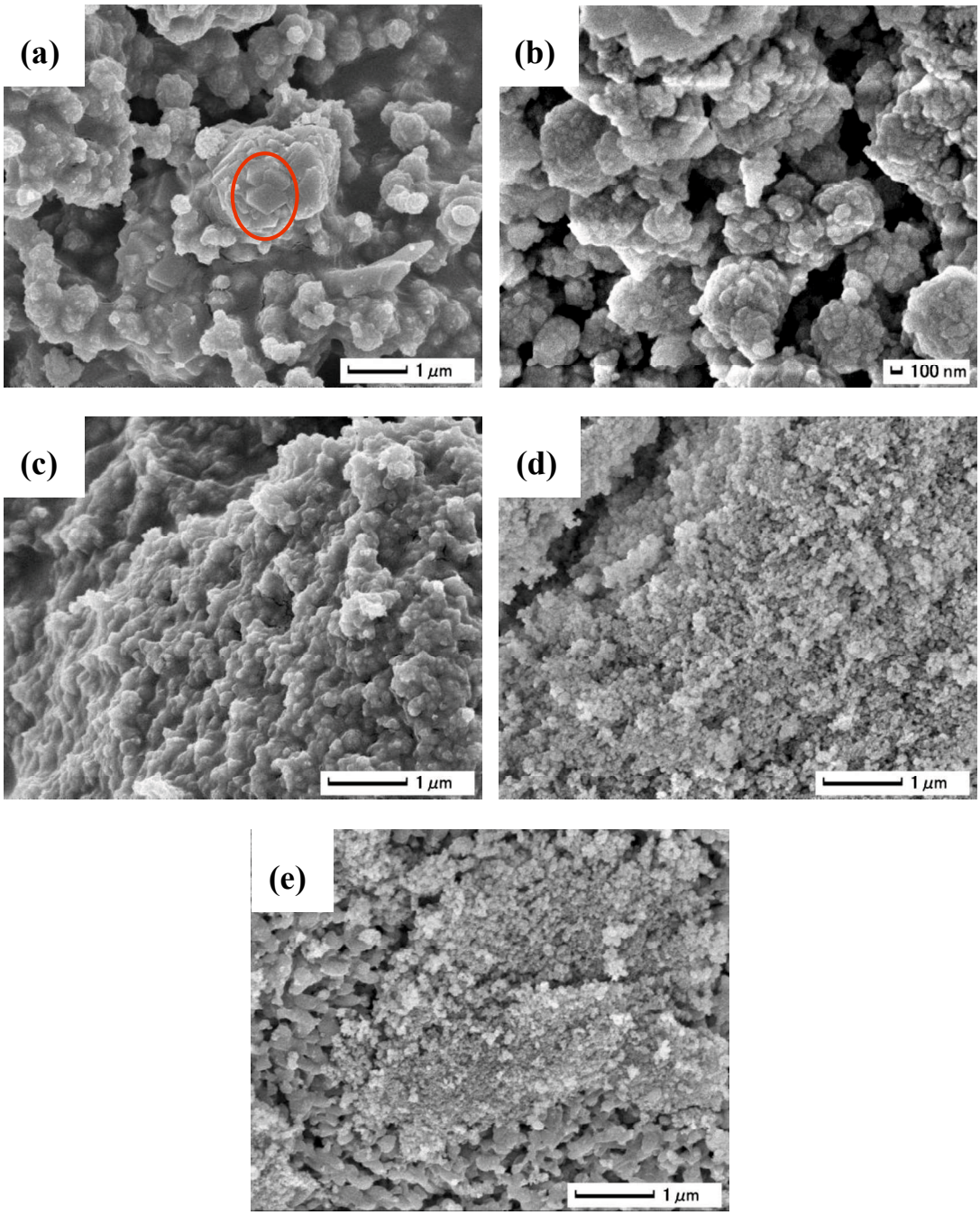

Figure 2-8 SEM images of powders prepared with (a) n (Na_2O/SiO_2) = 0.8, (b) n (Na_2O/SiO_2) = 0.96, (c) n (Na_2O/SiO_2) = 1.2, (d) n (Na_2O/SiO_2) = 1.4, (e) n (Na_2O/SiO_2) = 2.0.

2.3.4 Effect of n (Al_2O_3/SiO_2)

Lechert, H and Kosanovic et al. have studied the effect of the Si/Al ratio on the properties of zeolite crystals, such as A type, mordenite, and faujasite [24, 25].

Herein, in the case of sodalite, crystals were synthesized at the n (Al_2O_3/SiO_2) values of 0.10, 0.35, 0.40, 0.45, 0.50, 0.55, and 0.60 by adjusting the amount of aluminum hydroxide. The XRD patterns (not shown here) indicated that pure sodalite can be formed within such a wide range of n (Al_2O_3/SiO_2), which is in accordance with the high crystallinity as Figure 2-9 shows. However, the crystallite size was affected by n (Al_2O_3/SiO_2) significantly as the curve shown in **Figure 2-9**.

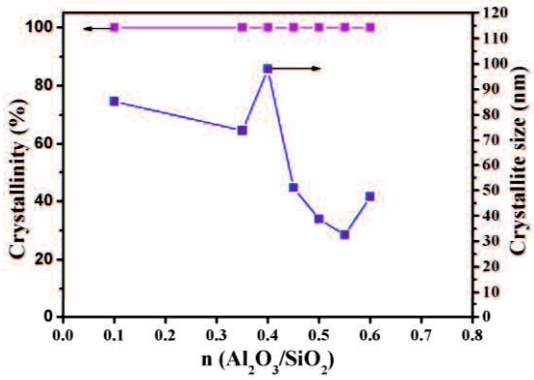

Figure 2-9 Crystallinity and crystallite size of powders prepared at 473 K as a function of n (Al_2O_3/SiO_2).

When n (Al_2O_3/SiO_2) changed from 0.10 to 0.40, the crystallite size was larger than 70 nm, and it reached the maximum of 98 nm when it was 0.40. As n (Al_2O_3/SiO_2) increased, the crystallites even decreased to 32 nm. It can be demonstrated by the reason that lower Si^{4+} concentration in the solutions favors the formation of small silicalte species such as double four-member ring (D4R) which is similar with the property of NaA zeolite. Therefore, higher n (Al_2O_3/SiO_2) should be better for preparing sodalite crystals high crystallinity and stability.

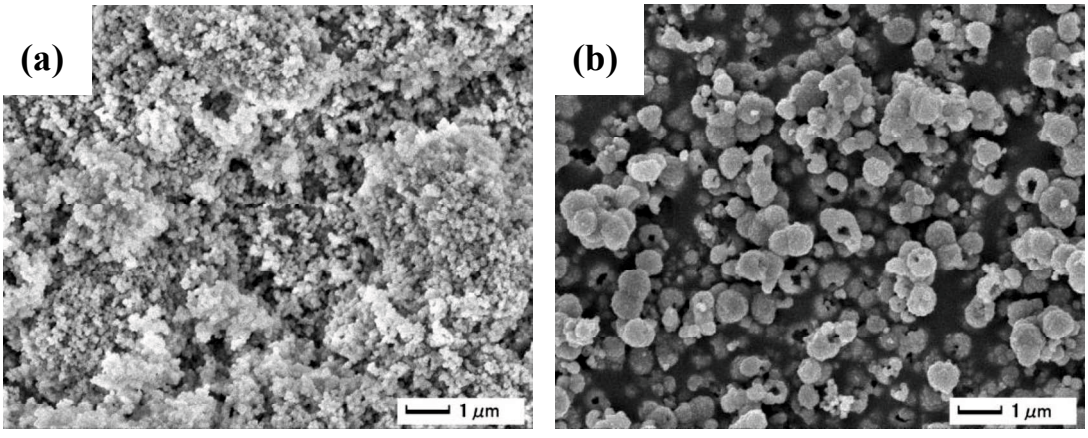

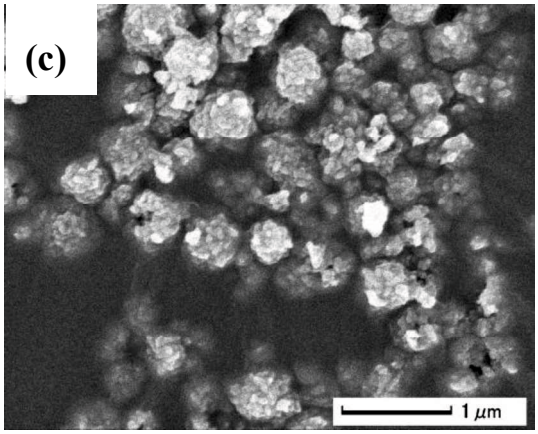

Figure 2-10 SEM images of powders prepared with (a) n (Al_2O_3/SiO_2) = 0.1, (b) n (Al_2O_3/SiO_2) = 0.4, and (c) n (Al_2O_3/SiO_2) = 0.6

Moreover, some SEM images of crystals synthesized with different n (Al_2O_3/SiO_2) were shown in **Figure 2-10**. When the n (Al_2O_3/SiO_2) was 0.10, large amount of clusters consisted of ball-like crystals were formed. As n (Al_2O_3/SiO_2) increased to 0.40, the particles showed hollow sphere shape. After the n (Al_2O_3/SiO_2) increased to 0.6, sodalite with common morphology was obtained. The results indicated that n (Al_2O_3/SiO_2) played an important role in the morphology of sodalite crystals.

2.3.5 Effect of n (H_2O/SiO_2)

Mohammad et al. has found that pure sodalite can be obtained with a wide range of water molar content (H_2O/SiO_2) varied from 140 to 260, and the particle size decreased as water molar content increased [18]. In this work, we tried to prepare sodalite powders with n (H_2O/SiO_2) varying from 15 to 35. However, when n (H_2O/SiO_2) increased to 35, ANA crystal phase appeared. The peaks were located at the angles showed in **Figure 2-11**. Even though the values of n (H_2O/SiO_2) were very different from the values as reported, pure sodalite can also prepared successfully. The similar n (Na_2O/H_2O) in this work (0.032-0.064) and the value reported (0.039-0.071) may be the main condition for sodalite growth.

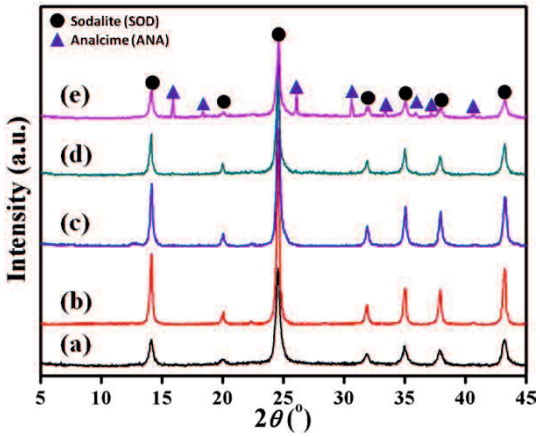

Figure 2-11 X-ray diffraction patterns of powders obtained with (a) n (H_2O/SiO_2) = 15, (b) n (H_2O/SiO_2) = 20.5, (c) n (H_2O/SiO_2) = 25, (d) n (H_2O/SiO_2) = 30 and (e) n (H_2O/SiO_2) = 35

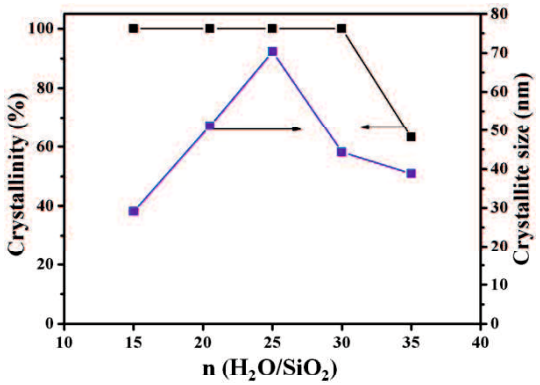

Figure 2-12 Crystallinity and crystallite size of powders prepared at 473 K as a function of n (H_2O/SiO_2).

As **Figure 2-12** showed, the crystallinity of sodalite decreased from 100% to 63.2% when water molar concentration increased to 35. From the corresponding curve of crystallite size, it can be estimated that when n (H_2O/SiO_2) was 25, the crystallite size of sodalite reached a peak. It was not the same as the results obtained by Mohammad et al [18]. It manifested that the same zeolite can perform differently during growth in different chemical environments.

2.3.6 Effect of silica source

Mintova et al. reported that the final silicalite-1 nanocrystal size was affected by

the type of silica source used [26]. Li et al. discovered that different type of silica source had notable effect on separation performance of as-synthesized CHA membranes [27]. Hence, the nature of silica source affects strongly on the growth of zeolite. In this work, four kinds of commercial available silica source were used, namely AS-40, TM-40, HS-40 and fumed silica. Fumed silica has largest particulate specific surface area (380 m^2/g) among the four silica sources. The particulate specific surface area of TM-40 (140 m^2/g) was similar to that of AS-40 (135 m^2/g). The proper value of HS-40 (220 m^2/g) was just smaller than fumed silica.

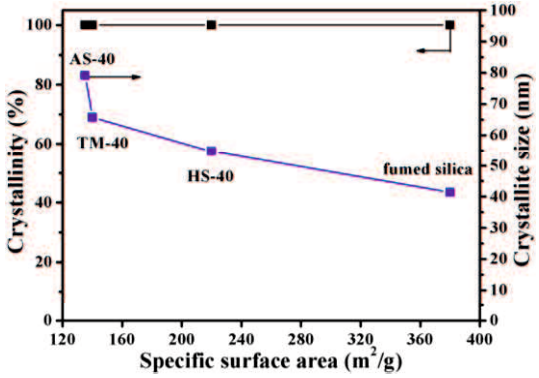

Figure 2-13 Crystallinity and crystallite size of powders prepared at 473 K as a function of specific surface area of silica source.

Figure 2-13 presented the crystallinity and crystallite size of sodalite in dependent on specific surface area of silica source types. Pure sodalite crystals were obtained by using all kinds of silica source. While fumed silica was used, sodalite has the smallest crystallite size. As the specific surface area of silica source decreased, crystallite size of as-synthesized sodalite increased from 41.4 nm to 79.1 nm. The average particle size decreases as silica particle size decreased. **Figure 2-13** provided a good illustration of it, which is in accordance with the result reported by Meise [28].

2.3.7 Effect of seeds on membrane morphology

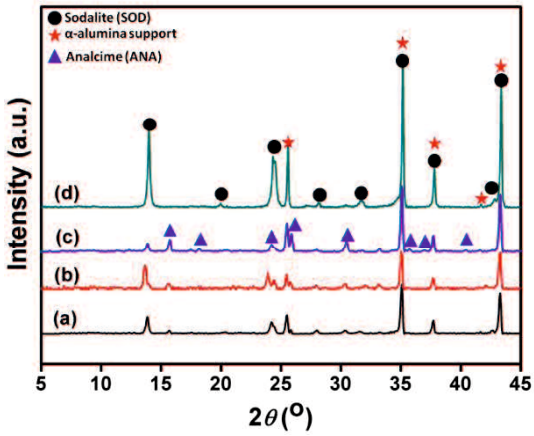

Figure 2-14 XRD patterns of membranes prepared with supports coated with sodalite crystals prepared at (a) 383 K, (b) 403 K, (c) 423 K, and (d) 448 K for 24 h. (Membranes were all synthesis at 448 K for 16 h in a sol with a molar composition of 1 SiO_2: 0.50 Al_2O_3: 0.96 Na_2O: 0.65 NaCl: 500 H_2O.)

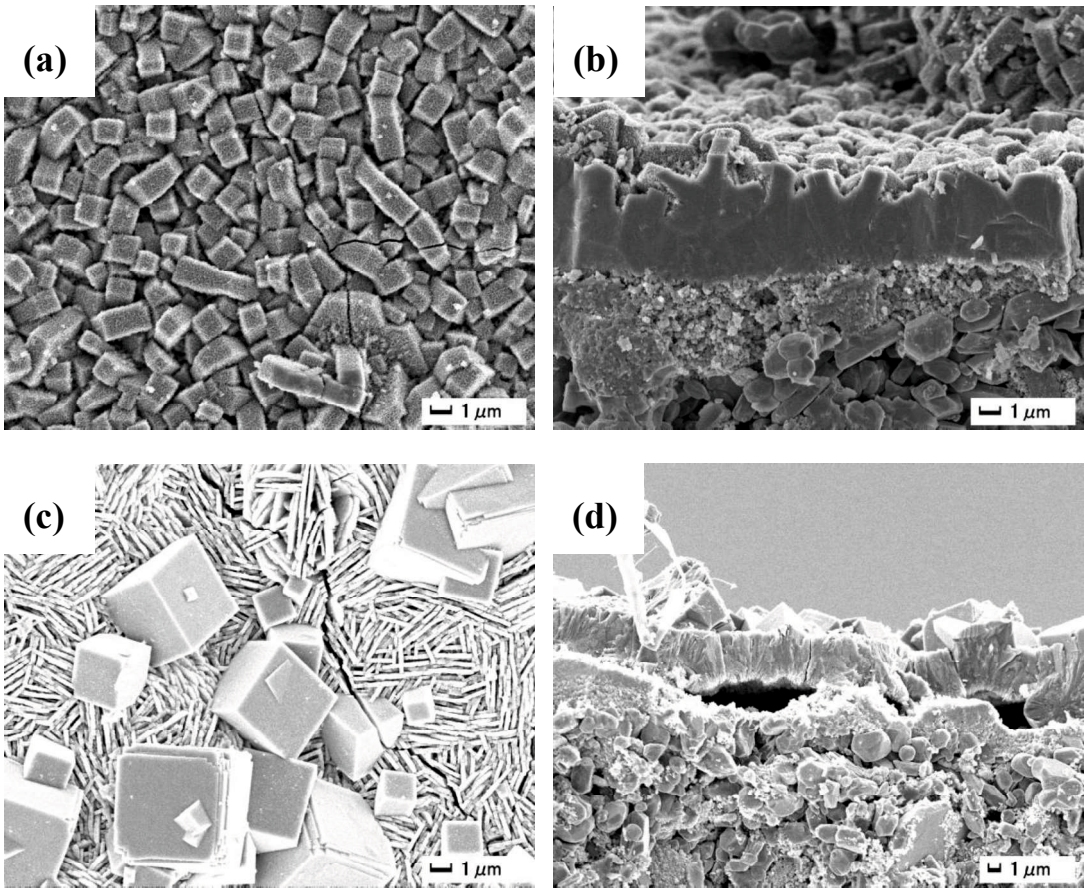

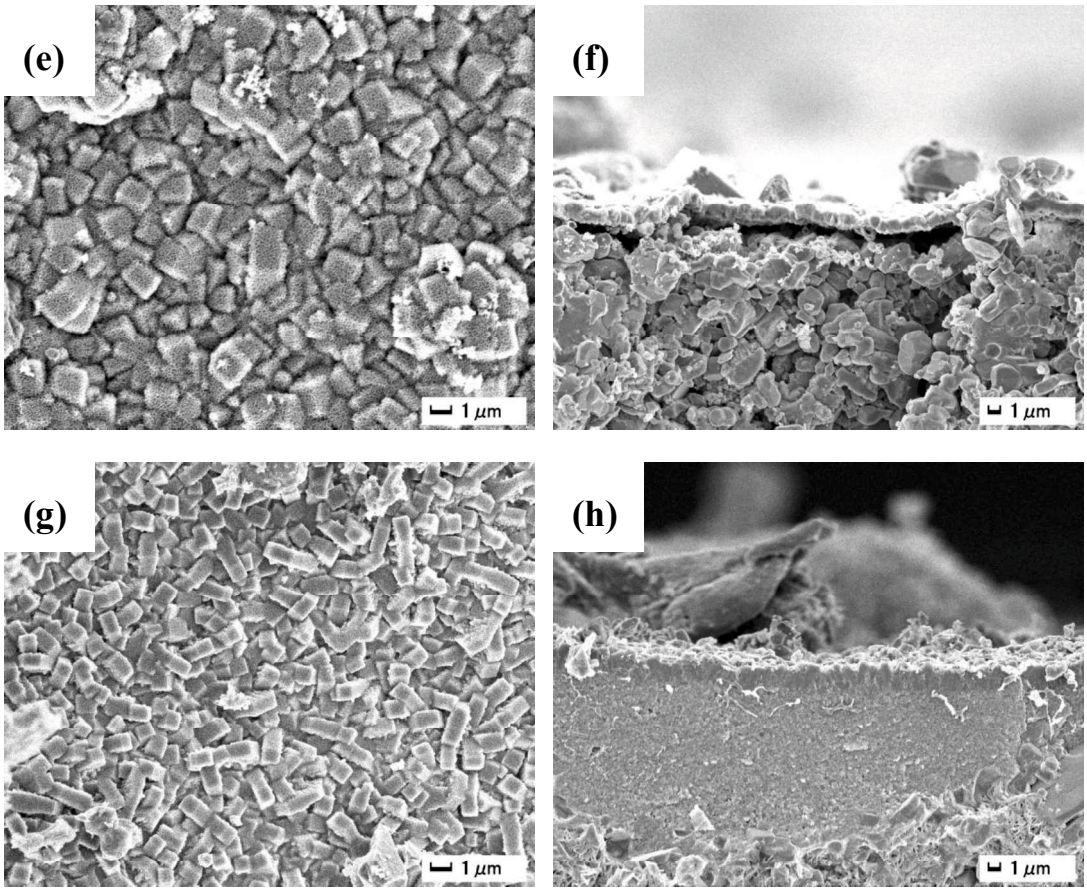

Figure 2-15 SEM images of membranes prepared with supports coated with sodalite crystals prepared at (a, b) 383 K, (c, d) 403 K, (e, f) 423 K, and (g, h) 473 K for 24 h. (Membranes were all synthesis at 448 K for 16 h in a sol with a molar composition of 1 SiO_2: 0.5 Al_2O_3: 0.96 Na_2O: 0.65 NaCl: 500 H_2O.)

To discuss the effect of seeds on membrane preparation, we attempted to prepare sodalite membranes using sodalite crystals prepared at different temperature as shown above. The SEM images of seeds were showed in **Figure 2-2**. Membranes were prepared with a molar composition of 1SiO_2: 0.5 Al_2O_3: 0.96 Na_2O: 0.65 NaCl: 500 H_2O. And the crystallization was carried out at 448 K for 16 h. **Figure 2-14** exhibited the XRD patterns of as-synthesized membranes. Pure sodalite membranes can be induced successfully except using sodalite crystals prepared at 423 K. When crystals prepared at 423 K were used, ANA crystal phase appeared.

The membrane morphologies were showed by SEM images in **Figure 2-15**. When crystals prepared at 403 K were used, inhomogeneous sodalite membrane was formed. On the surface of the membrane, both of cubic crystals with a side length of

2μm-5 μm and elongate crystals were formed. Pure sodalite membranes with cubic crystals can be obtained with seeds prepared at 383 K and 473 K, respectively. Especially for membrane prepared with seed synthesized at 473 K, there were no obvious cracks while much cracks appeared in membrane prepared with seed synthesized at 383 K. Moreover, **Figure 2-15(h)** showed a thin zeolite layer of 2 μm was formed on the support. Therefore, sodalite crystals prepared at 473 K will used for sodalite membrane preparation in **Chapter 3**.

2.4 Conclusions

The main purpose of this research is to investigate many factors influencing the synthesis of sodalite, including synthesis temperature, synthesis time, n (Na_2O/SiO_2), n (H_2O/SiO_2), n (Al_2O_3/SiO_2) and silica source. From the XRD patterns and SEM images, it was concluded that smaller and more uniform sodalite crystal particles were produced at higher synthesis temperature (473 K). Pure sodalite crystals were formed until the synthesis time was prolonged to 18 h at 423 K. Moreover, n (Na_2O/SiO_2) was effective on the crystallite size of synthesized zeolite and low n (Na_2O/SiO_2) reduced the crystallinity sharply. Herein, sodalite crystals which are as small as 50 nm have been synthesized with a high n (Na_2O/SiO_2) value of 2.0. Besides, higher n (H_2O/SiO_2) decreased the crystallinity of the samples obviously. In addition, n (Al_2O_3/SiO_2) affected the crystallite size of synthesized sodalite enormously even though the crystallinity was unchanged. Finally, the crystallite size of sodalite was only about 40 nm when the silica source is fumed silica, showing the positive effects of small silica particles on obtaining sodalite with small crystallite size. Uniform sodalite crystals prepared at 473 K is better for preparing sodalite membranes with good morphology.

References

[1] D.W. Breck, Zeolite molecular sieves, Krieger, 1984.

[2] N. Chen, W. Reagan, Evidence of autocatalysis in methanol to hydrocarbon reactions over zeolite catalysts, Journal of Catalysis, 59 (1979) 123-129.

[3] M. Iwamoto, H. Yahiro, Y. Mine, S. Kagawa, Excessively copper ion-exchanged ZSM-5 zeolites as highly active catalysts for direct decomposition of nitrogen monoxide, Chemistry Letters, (1989) 213-216.

[4] S.W. Blocki, Hydrophobic zeolite adsorbent: a proven advancement in solvent separation technology, Environmental Progress, 12 (1993) 226-230.

[5] K. Hernadi, A. Fonseca, J. Nagy, D. Bemaerts, A. Fudala, A. Lucas, Catalytic synthesis of carbon nanotubes using zeolite support, Zeolites, 17 (1996) 416-423.

[6] V.A. Bell, B.T. Desai, S.M. Kuznicki, I. Petrovic, Small-pored crystalline titanium molecular sieve zeolites and their use in gas separation processes, in, Google Patents, 2000.

[7] M. Climent, A. Corma, S. Iborra, J. Primo, Base catalysis for fine chemicals production: claisen-schmidt condensation on zeolites and hydrotalcites for the production of chalcones and flavanones of pharmaceutical interest, Journal of Catalysis, 151 (1995) 60-66.

[8] P. Leggo, B. Ledesert, Use of organo-zeolitic fertilizer to sustain plant growth and stabilize metallurgical and mine-waste sites, Mineralogical Magazine, 65 (2001) 563-570.

[9] O. Ahmed, H. Aminuddin, M. Husni, Reducing ammonia loss from urea and improving soil-exchangeable ammonium retention through mixing triple superphosphate, humic acid and zeolite, Soil use and management, 22 (2006) 315-319.

[10] W. Vermeiren, J. Gilson, Impact of zeolites on the petroleum and petrochemical industry, Topics in Catalysis, 52 (2009) 1131-1161.

[11] S. Wang, Y. Peng, Natural zeolites as effective adsorbents in water and wastewater treatment, Chemical Engineering Journal, 156 (2010) 11-24.

[12] T. Loeser, D. Freude, G. Mabande, W. Schwieger, ^{17}O NMR studies of sodalites, Chemical physics letters, 370 (2003) 32-38.

[13] A. Van den Berg, S. Bromley, E. Flikkema, J. Wojdel, T. Maschmeyer, J. Jansen, Molecular-dynamics analysis of the diffusion of molecular hydrogen in all-silica sodalite, Journal of Chemical Physics, 120 (2004) 10285-10289.

[14] N. Hiyoshi, Nanocrystalline sodalite: Preparation and application to epoxidation of 2-cyclohexen-1-one with hydrogen peroxide, Applied Catalysis A: General, 419-420 (2012) 164-169.

[15] M.M.M. Mostafa, K.N. Rao, H.S. Harun, S.N. Basahel, I.H.A. El-Maksod, Synthesis and characterization of partially crystalline nanosized ZSM-5 zeolites, Ceramics International, 39 (2013) 683-689.

[16] X. Xu, Y. Bao, C. Song, W. Yang, J. Liu, L. Lin, Microwave-assisted hydrothermal synthesis of hydroxy-sodalite zeolite membrane, Microporous and Mesoporous Materials, 75 (2004) 173-181.

[17] S. Khajavi, J.C. Jansen, F. Kapteijn, Performance of hydroxy sodalite membranes as absolute water selective materials under acidic and basic conditions, Journal of Membrane Science, 356 (2010) 1-6.

[18] M.S. Nabavi, T. Mohammadi, M. Kazemimoghadam, Hydrothermal synthesis of hydroxy sodalite zeolite membrane: Separation of H_2/CH_4, Ceramics International, 40 (2014) 5889-5896.

[19] A. Loiola, J. Andrade, J. Sasaki, L. Da Silva, Structural analysis of zeolite NaA synthesized by a cost-effective hydrothermal method using kaolin and its use as water softener, Journal of Colloid and Interface Science, 367 (2012) 34-39.

[20] M.M. Treacy, J.B. Higgins, Collection of simulated XRD powder patterns for zeolites fifth (5th) revised edition, Elsevier, 2007.

[21] D. Lin, X. Xu, F. Zuo, Y. Long, Crystallization of JBW, CAN, SOD and ABW type zeolite from transformation of meta-kaolin, Microporous and Mesoporous Materials, 70 (2004) 63-70.

[22] S. Khajavi, F. Kapteijn, J.C. Jansen, Synthesis of thin defect-free hydroxy sodalite membranes: New candidate for activated water permeation, Journal of

Membrance Science, 299 (2007) 63-72.

[23] P. Cubillas, M.W. Anderson, Synthesis mechanism: crystal growth and nucleation, Zeolites and Catalysis: Synthesis, Reactions and Applications, (2010) 1-55.

[24] H. Lechert, P. Staelin, C. Kuntz, Quantitative relations of the batch composition and the Si/Al ratio in the poduct of zeolites, Zeolites, 16 (1996) 149-156.

[25] C. Kosanović, T.A. Jelić, J. Bronić, D. Kralj, B. Subotić, Chemically controlled particulate properties of zeolites: Towards the face-less particles of zeolite A. Part 1. Influence of the batch molar ratio $[SiO_2/Al_2O_3]_b$ on the size and shape of zeolite A crystals, Microporous and Mesoporous Materials, 137 (2011) 72-82.

[26] S. Mintova, V. Valtchev, Effect of the silica source on the formation of nanosized silicalite-1: an in situ dynamic light scattering study, Microporous and Mesoporous Materials, 55 (2002) 171-179.

[27] X. Li, H. Kita, H. Zhu, Z. Zhang, K. Tanaka, K. Okamoto, Influence of the hydrothermal synthetic parameters on the pervaporative separation performances of CHA-type zeolite membranes, Microporous and Mesoporous Materials, 143 (2011) 270-276.

[28] F.E.S. W. MEISE, Kinetic Studies on the Formation of Zeolite A, in: Molecular Sieves, Advances in Chemistry, Germany, 1973, pp. 169-178.

Chapter 3 Dehydration performance of sodalite membranes prepared by secondary growth method

3.1 Introduction

Zeolites are crystalline aluminosilicates with well-defined pores and channels of molecular size. Intensive research efforts have been made in the last decades to shape various kinds of zeolite in thin films. Zeolite membranes have been examined in separating liquid mixtures and gaseous mixtures, including water [1], CO_2/CH_4 [1, 2], NH_3/H_2 [3], isomer separations [1] and other separations [2]. Successful commercial application of zeolite membranes is reported with LTA-type and T-type zeolite membranes in dehydration [4].

One of the unique properties of zeolite is the variety of zeolitic pore size. Sodalite has one of the smallest zeolitic pore size of 0.28 nm [5], allowing only small molecules, such as water, helium and hydrogen, penetrate into. Accordingly, defect-free sodalite membranes are expected to show significantly high selectivity of small molecules. Several attempts have been made to prepare sodalite membranes [6, 7]. However, single gas permeations of helium and nitrogen through sodalite membranes followed Knudsen diffusion mechanism, suggesting a large contribution of inter-crystalline pathways [7]. Besides enhancing the inter-crystalline growth, removing adsorbed water from zeolitic pores may be a challenge.

Recently, hydroxyl sodalite membranes synthesized on surface-polished disks are reported to show dehydration performance when alcohol/water mixtures were applied at 303-473K and 1.6-2.4 MPa [8]. Membranes showed dehydration performance also in vapor permeation performed at 398-473K [9]. In these preparation procedures, seed crystals were not applied. The polished flat surface may facilitate a formation of oriented zeolite membrane, which enhanced the intergrowth of crystals. In this research, sodalite membranes were prepared by seed assisted method on non-polished tubular supports. Effects of the composition of synthesis solution, synthesis

temperature and crystallization time on the formation of sodalite membranes were studied. Membrane performance was evaluated in pervaporation with ethanol and iso-propanol solutions at 348K, 0.1 MPa. Influence of feed compositions was also examined.

3.2 Experimental

3.2.1 Raw materials

Porous α-alumina tubes (o.d. 12 mm, i.d. 9 mm and length 100 mm with a membrane area of 37.68 cm^2), with an average pore size of 1.25 μm and porosity of 35.20 %, were used as supports. The surface SEM image was shown in **Figure 3-1**. Colloidal silica (Ludox HS-40, Aldrich), alumina hydroxide ($Al(OH)_3$, 100%, Wako), sodium hydroxide (NaOH, 97%, Wako) and sodium chloride (NaCl, 99.99%, Wako) were used as silica source, alumina source, sodium source and chloride source, respectively. Distilled water was used as the solvent.

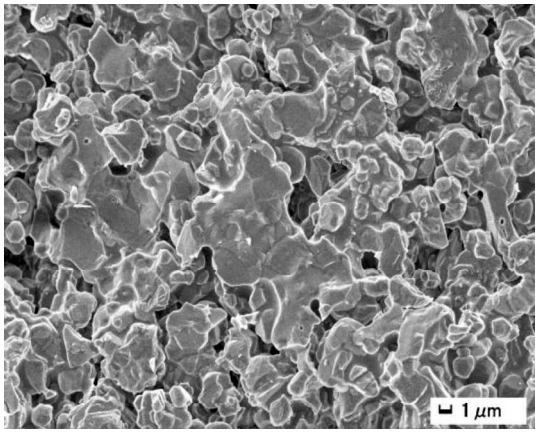

Figure 3-1 The SEM photograph of the alumina support (surface section)

3.2.2 Synthesis of sodalite seed crystals

The procedure of preparing sodalite crystals as seed has been described in detail in **Chapter 2**. It can be explained briefly as follows. In typical synthesis, $Al(OH)_3$, NaOH and the required distilled water were mixed and heated until the solution became apparent. After cooling the solution to room temperature, NaCl and Ludox

HS-40 colloidal silica were added sequentially and the resulting solution was stirred vigorously for 1 h. The final solution had a molar composition of 1.00 SiO_2: 0.50 Al_2O_3: 0.96 Na_2O: 0.65 NaCl: 20.50 H_2O. The solution was placed in a sealed autoclave with Teflon and treated hydrothermally at 473 K for 24 h in a conventional oven. After the particles were rinsed until neutral, the resultant precipitate was dried overnight at 353 K before use.

3.2.3 Preparation of sodalite membranes

Sodalite membranes were grown by secondary seeded growth. The synthesis gel for sodalite membranes had a molar ratio of 1.0 SiO_2: 0.50 Al_2O_3: 0.96 Na_2O: 0.65 NaCl: (30-500) H_2O. The tubes with 10 cm length were cleaned with distilled water and dried at 353 K over night before use. The reaction solution was prepared as follows. Initially, $Al(OH)_3$ was mixed with some water. While the mixture was being heated and stirred, NaOH was added. After the mixture became apparent and cooled to room temperature, the surplus water was supplemented. After several minutes, NaCl was added. Finally, silica source HS-40 was added cautiously, dropwise after NaCl was dissolved. The solution will be stirred for 24 h at room temperature. After aging, the reaction solution was transferred into a 300 ml autoclave. And then the outer side seeded supports were placed vertically into the autoclave. Secondary hydrothermal synthesis was carried out at 383~448 K for 4~20 h in a traditional oven which was preheated to the desired temperature. After crystallization, the membranes were racked from the cooled autoclave, and then washed with water thoroughly until the neutral and dried overnight at 353 K.

3.2.4 Characterization

X-ray diffraction (XRD, SHIMADZU XRD-6100) with Cu-$K\alpha$ radiation was used to identify the crystal structures of sodalite crystals and sodalite membranes. These spectra were scanned in the range of $2\theta = 5^o$-45^o at a scanning rate of 4^o/min. Scanning electron microscopy (FE-SEM, JEOL JSM 6335F) was used to observe the morphology and thickness of obtained samples.

3.2.5 Permeation performance

3.2.5.1 Pervaporation (PV)

The membrane performance was firstly determined by using it to dehydrate ethanol (EtOH)/water (H_2O) and isopropanol (IPA)/water (H_2O) mixtures at 348 K by pervaporation (PV). The schematic representation of the PV apparatus was shown in **Figure 3-2**. The seeded supports were directly immersed in the feed solution. The capacity of each permeation cell was about 140 mL and the effective area of the membranes was 23 cm^2. The permeated vapor was completely condensed in a trap placed in a Dewar Flask cooled to 77 K using liquid nitrogen. The compositions of feed and permeate solutions were analyzed by gas chromatography (GC, SHIMADZU GC-8A).

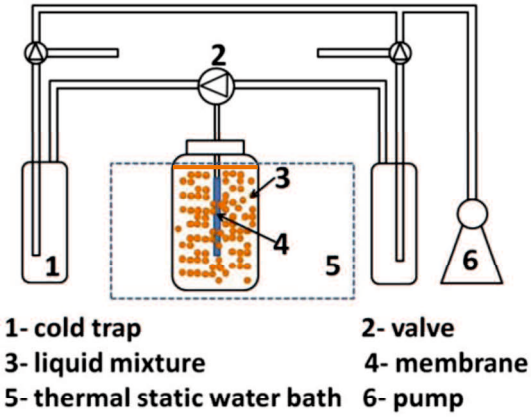

Figure 3-2 Schematic diagram of pervaporation.

The performance of a membrane in PV is characterized by permeation flux (J), selectivity (α) and permeance (P) calculated by the following equations:

$$J = Q/At \qquad (1)$$

where Q is the mass of permeate (g) collected during a time interval of t (h) and A is the effective membrane area in contact with the feed (m^2).

$$\alpha = (y_i/y_j)/(x_i/x_j) \qquad (2)$$

where y_i and y_j represent the weight fraction of water and alcohols in the permeate, and x_i and x_j represent those of water and organics in the feed, respectively.

$$P_{i(j)} = (10^3 \times Q)/(3600 \times M\Delta P) \quad (3)$$

where $P_{i(j)}$ is the permeance ($mol \cdot m^{-2} \cdot s^{-1} \cdot Pa^{-1}$) of component of *i* or *j*. Q is the same parameter in Eq. (1). M is the molar mass ($g \cdot mol^{-1}$) of the correspondence component. ΔP is the pressure difference (Pa) across the membrane.

3.2.5.2 Nanopermporometry

Adsorption-branch N_2/water nanopermporometry data were recorded for sodalite membranes at room temperature using the experimental set-up illustrated in **Figure 3-3**. A sodalite membrane was mounted in a stainless steel module and sealed with o-rings. The membrane was dried over night before the measurement. The pressure difference was adjusted to 30 kPa. The permeate side was kept at atmospheric pressure. N_2 gas and water vapor were fed to the membrane via two mass flow controllers. One of the N_2 streams was saturated with water vapor by bubbling through a water bath. The two N_2 streams were mixed to arrive at the required relative pressure. The total flow rate was measured by a flow meter. Increasing concentrations of water vapor was added to the feed and the N_2 permeance was continuously recorded using a digital flow meter. The basic principle of nanopermporometry is based on capillary condensation of vapor and the blocking effect of permeation of a non-condensable gas.[10]

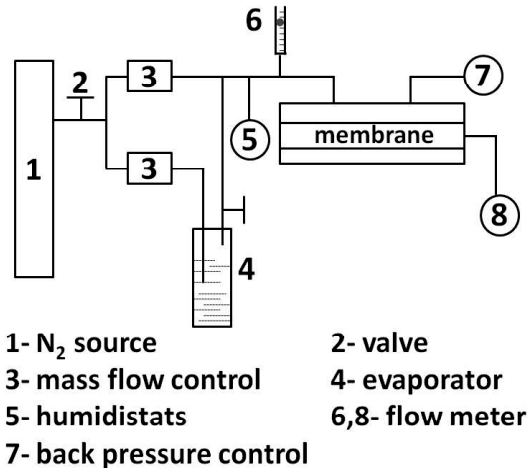

Figure 3-3 Schematic diagram of nanopermporometry.

In a capillary having a smaller pore size (radius *r*), vapor condenses at vapor pressure p lower than the saturated vapor pressure p_0. The capillary radius can be estimated by the water vapor pressure in the feed and under a standard saturated condition, using the well-known Kelvin equation:

$$RT \ln(p/p_0) = -2v\sigma\cos\theta/r \qquad (4)$$

where v, σ and θ are molar volume, surface tension and contact angle, respectively.

For the calculation of capillary condensation diameter based on Eq. (4), complete wetting, i.e. contact angle $\theta = 0$, was assumed irrespective of the types of vapors.

3.3 Results and discussion

3.3.1 Preparation of sodalite seed crystals

Formation of a uniform seed layer on the support surface is one of the keys in preparing defect-free zeolite membranes via seed-assisted method. Seed crystals should be in pure phase to avoid any contamination to the zeolite membrane, for impurity often causes defect formation. Synthesis conditions were optimized to form pure sodalite crystals in sub-micrometer size. **Figure 3-4 (a)** shows the morphology of the sodalite crystals used as seed in this study. The crystal size was in the range of 100 to 200 nm. XRD pattern of crystals is shown in **Figure 3-4 (b)**. Typical peaks at 2θ =14.16°, 24.65°, 31.99° and 35.13° associated with sodalite zeolite can be observed in this pattern. Impurities are not found from the XRD analysis.

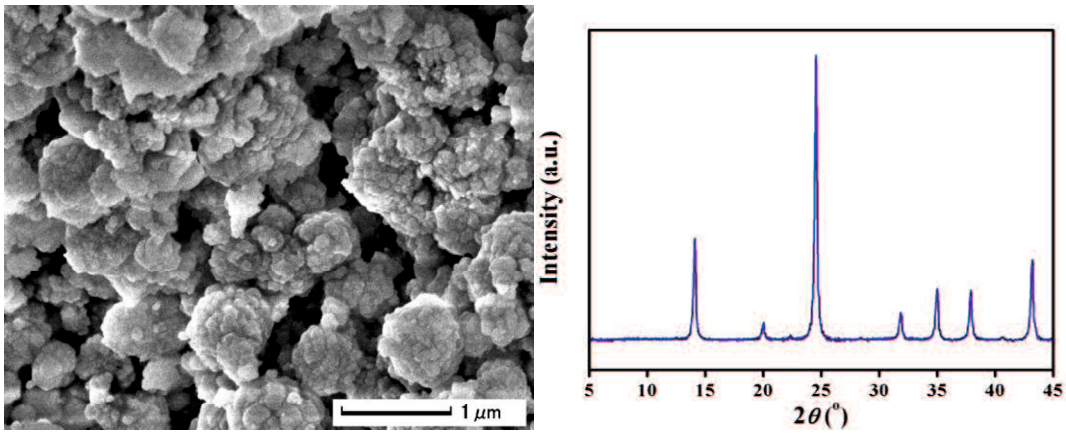

Figure 3-4 Sodalite powder used as seed: (a) SEM image and (b) XRD pattern

3.3.2 Influence of synthesis conditions on the formation of sodalite membranes

Membranes synthesized under the same conditions as the seed preparation conditions were consisted with loosely packed crystals and very fragile. Crystals formed in the synthesis solution seemed to be accumulated on the support. To reduce the contribution of crystals formed in the solution to the membrane formation, synthesis solutions with higher water contents were investigated.

Figure 3-5 shows the membrane morphologies prepared from solutions having composition of 1.0 SiO_2: 0.50 Al_2O_3: 0.96 Na_2O: 0.65 NaCl: x H_2O (x = 30, 50, 200 and 500). Hydrothermal conditions were fixed to 448K for 4 hours. Crystals at the surface of sodalite membrane became larger when water content in the solution was higher. However, many cracks were found when the synthesis solution was too dilute (x = 200 and 500). Some of the cracks were formed throughout the sodalite layer, as can be seen in **Figure 3-5 (h)**. The thickness of the sodalite membrane differed to the synthesis solution compositions. Membrane prepared from solution with water content of x = 50 had thickness of ca. 2-3 μm and other membranes had thickness of ca. 5 μm. As cracks were only found in the latter membranes, crack formation may be associated with the membrane thickness.

Influence of hydrothermal synthesis temperature and time on the membrane formation was examined by fixing the solution composition to x = 50. **Figure 3-6 (a)** shows the XRD patterns of membranes synthesized at different temperatures. The major peaks were corresponding to sodalite crystals [11] and to support for all the membranes. Contamination of LTA-type zeolite, having typical peak at $2\theta = 7.2^{o}$, was found when membranes were prepared at lower temperatures as 383 K and 403 K. LTA-type zeolite is a common impurity phase when preparing sodalite crystals, especially at lower temperature or shorter synthesis time [12]. On the contrary, impurities were not found when synthesis temperature was over 423 K.

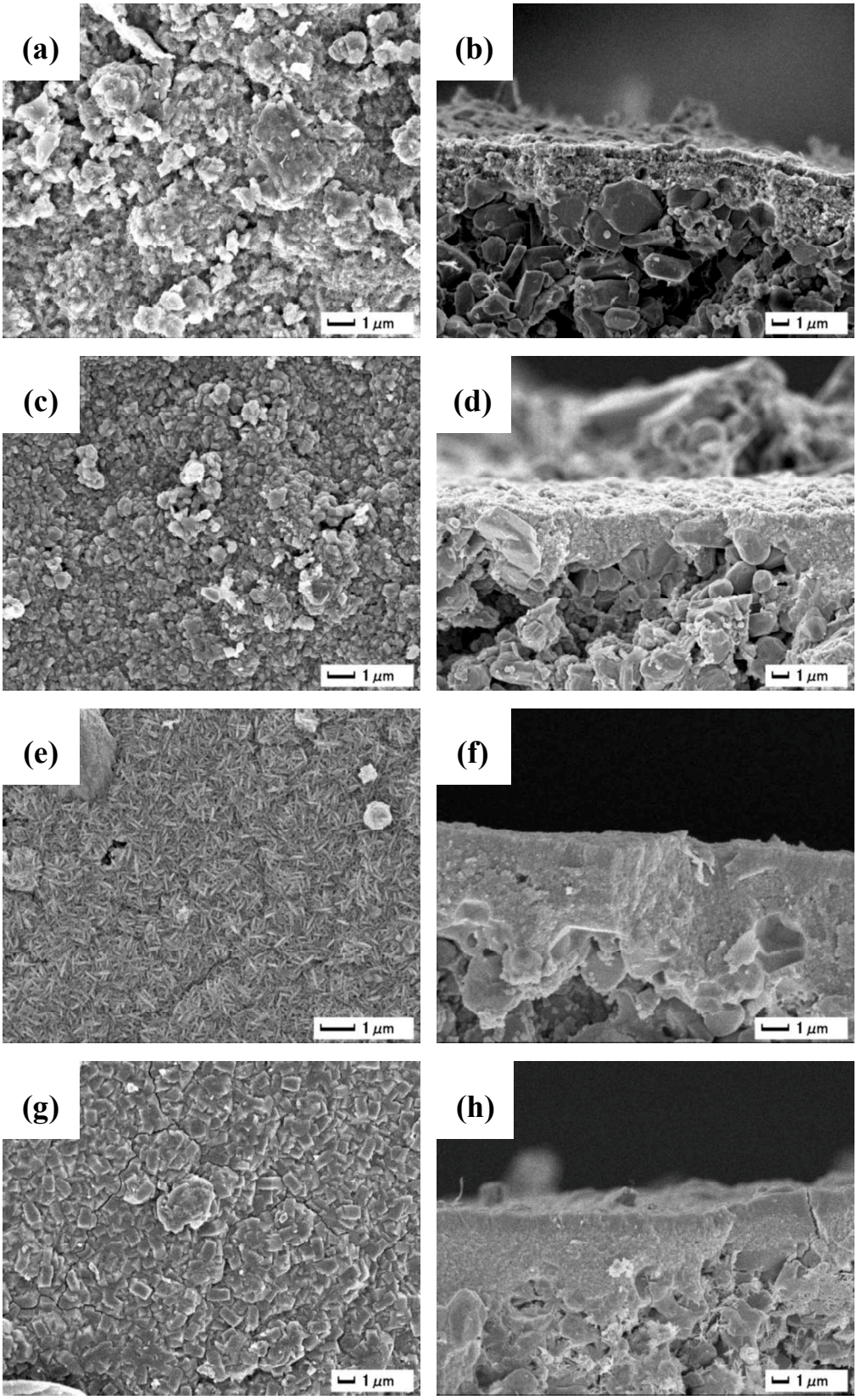

Figure 3-5 SEM images of membranes prepared from solutions having composition of SiO_2: 0.50 Al_2O_3: 0.96 Na_2O: 0.65 NaCl: xH_2O, x = (a-b) 30, (c-d) 50, (e-f) 200 and (g-h) 500. (Hydrothermal conditions were fixed to 450 K for 4 h.)

Figure 3-6 (b) shows the XRD patterns of membranes synthesized for different time at a fixed temperature of 448K. Peaks corresponding to sodalite phase were observed in all the membranes, however, impurities were found in membranes synthesized for 4 hours and 20 hours. Impurity in the membrane synthesized for 4 hours is P-type zeolite, having typical peaks at 2θ = 12.5°, 17.8° and 21.8°. P-type zeolite is another common impurities formed together with sodalite as reported by S. Khajavi et al. [12]. On the contrary, when the synthesis time was over 20 h, analcime (ANA)-type zeolite appeared that has typical peaks at15.81° and 30.54°. This may be an indication of transformation of sodalite to ANA phase.

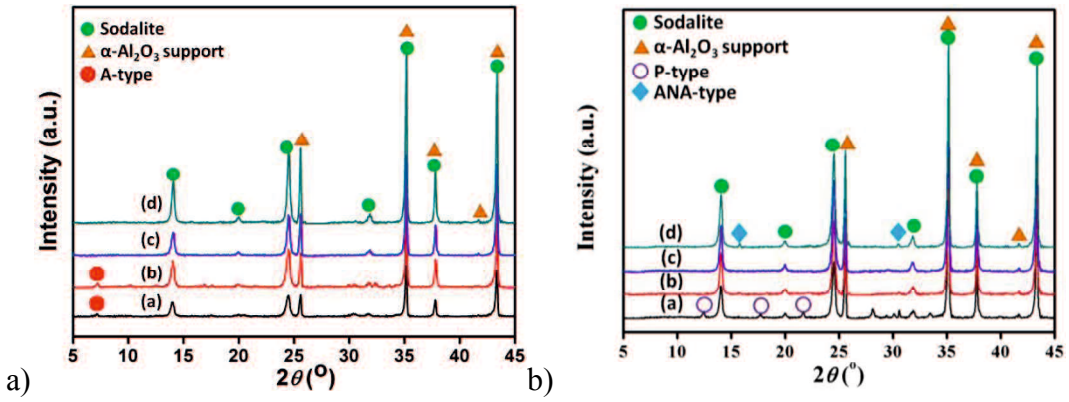

Figure 3-6 a) The XRD patterns of sodalite membranes prepared for 6 h at different temperatures: (a) 383 K, (b) 403 K, (c) 423 K, and (d) 448 K, respectively.
b) The XRD patterns of sodalite membranes prepared at 448 K for (a) 4 h, (b) 6 h, (c) 12 h and (d) 20 h

Figure 3-7 shows the SEM images of membranes prepared for different synthesis time at 383 K, 423 K and 448 K, respectively. The SEM images were taken with membranes after pervaporation tests. Supports were fully covered with crystals in all the cases. The findings showed that the morphology of the membranes was closely related to crystallization temperature. By comparison, the images clearly revealed that the surface morphology of pure sodalite membranes became smoother and the zeolite layer was more continuous when synthesis temperature increased. Moreover, the morphology of membrane (S-2) was dominated by the impurity of A-type crystal phase.

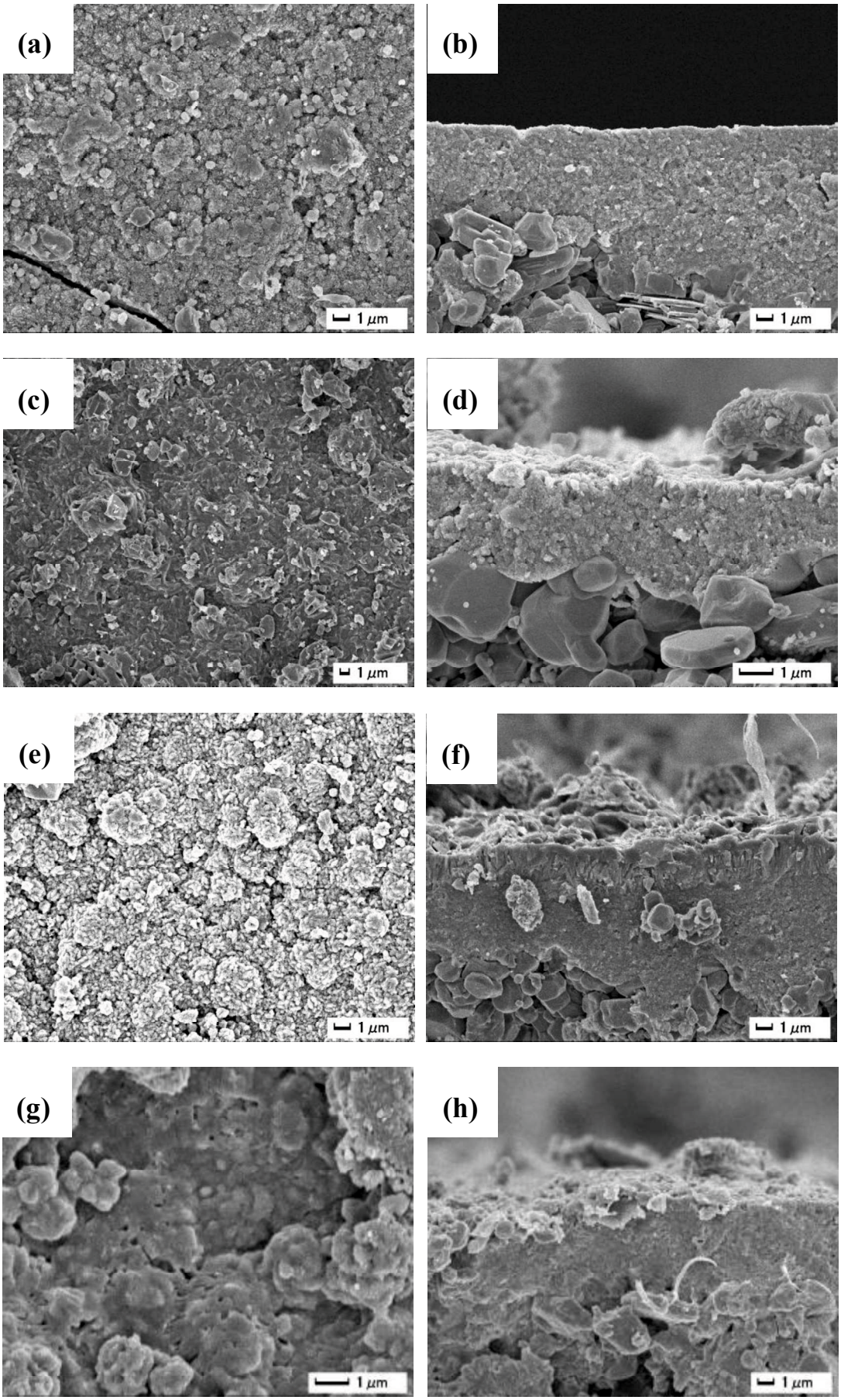
(a)
1 μm
(b)
1 μm
(c)
1 μm
(d)
1 μm
(e)
1 μm
(f)
1 μm
(g)
1 μm
(h)
1 μm

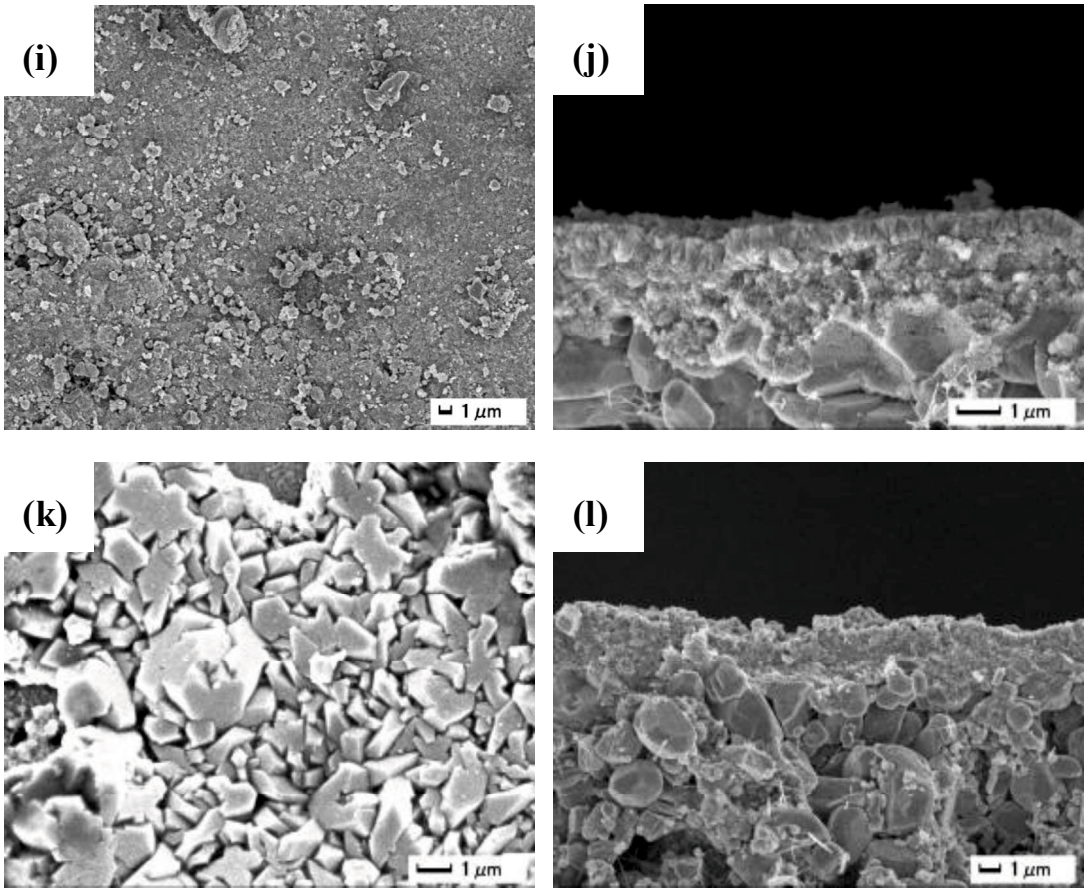

Figure 3-7 SEM images of membranes prepared (a-b) at 383 K for 6 h, (c-d) at 403 K for 6 h, (e-f) at 423 K for 6 h, (g-h) at 448 K for 6 h, (i-j) at 448 K for 12 h and (k-l) at 448 K for 20 h, respectively.

For membranes prepared at 448 K, continuous layers of ca. 1-5 μm were observed on the porous supports. Crystals at the surface of the membrane were inter-grown each other. The gap between crystals became smaller with prolonging the synthesis time from 6 hours to 12 hours. On the contrary, a drastic morphology change was observed after 20 hours of synthesis. The surface of the membrane was consisting of micron-meter sized crystals. Voids between crystals were clearly observed. The shape of crystals were similar to those reported for ANA zeolite [13], which existence was observed by XRD.

Table 3-1 Synthesis conditions and crystal phases of synthesized membranes.

No.	Synthesis condition		Crystal phase
	Temperature (K)	Time (h)	
S-1	383	6	SOD, A
S-2	403	6	SOD, A
S-3	423	6	SOD
S-4	448	4	SOD, P
S-5	448	6	SOD
S-6	448	12	SOD
S-7	448	20	SOD, ANA

Table 3-1 summarizes some of the results showing the influence of hydrothermal synthesis conditions on the zeolite phase. Higher synthesis temperature than 423K is required for the formation of pure sodalite membranes. As defects in zeolite membranes are expected to be reduced with the growth of crystals, prolonging the synthesis time is one way to improve the membrane selectivity. However, undesired zeolite phase started to appear in this study when the synthesis time was too long. Sodalite membranes with impurities observed by XRD were not applicable for PV tests due to large defects in the membranes. These results suggested the importance of forming sodalite membranes in pure phase.

3.3.3 Dehydration properties

Figure 3-8 shows the dehydration performance of a membrane synthesized at 448K for 12 hours. No other phase than sodalite was observed in the membrane by XRD analysis. Steady state of permeation was confirmed at each measurement by performing the test for more than 10 hours. Sodalite membrane showed water-selectivity with both water/EtOH and water/IPA mixture feeds. Selectivity was higher in water/IPA separation than in water/EtOH separation as observed in different zeolite membranes[14]. Flux was about one order smaller when compared with the flux through zeolite A membrane[14], which might be due to the smaller zeolitic pore size of sodalite than zeolite A. Permeation of alcohols suggests a contribution of non-zeolitic pore permeation.

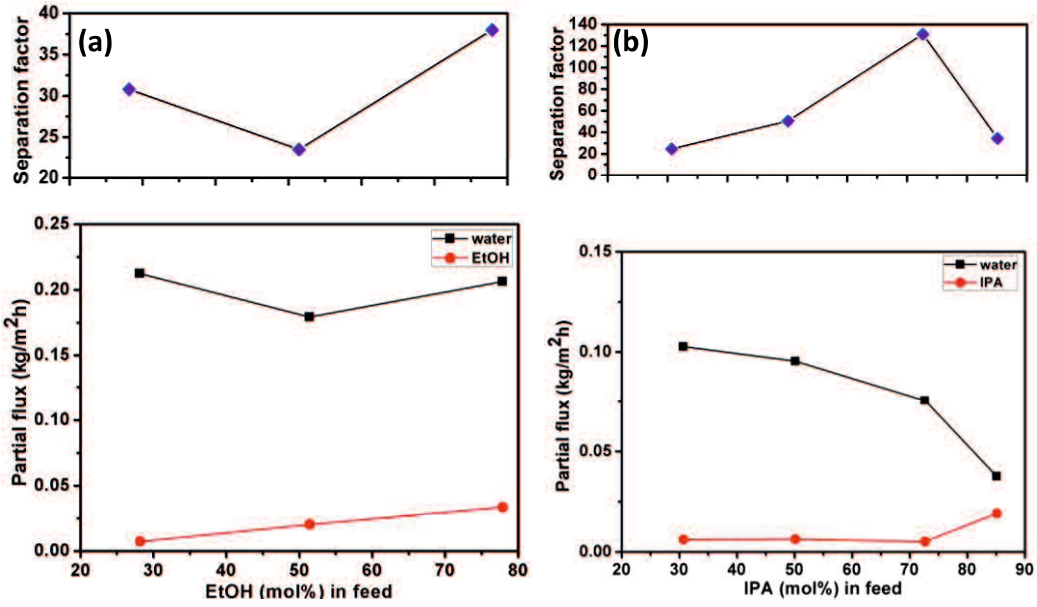

Figure 3-8 Separation factor and feed composition dependence of partial flux of each component for (a) EtOH/H_2O and (b) IPA/H_2O mixtures at 348 K.

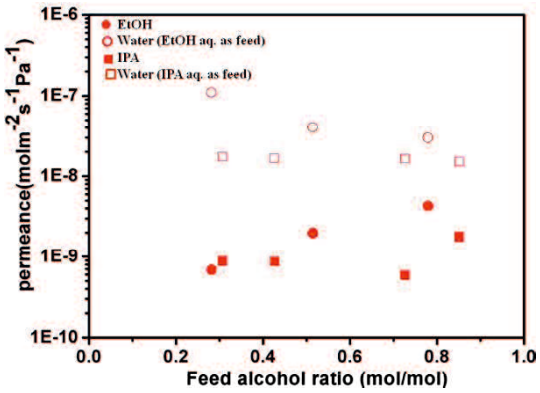

Figure 3-9 Feed composition dependence of water permeance in EtOH/H_2O and IPA/H_2O mixtures at 348 K.

Figure 3-9 shows the water permeance calculated according to Eq. (3). Permeance of water was about half in water/IPA separations than in water/EtOH separations. In both cases, permeance of water was constant to the feed composition in the concentration ranges studied. S. Khajavi et al. [8] reported different profiles of water flux by the type of alcohol in the feed solution; secondary-alcohol drastically hindered water flux through sodalite membranes when alcohol concentration was above 60-65 mol%. They presumed the cause as a different packing of molecules on

the surface of the membrane. Such differences in profile of water permeation by the type of co-existing alcohol were not observed in this study. Lower operation temperature applied in this study facilitates water adsorption and, thus, the different adsorption profiles of alcohol to the sodalite surface may not be relevant.

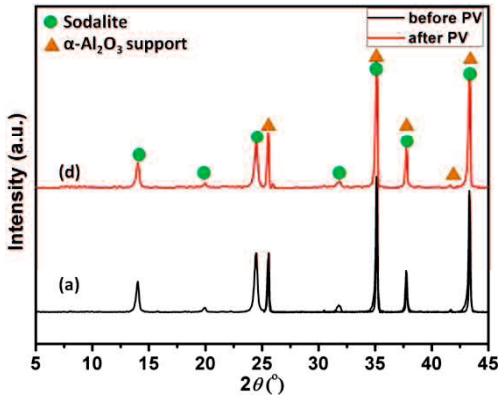

Figure 3-10 The XRD patterns of sodalite membrane prepared for 6 h at 448 K: (a) before pervaporation, (b) after pervaporation (I(110),14.16°/Isupport, 35.2°, before PV = 0.21, I(110), 14.16°/Isupport, 35.2°, after PV = 0.19)

Sodalite membranes showed stable separation performance in each PV test condition, measured for 10-20 hours. However, after several runs of PV test with washing and drying at 353K in between the measurements, membranes lost selectivity. Sodalite membrane prepared from longer synthesis time had better stability, but yet, defect formation was suspected after several tests. No other phases than sodalite and support alumina were observed by XRD after the membranes got damaged as shown in **Figure 3-10**. Peak intensity ratios between sodalite (2θ = 14.2°) and support (2θ = 35.1°) give an indication of the thickness of the sodalite layer. The values calculated from the XRD patterns obtained for the same membrane before and after PV test were 0.21 and 0.19, respectively. While no significant change was suggested by XRD analyses, larger defects than ca. 20 nm were observed by permporometry measurement using water and nitrogen in the membrane after PV tests. Small amount of solution may have remained in between crystals and triggered defects formation. Synthesis conditions and micro-structure of the sodalite membrane requires further investigations to improve the membrane property and stability.

3.4 Conclusions

Sodalite membranes were synthesized by the secondary growth method on α-Al_2O_3 tubular supports. Zeolite A was contaminated into sodalite when the synthesis temperature was lower than 403K. Pure sodalite phase can be obtained at higher temperature than 423K, however, too short or too long synthesis time resulted in a formation of undesired phase. Sodalite membranes having impurities had large defects, suggesting the importance of forming sodalite membranes without any contamination. Sodalite membranes, without impurities, showed water selectivity in water/EtOH and water/IPA mixtures with different alcohol concentrations at 348 K.

References

[1] H. Kita, K. Horii, Y. Ohtoshi, K. Tanaka, K. Okamoto, Synthesis of a zeolite NaA membrane for pervaporation of water/organic liquid mixtures, Journal of Materials Science Letters, 14 (1995) 206-208.

[2] K. Kusakabe, T. Kuroda, A. Murata, S. Morooka, Formation of a Y-type zeolite membrane on a porous α-alumina tube for gas separation, Industrial and Engineering Chemistry Research, 36 (1997) 649-655.

[3] O. Camus, S. Perera, B. Crittenden, Y.C. van Delft, D.F. Meyer, P. PAC Pex, I. Kumakiri, S. Miachon, J.A. Dalmon, S. Tennison, Ceramic membranes for ammonia recovery, AIChE Journal, 52 (2006) 2055-2065.

[4] K. Sato, K. Aoki, K. Sugimoto, K. Izumi, S. Inoue, J. Saito, S. Ikeda, T. Nakane, Dehydrating performance of commercial LTA zeolite membranes and application to fuel grade bio-ethanol production by hybrid distillation/vapor permeation process, Microporous and Mesoporous Materials, 115 (2008) 184-188.

[5] M.S. Nabavi, T. Mohammadi, M. Kazemimoghadam, Hydrothermal synthesis of hydroxy sodalite zeolite membrane: Separation of H_2/CH_4, Ceramics International, 40 (2014) 5889-5896.

[6] A. Julbe, J. Motuzas, F. Cazevielle, G. Volle, C. Guizard, Synthesis of sodalite/α-Al_2O_3 composite membranes by microwave heating, Separation and Purification Technology, 32 (2003) 139-149.

[7] A. Van Niekerk, J. Zah, J.C. Breytenbach, H.M. Krieg, Direct crystallisation of a hydroxy sodalite membrane without seeding using a conventional oven, Journal of Membrance Science, 300 (2007) 156-164.

[8] S. Khajavi, J.C. Jansen, F. Kapteijn, Application of hydroxy sodalite films as novel water selective membranes, Journal of Membrance Science, 326 (2009) 153-160.

[9] N. Wang, Y. Liu, A. Huang, J. Caro, Hydrophilic SOD and LTA membranes for membrane-supported methanol, dimethylether and dimethylcarbonate synthesis, Microporous and Mesoporous Materials, 207 (2015) 33-38.

[10] T. Tsuru, T. Hino, T. Yoshioka, M. Asaeda, Permporometry characterization of

microporous ceramic membranes, Journal of Membrance Science, 186 (2001) 257-265.

[11] N. Wang, Y. Liu, A. Huang, J. Caro, Supported SOD membrane with steam selectivity by a two-step repeated hydrothermal synthesis, Microporous and Mesoporous Materials, 192 (2014) 8-13.

[12] S. Khajavi, F. Kapteijn, J.C. Jansen, Synthesis of thin defect-free hydroxy sodalite membranes: New candidate for activated water permeation, Journal of Membrance Science, 299 (2007) 63-72.

[13] M. Tatlier, K. Barış Cigizoglu, B. Tokay, A. Erdem-Şenatalar, Microwave vs. conventional synthesis of analcime from clear solutions, Journal of Crystal Growth, 306 (2007) 146-151.

[14] Y. Morigami, M. Kondo, J. Abe, H. Kita, K. Okamoto, The first large-scale pervaporation plant using tubular-type module with zeolite NaA membrane, Separation and Purification Technology, 25 (2001) 251-260.

Chapter 4 Preparation of zeolite T membranes by a two-step temperature process for CO_2 separation

4.1 Introduction

Carbon dioxide, one of the major greenhouse gases, has become an important global concern over past decades due to the significant and continuous rise in atmospheric CO_2 concentrations, thus leading to global warming [1, 2]. Therefore, controlling and minimizing CO_2 emissions and separation and capture of CO_2 in industry are of great interest from the perspectives of global warming and energy production and conservation [3, 4].

Currently, polymeric membranes are widely developed in the application of CO_2 separation due to their relatively high CO_2 separation performance, relatively low cost, and large-scale production. However, they also have disadvantages of severe decomposition, lower selectivity at high temperatures, and a limitation of Robeson's upper bound, which will cause negative reliability in the large-scale application of polymeric membrane-based separation processes [3, 5, 6].

Zeolite T membrane has been developed as a novel membrane material for CO_2 separation for the past decade [7, 8]. The effective pore size of zeolite T for permeation is 0.36 nm × 0.51 nm [9]. Therefore, N_2 and CH_4 gas molecules with of 0.364 and 0.38 nm, respectively, could hardly penetrate through the dense layer of zeolite T crystals. However, CO_2 gas molecules with a smaller kinetic diameter of 0.33 nm may permeate through the zeolite T membrane without difficulty. Thus, the selective membrane covered with well-intergrown zeolite T crystals is especially advantageous in removing CO_2 from gas mixtures due to molecular sieving and competitive adsorption [10]. Therefore, it has great potential application in the permselective separation of CO_2 from CH_4 and N_2 through zeolite T membranes [7].

A two-step varying-temperature synthesis procedure, which involves a rapid change in temperature at some point during the crystallization process, was intensively reported to silicalite-1 and ZSM-5 zeolites, and MFI-type zeolite

membranes [11-13]. Recently, we prepared zeolite T membranes using a clear aluminosilicate solution or a fluoride media and the two-step method [14, 15]. These membranes showed high selectivity for water/organic mixture separation by pervaporation and high reproducibility. Two-step method leads to shortened crystallization time and improved membrane density. But there are no any investigations on the gas separation properties such as CO_2 separation performance through zeolite T membranes in our previous work. Also, there are few reports on detailed investigations for the relationship among synthesis conditions of zeolite T membrane growth and CO_2 separation performance in the literature.

Herein, thin and well-intergrown zeolite T membranes with high permeation performance for CO_2 separation were successfully prepared with the two-step varying-temperature hydrothermal process. The influence of synthesis parameters such as synthesis temperature, crystallization time on membrane growth and CO_2 separation performance of zeolite T membranes were investigated systematically. The formation mechanism of zeolite T membranes during the two-step method was also discussed. The as-synthesized membranes displayed high permeation properties from CO_2/CH_4 and CO_2/N_2 mixtures.

4.2 Experimental

4.2.1 Membrane synthesis.

Porous α-Al_2O_3 tubes (Nikkato Corp.) 100 mm in length were used as membrane supports, which had an outer diameter of 12 mm, a thick wall of 1 mm, an average pore size of 1.3 μm, and a porosity of about 40%. These tubes were polished with SiC sandpaper, washed with deionized water in an ultrasonic bath for 30 min, and then dried in an oven at 373 K overnight. Before hydrothermal treatments, the support tubes were rub-coated with homemade nanometer sized (about 100 nm) zeolite T powder and were dried. Zeolite T powders were prepared with a molar composition of SiO_2: Al_2O_3: Na_2O: K_2O: H_2O: $(TMA)_2O$ = 1: 0.055 :0.075: 0.025: 11.6: 0.25 at 358 K for 120 h in an oil bath.

The detailed preparation procedure of nanosized seeds and seeded support were described previously [14]. The aluminosilicate gel was prepared by mixing colloidal silica (TM-40, 40 wt % SiO_2 suspension in water, Aldrich), $Al(OH)_3$ (Wako Pure Chemical), NaOH (Aldrich), KOH (Aldrich), NaF (Aldrich), and de-ionized water under vigorous stirring at room temperature for 24 h. The molar composition of the resulting synthesis gel was SiO_2: Al_2O_3: (Na_2O +K_2O): NaF: H_2O = 1: 0.05: 0.35: 0.50: 30 (n(Na)/n(K) = 3/1). Then, the seeded support tubes were vertically placed in a stainless steel autoclave filled with the above synthesis solution for membrane preparation.

One-step constant-temperature synthesis method (one-step method)

After sealing the autoclave, the autoclave was kept in an oven at a constant temperature of 353 K (or 423 K) for different periods of time.

Two-step varying-temperature synthesis method (two-step method)

After sealing the autoclave, the autoclave was kept in an oven and preheated to 353 K (or 473 K) for specific hours (denoted as "the first-step"), followed by quickly moving into another oven preheated to 398-448 K for crystal growth (denoted as "the second step"). By finishing the synthesis process, the as-synthesized membrane samples were taken out and washed thoroughly with hot deionized water (~333 K) for 2 h to remove excess materials, and then dried at 373 K overnight.

4.2.2 Gas permeation measurements.

The gas permeation through the zeolite T membrane was evaluated in a membrane permeation system as shown in **Figure 4-1**. The membrane was mounted in a stainless-steel membrane module and sealed with silicone Orings on both ends. Feed gases flowed to the outside of the tubular membrane (retentate side), and the permeated gases were collected on the inside of the tubular membrane (permeate side). Mass flow controllers (MFC) were used to mix pure CO_2, CH_4, and N_2 gases. Hydrogen gas was used as the sweep gas on the permeate side. Gas permeating through the membrane was led into a MFC detector and an online gas chromatograph

(GC7100, equipped with a thermal conductivity detector, hydrogen gas as carrier gas) to determine the flow rate and component of permeated gases, respectively. The pressure in the retentate side was controlled by a back pressure regulator, while that of the permeate side was kept at an ambient atmosphere. The effective permeation area of the membrane was 18.8 cm^2. The operation measurements of mixed-gas permeation were conducted with equal molar binary gaseous mixtures (CO_2/CH_4 or CO_2/N_2, 50/50 mol %) with a total feed flow rate of 300 ml/min and H_2 sweep gas of 400 ml/min under a pressure gradient of 0.1 MPa at 308 K. The gas permeation performance of the membrane was evaluated in terms of permeance and selectivity. The permeance is related to the transport flux by the driving force across a membrane. The selectivity is defined as the ratio of the compositions of components A and B in the permeate side relative to the composition ratio of these components in the retentate side. The permeance and selectivity were calculated from the following equations, respectively:

$$Q = N/\Delta PSt \quad (1)$$

$$\alpha\ (A/B) = (Y_A/Y_B)/(X_A/X_B) \quad (2)$$

where N is the molar amount of the permeate gas (mol) over a period of time (t, s); ΔP is the partial pressure difference of the permeate gas (Pa); S is the effective membrane area for permeation (m^2); and X_A, X_B, Y_A, and Y_B are the mole fractions of each component in the retentate and permeate sides, respectively.

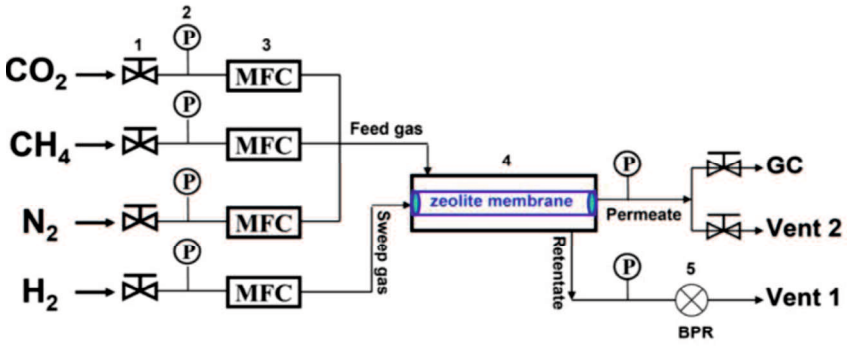

Figure 4-1 Scheme of membrane permeation system for gas separation experiments. (1. valve; 2. pressure gauge; 3. mass flow controller; 4. membrane module; 5. back pressure regulator)

4.2.3 Characterization

The crystal structure of zeolite seeds and as-synthesized membranes were characterized by X-ray diffraction (XRD, Ultima IV, Rigaku) with Cu Kα radiation at 40 kV and 40 mA. The morphology and thickness of zeolite membranes were observed using a scanning electron microscope (SEM, VEGA3 SBU, Tescan), equipped with an energy dispersive X-ray analyzer (EDX, Hitachi S-3400N) for composition analysis (e.g., Si/Al ratio) of the zeolite membranes.

4.3 Results and discussion

4.3.1 Effects of crystallization temperature and time during the one-step method.

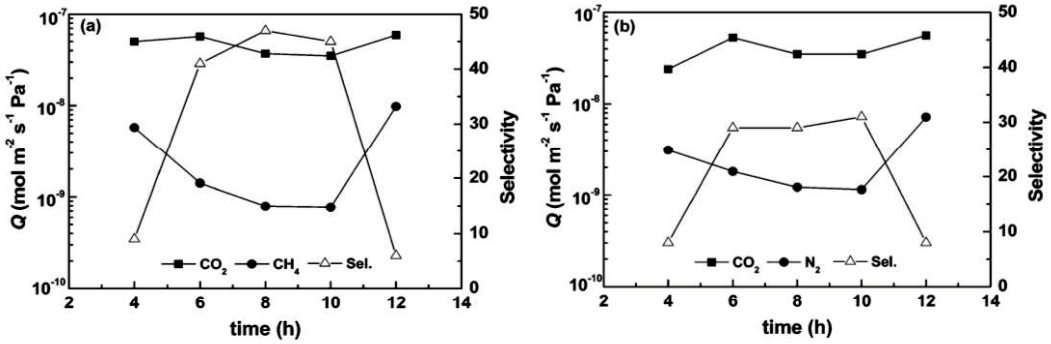

Figure 4-2 Effect of crystallization time on the CO_2 separation performance of zeolite T membranes prepared at 423 K by the one step method.

Figure 4-2 shows the effect of crystallization time on the CO_2 separation performance of zeolite T membranes prepared at 423 K with a one-step method.

As shown in **Figure 4-2(a)**, for CO_2/CH_4 mixtures, the CO_2 permeance fluctuated slightly with the increasing crystallization time, which ranged from 3.5×10^{-8} $mol\cdot m^{-2}\cdot s^{-1}\cdot Pa^{-1}$ to 5.9×10^{-8} $mol\cdot m^{-2}\cdot s^{-1}\cdot Pa^{-1}$. However, the CH_4 permeance first rapidly decreased with synthesis time until 10 h, then increased sharply when the synthesis time was further increased, showing a maximum value of 9.8×10^{-9} $mol\cdot m^{-2}\cdot s^{-1}\cdot Pa^{-1}$at 12 h. Thus, the membranes prepared for 6-10 h at 423 K displayed good permselectivity ranged from 41 to 47 for CO_2/ CH_4 mixtures. Similar trends as

shown in **Figure 4-2(a)** appeared in the results, as represented in **Figure 4-2(b)** for CO_2/N_2 mixtures.

In addition, it should be noted that the membrane prepared for 12 h exhibited higher CH_4 or N_2 permeance and lower CO_2 permselectivity of 6-8 in both CO_2/CH_4 and CO_2/N_2 mixtures tests. Normally, zeolite membranes would grow more continuous and denser with the increasing crystallization time, thus showing good permselectivity. However, as shown in **Figure 4-3**, the surface of this membrane prepared for 12 h was covered with randomly oriented rod-like zeolite T crystals, while their packing like small floccules about 20 μm in thickness was rather loose. Therefore, it showed lower CO_2 separation performance. The effect of crystallization time on CO_2 separation performance of zeolite T membranes prepared at 353 K by the one-step method was also investigated.

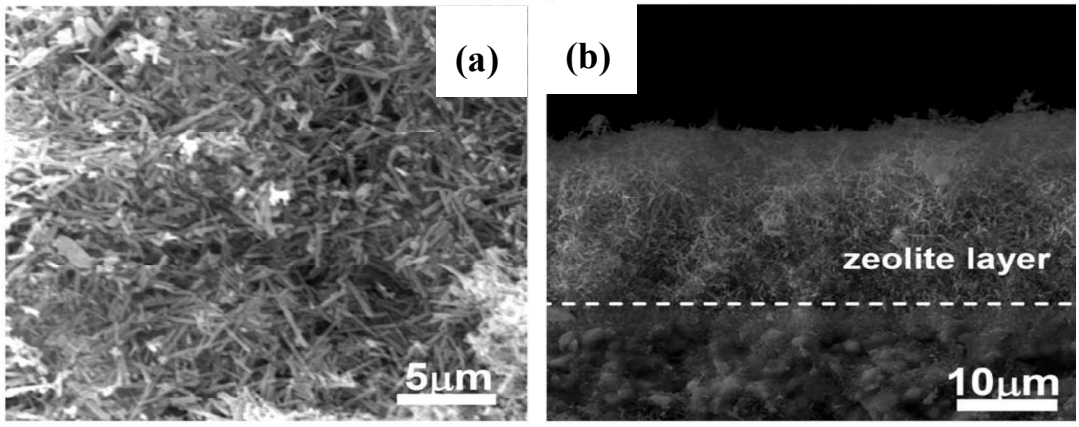

Figure 4-3 SEM images of zeolite T membrane synthesized at 423 K for 12 h with the one-step method: top view (a) and cross-sectional view (b).

As seen in **Figure 4-4**, for both CO_2/CH_4 and CO_2/N_2 mixture systems, all the gas permeances of CO_2, CH_4, and N_2 for these membranes nearly remained constant, and the CO_2 permselectivity was about 10 with the increasing synthesis time, even though the membrane was a prolonged crystallization of 96 h.

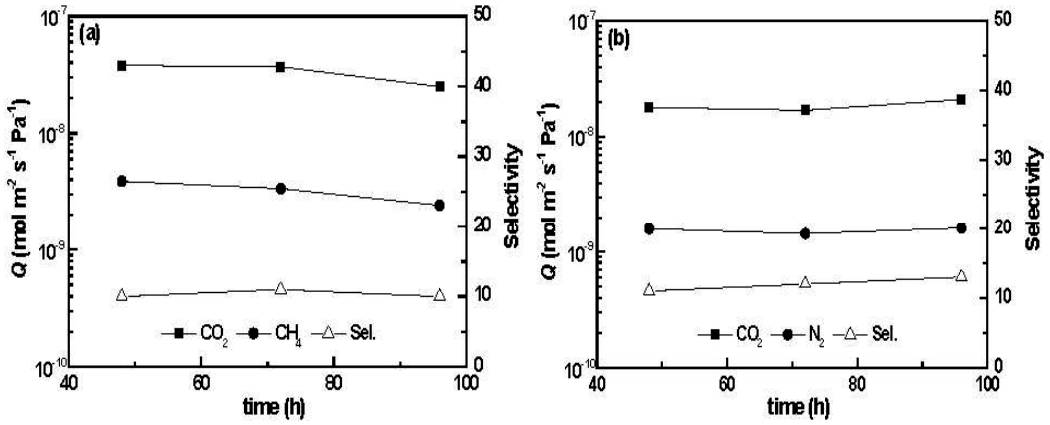

Figure 4-4 Effect of crystallization time on the CO_2 separation performance of zeolite T membranes prepared at 353 K with the one-step method.

Figures 4-5 and Figure 4-6 show the SEM images and XRD patterns for the zeolite membranes synthesized at 423 K for 8 h and at 353 K for 96 h, respectively. As illustrated in Figures 4-5, it can be seen that all the seeded support was fully covered with zeolite T crystals with random intergrowth. For the membrane prepared at 423 K for 8 h, the rod-like crystals with the a particle size over 5 μm were grown on the outer surface of the support (**Figures 4-5(a)**), which would influence the CO_2 separation performance. And the top thickness of randomly oriented crystal layers was approximately 3 μm (**Figures 4-5(b)**). However, it was seen that the support surface was covered with smaller ricelike zeolite T particles of less than 1 μm in diameter (**Figures 4-5(c)**), and a zeolite layer as thin as 1.5-2 μm was observed for the membrane prepared at 353 K for 96 h (**Figures 4-5(d)**). Compared with the membrane prepared at 423 K for 8 h, as seen in **Figures 4-6**, the membrane prepared at 353 K displayed weaker characteristic peaks of T-type zeolite while showing the stronger typical peaks of Al_2O_3 support. The XRD results were consistent with the surface images of zeolite T layers (**Figures 4-5**) and CO_2 separation performance, indicating that the nuclei grew rapidly to form larger zeolite crystals at higher crystallization temperatures [11, 16]. The above results suggested that the synthesis temperature or crystallization time is one of the most important variable factors, which strongly affects the membrane growth and CO_2 separation performance.

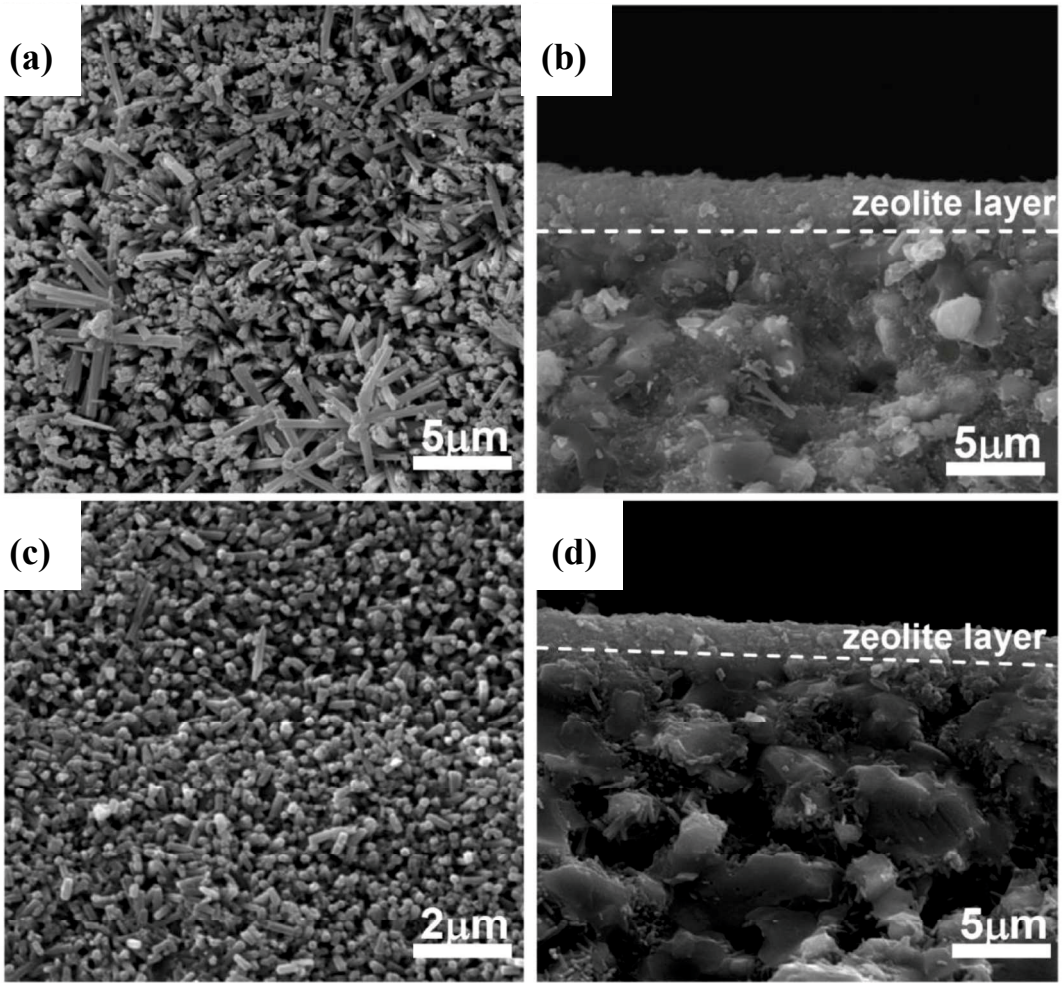

Figure 4-5 SEM images of zeolite T membranes synthesized at 423 K for 8 h (a, b) and at 353 K for 96 h (c, d) with the one-step method.

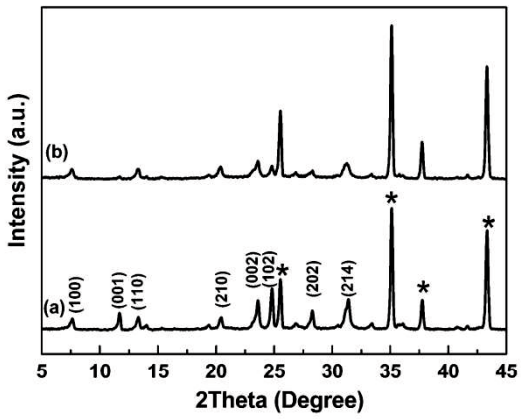

Figure 4-6 XRD patterns of zeolite T membranes synthesized at 423 K for 8 h (a) and at 353 K for 96 h (b) with the one-step method. Asterisk represents the patterns of α-Al_2O_3 support

4.3.2 Effects of synthesis temperature and crystallization time for each step during the two-step method

Table 4-1 Permeation properties of as-synthesized zeolite T membranes with the two-step method

No.	First step		Second step		Permeance ($mol \cdot m^{-2} \cdot s^{-1} \cdot Pa^{-1}$)		α	Permeance ($mol \cdot m^{-2} \cdot s^{-1} \cdot Pa^{-1}$)		α
	T (K)	t (h)	T (K)	t (h)	CO_2 ($\times 10^8$)	CH_4 ($\times 10^{10}$)	(CO_2/CH_4)	CO_2 ($\times 10^8$)	N_2 ($\times 10^{10}$)	(CO_2/N_2)
T1	353	4	398	14	2.1	9.2	23	1.8	11.3	16
T2	353	4	398	18	2.4	17.0	14	1.9	15	13
T3	353	4	423	8	6.2	7.8	80	5.9	13.7	43
T4	353	4	423	10	2.3	5.9	39	2.4	10.1	24
T5	353	4	448	3	4.2	10.3	41	3.8	13.2	29
T6	353	4	448	4	3.8	20.0	19	3.3	20.0	17
T7	473	1	423	8	5.2	309.0	2	4.6	261.0	2
T8	473	2	423	8	5.1	383.0	1	4.7	312.0	2

In order to investigate the effects of crystallization temperature and synthesis time for each step during the two step method, two series of zeolite T membranes were synthesized. One is to investigate the effect of synthesis time of the first step at a low temperature of 353 K on the membrane crystallization and separation performance by keeping the second step at 423 K for 4 h. The other is to explore the effects of crystallization temperature and time of the second step at a higher temperature of 398-448 K on the membrane crystallization and permeation performance by keeping the first step at 353 K for 4 h (see **Table 4-1**). It may provide valuable insights into the nucleation and crystallization stages during the two-step method and obtain the best membranes with high CO_2 permeance and permselectivity under the optimized synthesis conditions.

4.3.2.1 Effect of crystallization time for the first step.

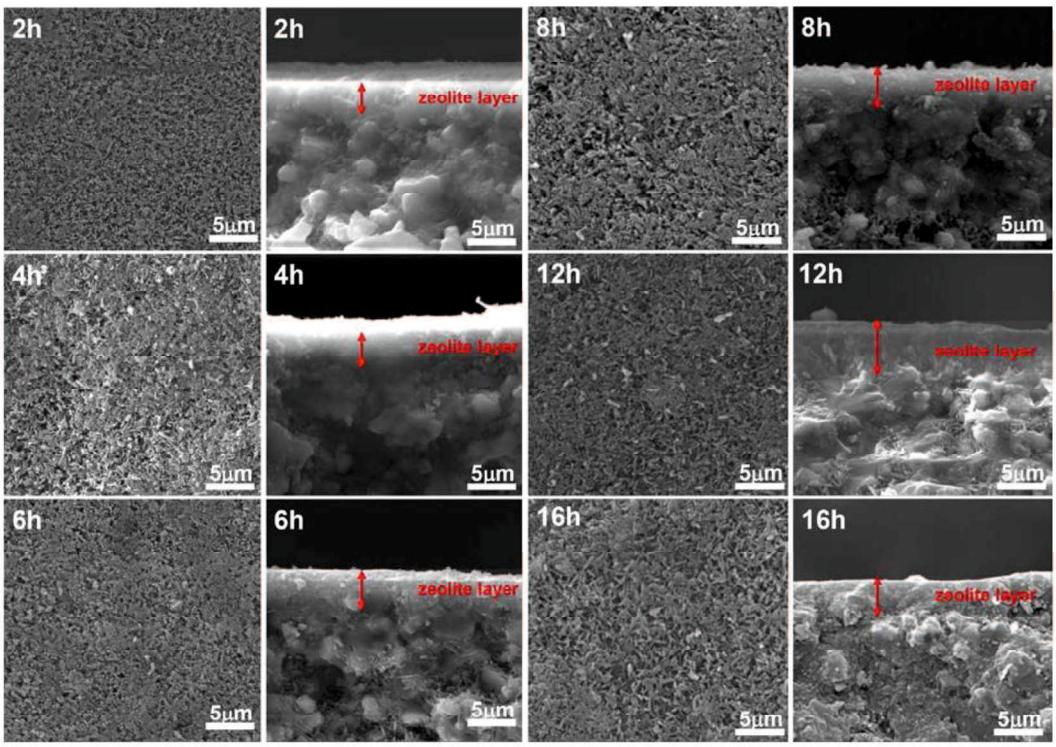

Figure 4-7 SEM images of as-synthesized membranes prepared at the first step of 353 K for different crystallization time with the two-step method (the second step at 423 K for 4 h).

Figure 4-7 shows the surface and cross-sectional SEM views of as-synthesized zeolite membranes prepared over a crystallization time from 2 to 16 h at a first step of 353 K with the two-step method. After thermal treatment at 353 K for a certain duration and subsequent synthesis at 423 K for 4 h during the two-step method, as seen in **Figure 4-7**, all the as-synthesized membranes were covered with randomly oriented small zeolite T crystals with a size less than 1 μm. The thickness of the top crystal layers increased from about 3.5 to 6 μm on increasing the first-step time from 2 to 16 h. And few zeolite T crystals were grown inside the supports after 8 h. It can be found that the XRD patterns of these zeolite membranes (**Figure 4-8**) were consistent with the strong characteristic peaks of the α-Al_2O_3 tube together with those of the zeolite T crystals, confirming that the outer surface of the mullite support was not fully covered by the zeolite layers. The relative intensity of the main characteristic

peaks of zeolite T (2θ = 7.7°, 13.3°, 20.4°, 23.6°, 24.8°, 28.3°, and 31.4°) increased greatly under the synthesis time of the first step.

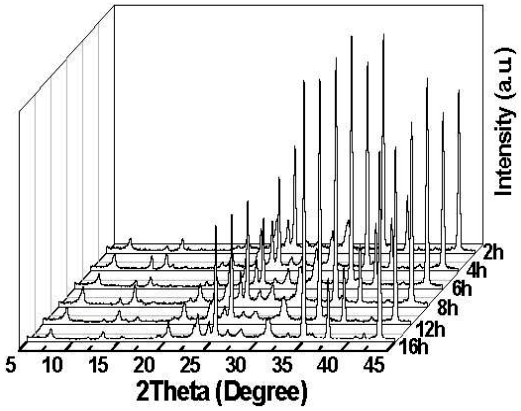

Figure 4-8 XRD patterns of as-synthesized membranes prepared at the first step of 353 K for different crystallization time with the two-step method (the second step at 423 K for 4 h).

Figure 4-9 shows the CO_2 separation performance of these membranes. It indicates that the gas permeance mostly decreased with the increasing crystallization time of the first step; especially CH_4 permeance (**Figure 4-9**) decreased drastically from 2.0×10^{-9} mol· $m^{-2}\cdot s^{-1}\cdot Pa^{-1}$ to 3.0×10^{-10} mol· $m^{-2}\cdot s^{-1}\cdot Pa^{-1}$ in this work. Generally, the membrane grows thicker, and the gas-tightness of the membrane becomes denser, thus depressing the permeance of non-adsorbing gas. For further treatment, the permselectivity increased and the permeation flux of the membrane decreased, maybe because of increasing the membrane thickness and density. The drastic decreasing permeance of gaseous mixtures shown in **Figure 4-9** is consistent with the previous observations of SEM images and XRD spectra (**Figures 4-7** and **Figure 4-8**). The selectivity of CO_2/CH_4 and CO_2/N_2 first increased with the first-step synthesis time, and then decreased sharply when synthesis time further increased to 16 h, resulting in a higher value of selectivity obtained at 4 h for the first step. Moreover, the CO_2 separation performance during the CO_2/ CH_4 mixture system was obviously higher than that of the CO_2/N_2 mixtures test, which was consistent with that of previous reports [7, 8]. On the basis of above considerations, the more effective crystallization time of the first step seems be 4 h at 353 K.

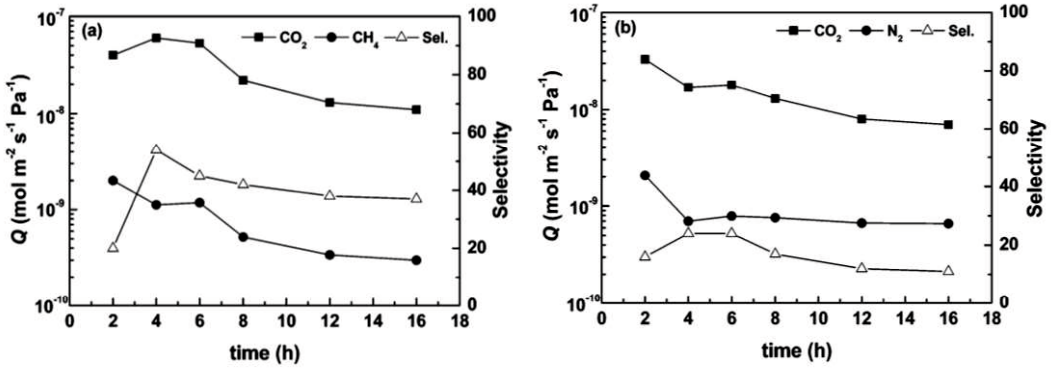

Figure 4-9 Effect of crystallization time of the first step at 353 K with the two-step method on the CO_2 separation performance (the second step at 423 K for 4 h).

4.3.2.2 Effect of synthesis temperature and crystallization time for the second step.

Table 4-1 shows the permeation performance of zeolite T membranes prepared in the second step with different synthesis temperatures from 398 to 448 K by keeping the first step at 353 K for 4 h. As seen in **Table 4-1**, the membranes T1 and T2 prepared with the second step at 398 K for 14-18 h displayed a lower CO_2 permeance of 1.8×10^{-8} mol·m^{-2}·s^{-1}·Pa^{-1} to 2.4×10^{-8} mol·m^{-2}·s^{-1}·Pa^{-1} and a poorer CO_2 selectivity of about 13-23, respectively.

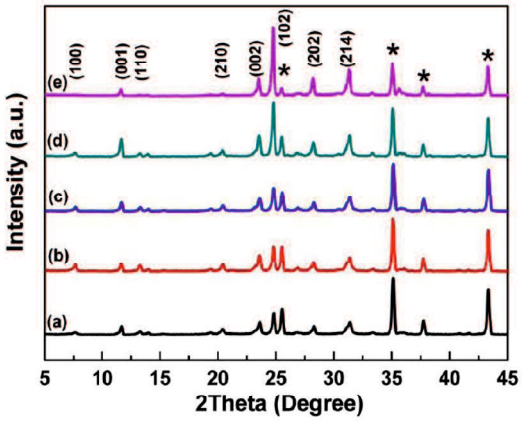

Figure 4-10 XRD patterns of as-synthesized membranes: T1 (a), T3 (b), T5 (c), T7 (d), and T8 (e). Asterisk represents the patterns of α-Al_2O_3 support

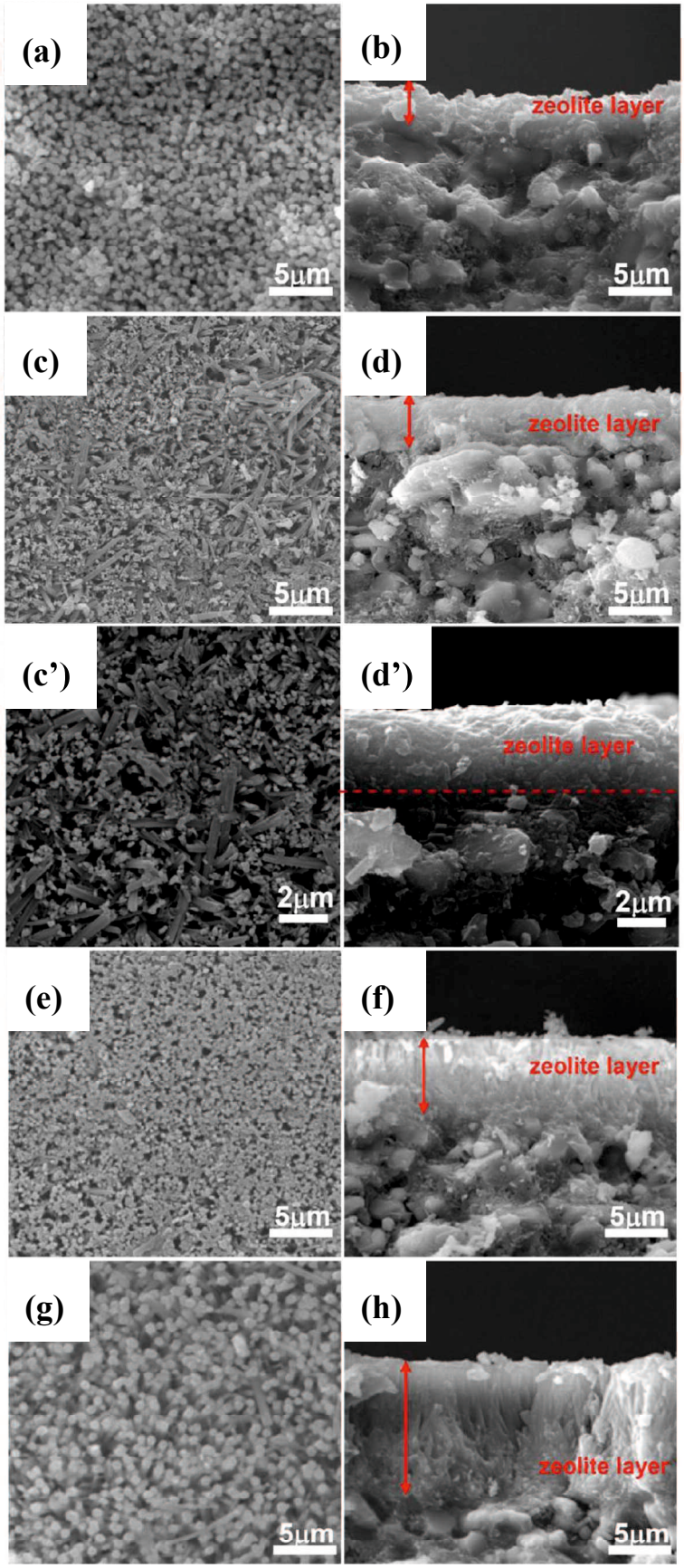

Figure 4-11 Surface and cross-sectional SEM images of T membranes: T1 (a, b), T3 (c−d′, c′and d′ are magnified c and d, respectively), T5 (e, f) and T8 (g, h).

The CH_4 and N_2 permeance of membrane T2 was about 1.3-1.8 times those of membrane T1. Membrane T2 did not become denser with the increasing crystallization time prolonged to 18 h. Moreover, for membrane T1, there were stronger characteristic peaks of the α-Al_2O_3 support and relatively weaker characteristic peaks of zeolite T crystals (**Figure 4-10 (a)**) and the loose packed zeolite T layer covered on the seeded support (**Figure 4-11 (a-b)**).

As a result, the membrane T1 showed poor gas permeation properties. Similar results were observed for membranes T5 and T6 with the second step at 448 K for 3-4 h. Although there were also stronger characteristic peaks of support as seen in Figure 5c, the membrane T5 showed high crystallinity of zeolite T together with preferential growth of the (102) direction, and a lot of smaller zeolite T crystals with poorer intergrowth were observed in the depths of the seeded supports (**Figure 4-11 (e-f)**). Thus, it also showed poorer CO_2 selectivity as seen in Table 1. However, as shown in **Table 4-1**, the membrane T3 prepared with the second step at 423 K for 8 h displayed the highest CO_2 permeance of 6.2×10^{-8} $mol\cdot m^{-2}\cdot s^{-1}\cdot Pa^{-1}$ and CO_2 permselectivity of 80 in CO_2/CH_4 mixtures compared with other membranes. As shown in **Figure 4-11 (c, d')**, a continuous and dense zeolite T layer as thin as 4 μm randomly covered the support surface. The membrane exhibited much stronger relative intensity of the main characte

The above results repeatedly indicate that synthesis temperature and crystallization time are the most important variable factors, which strongly affect the zeolite membrane growth and permeation performance [12, 13, 17, 18]. It also suggested that it was difficult to control the crystal growth at lower temperature or higher temperatures during the second-step and to subsequently form dense zeolite T layers on a seeded support surface under such synthesis conditions in this work.

The effect of crystallization time of the second step at 423 K on the membrane crystallization and the permeation performance was also investigated in this work (keeping the first step at 353 K for 4 h). After 2 h of hydrothermal treatment during the second step, as seen in **Figure 4-12**, there were weaker characteristic peaks of zeolite T while showing the stronger characteristic peaks of support. Loose zeolite T

crystals could not fully cover all the pores of the support (**Figure 4-13**), and thus, this membrane did not have a separation property (**Figure 4-14**). After 6 h, although this membrane showed the main characteristic peaks of zeolite T, there were also stronger characteristic peaks of support. It illustrated that zeolite T layers with random intergrowth did not completely cover the pores of the support, showing a relatively lower CO_2 permeation performance. After 8 h, as described above, the membrane T3 (**Table 4-1**) exhibited a continuous zeolite T layer with good intergrowth morphology, showing the highest CO_2 permeance and separation performance.

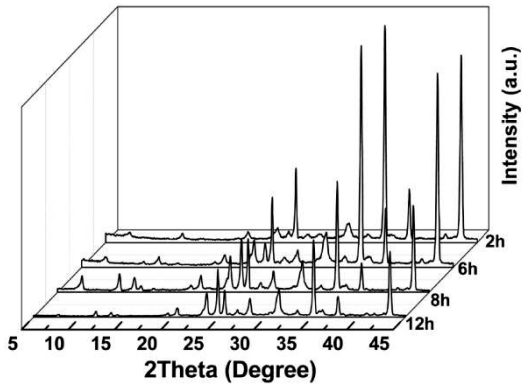

Figure 4-12 XRD patterns of as-synthesized membranes for different crystallization times of the second step at 423 K with the two-step method (the first step at 353 K for 4 h).

However, for further treatment to 12 h, the membrane showed the oriented zeolite T layer with about a thickness of 7 μm covered in the depths of the supports, which was similar to the membrane T5 as seen in **Figure 4-11 (e-f)**. It was also consistent with the XRD results for this membrane, as shown in **Figure 4-12**. The (102) peaks (2θ = 24.8°) became obvious and strong in the membrane. Generally, zeolite membranes with preferred crystal orientation would exhibit high permeation performance. Nevertheless, this membrane prepared over 12 h in this work still showed poor CO_2 perm-selectivity (**Figure 4-14**) due to no dense zeolite layer being fully covered on the seeded support, as illustrated in **Figure 4-13**. Further study of the influence of zeolite crystal orientation on CO_2 separation performance of zeolite T membranes is necessary.

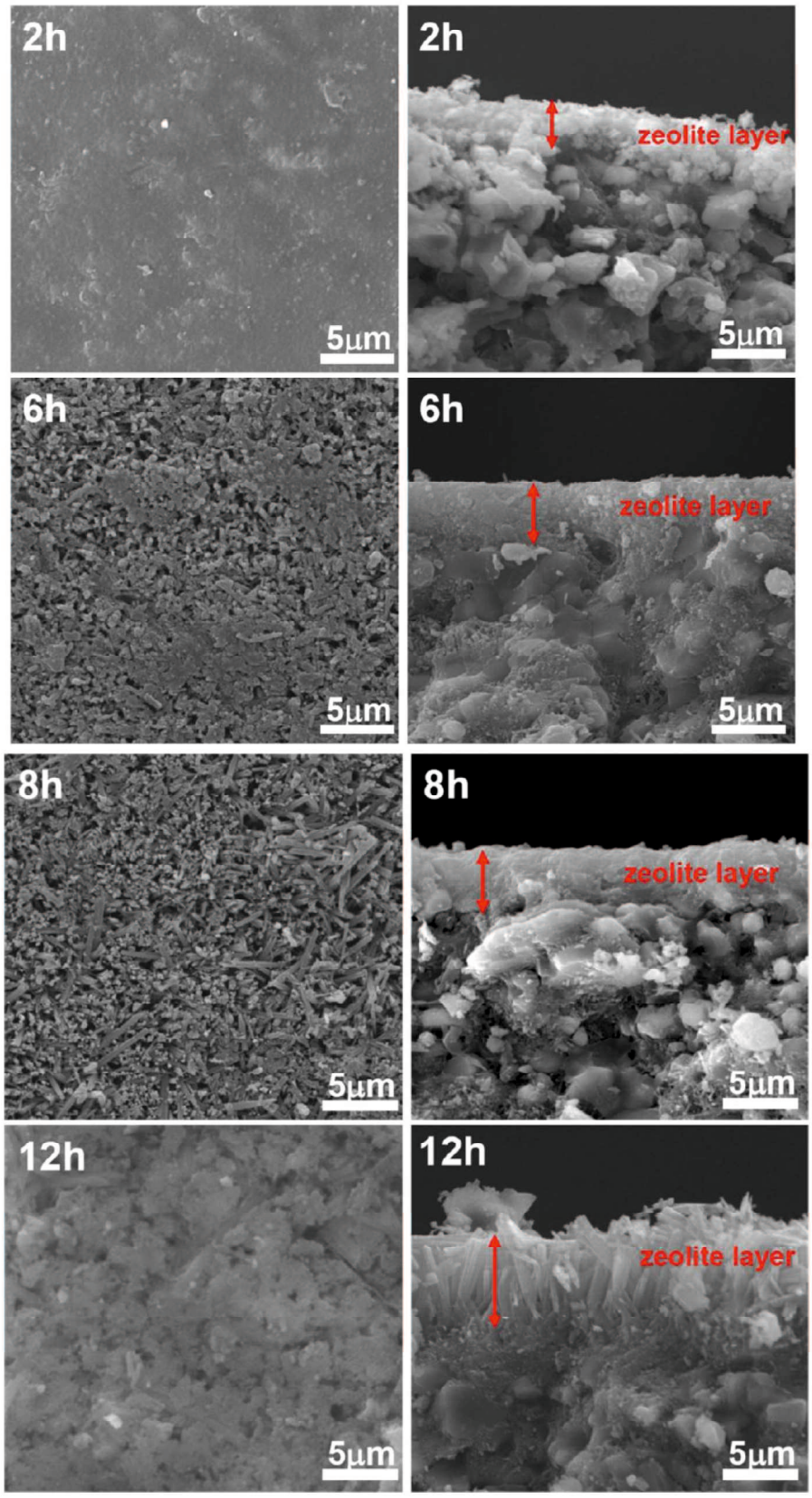

Figure 4-13 Surface and cross-sectional SEM images of membranes prepared for different crystallization times of the second step at 423 K by the two-step method (the first step at 353 K for 4 h).

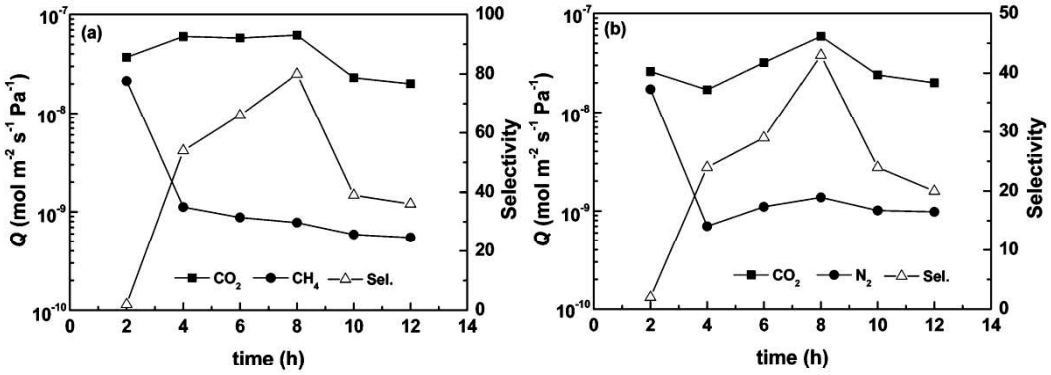

Figure 4-14 Effect of crystallization time of the second step at 423 K with the two-step method (the first step at 353 K for 4 h) on the CO_2 separation performance.

4.3.3 Comparison of the synthesis process at higher temperatures for the first step.

In order to investigate the effect of the synthesis process at higher temperatures for the first step, the membranes T7 and T8 (see **Table 4-1**) were also prepared at 473 K for the first step and then synthesized at 423 K for 4 h with the two-step method. Compared with other zeolite T membranes, as seen in **Figure 4-13**, it can be seen that the peaks (100), (110), and (210) were absent (or very weak) while the (102) peak became obvious and the strongest for the membranes T7 and T8. The intensity ratio of I(102)/I(100) in zeolite T seeds was as small as 1.1 (see **Figure 4-15(b)**).

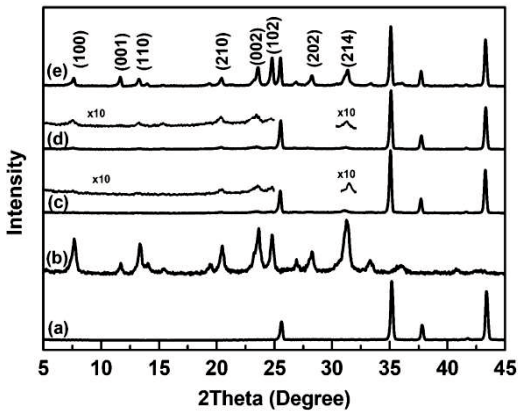

Figure 4-15 XRD patterns of α-Al_2O_3 support (a), zeolite T crystal (b), support seeded with zeolite T (c), zeolite T membrane prepared at 353 K for 4 h (d), and as-synthesized membrane T3 (Table 1) with the two-step method (e)

However, the I(102)/I(100) ratio increased to 12.6 for membrane T7 (**Figure 4-10(d)**) and then increased to 36.5 for membrane T8 (**Figure 4-10**). The length direction of the column-like crystals with stronger (h0l) orientation was perpendicularly grown onto the support outer surface for membrane T8 (**Figure 4-11(g-h)**). This morphology of crystal layers was very similar to that of the membrane prepared at 423 K for 12 h during the second step (**Figure 4-13**) and that described in our previous reports [19] which suggests that a higher synthesis temperature over 423 K favored the formation of oriented zeolite layers under such synthesis conditions. However, the membranes T7 and T8 exhibited a high CO_2 permeance of 5.1×10^{-8} mol·m^{-2}·s^{-1}·Pa^{-1} to 5.2×10^{-8} mol·m^{-2}·s^{-1}·Pa^{-1} and a lower CO_2 permselectivity of about 1-2 (see **Table 4-1**). This crystallization process at higher temperatures over 423 K for the first step is not suitable for nucleation (also see SEM images in **Figure 4-16**). Therefore, it seems that this crystallization process at higher temperatures for the first step is not favorable to preparing high quality membranes for CO_2 separation with the two-step method in this work.

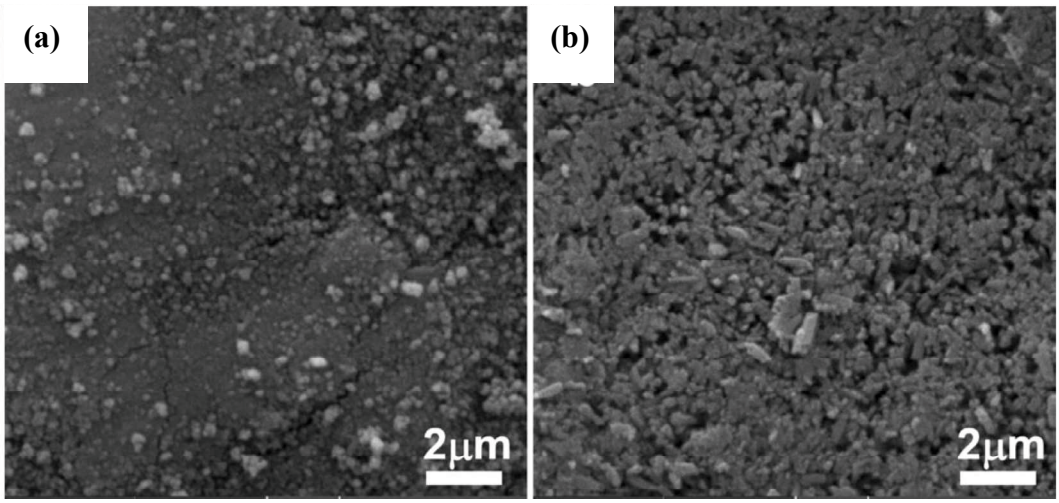

Figure 4-16 Surface-sectional SEM images of as-synthesized membranes at the first step of 423 K (a) and 473 K (b) for nucleation, respectively.

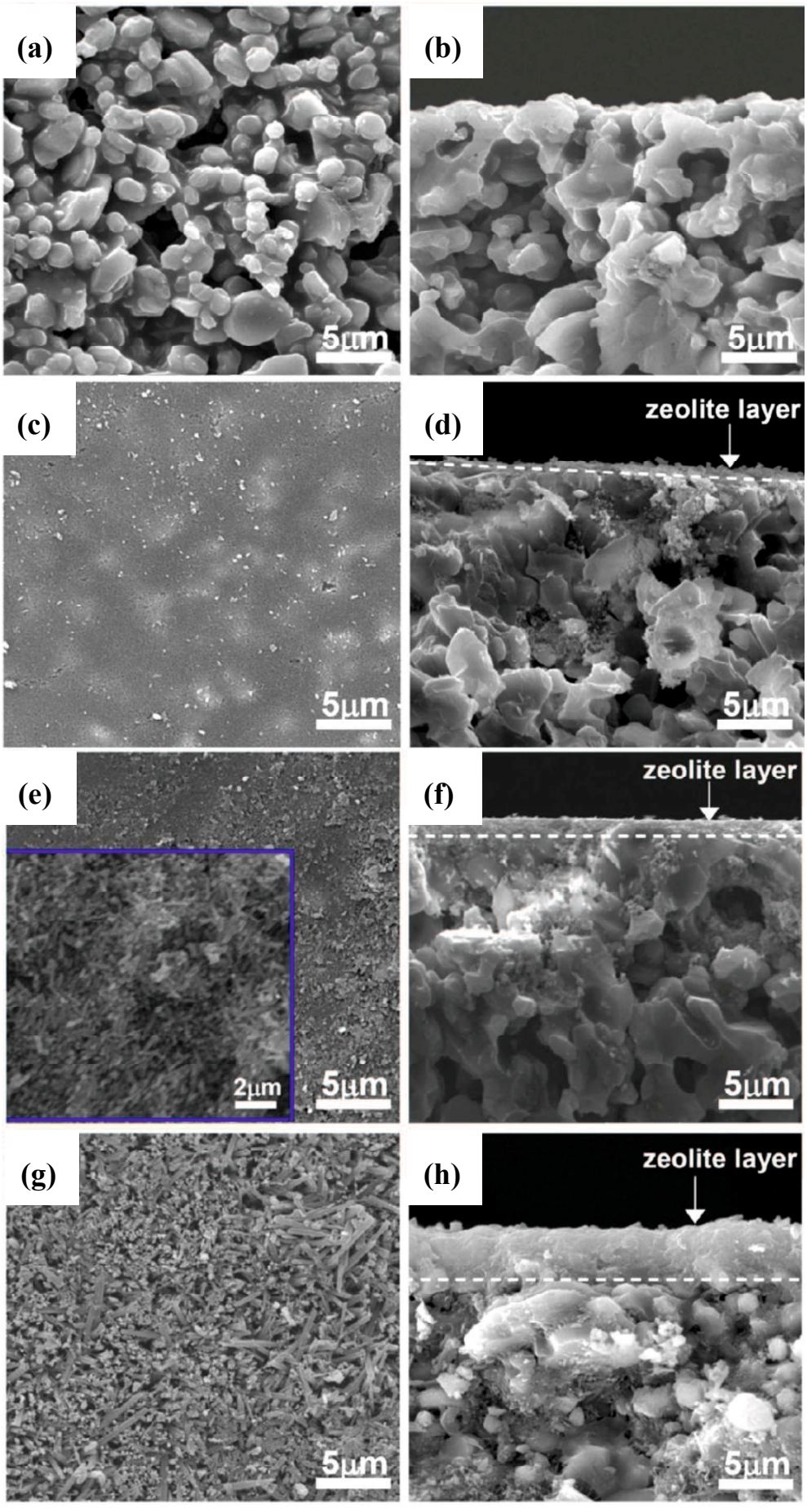
(a)
5μm
(b)
5μm
(c)
5μm
(d)
zeolite layer
5μm
(e)
2μm
5μm
(f)
zeolite layer
5μm
(g)
5μm
(h)
zeolite layer
5μm

Figure 4-17 Surface and cross-sectional SEM images of as-synthesized membranes during the two-step method process: Al_2O_3 support (a, b), support seeded with zeolite T (c, d), zeolite T membrane prepared at 353 K for 4 h (e, f), and as-synthesized membrane T3 (Table 1) with the two-step method (g, h).

4.3.4 Formation mechanism of zeolite T membranes with the two-step method.

Figures 4-(15, 17, and 18) show the XRD patterns, SEM images, and Si/Al ratios (EDX measurements) of zeolite T membranes prepared during each step with the two-step method, respectively. Compared to the microstructure characteristic of porous Al_2O_3 support (**Figures 4-17 (a-b) and Figures 4-15(a)**), the seeded support with nanosized seeds displayed the disjunctive layer as thin as approximately 0.2 μm on the support (**Figure 4-17 (c-d)**), and only very weak peaks of (210), (002), and (214) of zeolite T appeared for the seeded support (**Figure 4-15 (c)**). After 4 h of treatment at 353 K for the first step, many small crystals formed either on the support surface or in the interval of the pre-coated seeds layer (**Figure 4-17(e)**) and the membrane became dense with a thickness of about 1.0 μm (**Figure 4-17(e)**). At such a moment, Si/Al ratio of this membrane increased from 1.0 of seeded support to 1.6 as shown in **Figure 4-18**. Although the very weak peaks of (100) and (110) were newly formed, the characteristic peaks of zeolite T were still very weak (**Figure 4-15(d)**). It demonstrated that large amounts of nuclei could form at low temperatures by seed induction [11-13, 20]. Subsequently, these small zeolite T crystals grew into larger crystals quickly at higher temperatures, and a continuous and well-intergrown zeolite layer was rapidly formed at 423 K for 8 h (**Figure 4-17(g)**). Moreover, this zeolite T membrane was bound firmly to the support with a thickness of about 4 μm (**Figure 4-17(h)**), and the stronger characteristic peaks of zeolite T were obviously observed (**Figure 4-15(e)**). The Si/Al ratio of this as-synthesized membrane with the two-step method increased significantly to 3.8, which was consistent with that of the T-type zeolite of (3-4) [9, 21-23]. As mentioned above, the formation process of zeolite T membranes prepared with the two-step method can be depicted as follows. In the first

step, incremental nucleation and maturation of zeolite precursors was carried out at low temperature (353 K) by the nanometer sized seed induction, which was deposited on the support surface using the rub-coating method. Many new small zeolite T crystals and small secondary aggregates were formed among the originally coated seeds. Moreover, as described in **Chapter 4.3.3**, the crystallization process at higher temperature over 423 K for the first step is not suitable for nucleation and not for preparing high quality membranes for CO_2 separation using the two-step method in this work. After completion of the nucleation period, subsequently, the second step at high temperatures (i.e., 423 K) was carried out to promote the crystallization. Zeolite crystal growth over already formed nuclei is much favored to formation of new crystallites [20]. Therefore, more and more zeolite T crystals grew quickly, and eventually a continuous dense zeolite T membrane formed on the support surface [12]. In summary, a lower temperature (i.e., 353 K) favored the smaller size crystallite or nucleation, while a higher crystallization temperature (i.e., 423 K) promoted the zeolite crystallization under such synthesis conditions in this work [11-13, 20].

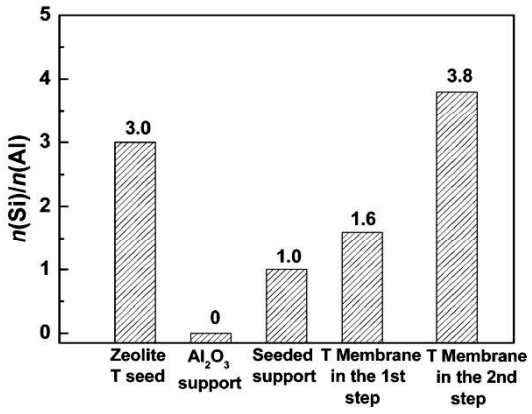

Figure 4-18 The Si/Al ratios of zeolite T seeds, support, and zeolite T membranes during the zeolite crystallization procedure with the two-step method. The membranes were prepared in the first step at 353 K for 4 h and then in the second step at 423 K for 8 h.

4.3.5 Comparison of membrane separation properties.

Using the two-step method under optimized conditions, five series of parallel

tubes of zeolite T membranes were successfully prepared on seeded supports. All the samples were characterized by SEM and XRD. It showed that these membranes were defect-free and purely crystalline with a typical T-type zeolite structure without other zeolite phases (not shown in this work). These membranes showed good reproducibility, high CO_2 permeance, and relative high CO_2/ CH_4 permselectivity under the same test conditions ((5.7-6.2)×10^{-8} mol·m^{-2}·s^{-1}·Pa^{-1} and 68-80, respectively). Here, compared with zeolite T membranes and other membranes in the literature, the higher CO_2 separation performance of the assynthesized zeolite T membrane (T3) is clearly demonstrated in **Figure 4-19**. As seen in **Figure 4-19**, Cui et al. [7, 8] reported that CO_2 permeance and maximum permselectivity of their zeolite T membranes were 4.6×10^{-8} mol·m^{-2}·s^{-1}·Pa^{-1} and 400 using the vacuum measurement method for equimolar binary CO_2/ CH_4 gaseous mixtures at 308 K, respectively. In comparison with their membranes, the membrane in this work exhibited higher CO_2 permeance (6.2×10^{-8} mol·m^{-2}·s^{-1}·Pa^{-1}) and relatively high CO_2 permselectivity (80) under the same conditions using the sweep gas measurement method. In addition, the synthesis time in this study (12 h) was much shorter than that of their reports (30 h). Moreover, as shown in **Figure 4-19**, the zeolite T membranes in this work also showed good CO_2 permeation performance in the CO_2/CH_4 and CO_2/ N_2 mixtures systems compared to other zeolite T or other-type membranes [2, 4, 17, 18]. Of course, it should be noted that it is a complex system to synthesize a zeolite membrane that exhibits high separation performance. Many effects or steps such as the choice of substrate, synthesis method, seed size, separation measurement techniques, etc. would influence the gas separation properties [3]. Sometimes, improving membrane permeance is more important than increasing selectivity to further reduce the cost of CO_2 separation and capture from flue gas when the CO_2 permselectivity is over 50.6 Moreover, the permselectivity of zeolite T membranes can be further improved by optimizing the synthesis conditions to improve the membrane density for potentially practical applicability, which is currently under investigation.

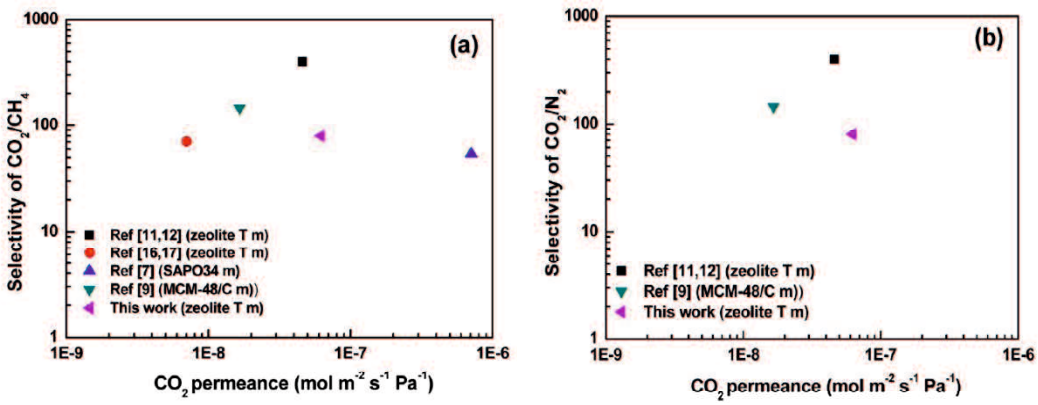

Figure 4-19 The permeation performance curves with permeance *vs* selectivity through zeolite T membranes in this work and other membranes in the literature.

4.4 Conclusions

The well-intergrown zeolite T membranes were successfully synthesized on seeded support with the two-step temperature process. The synthesis parameters such as synthesis temperature and crystallization time during the two-step durations could seriously influence the zeolite T crystal growth and CO_2 separation properties. Compared with the conventional hydrothermal synthesis at a constant temperature (i.e., one-step method), the two-step method is more effective in synthesizing a thin and continuous membrane in a short time under optimum synthesis conditions. During the two-step method, a lower temperature favored nucleation, while a higher crystallization temperature promoted crystallization, thus improving zeolite T crystal growth and membrane separation properties. The permeation performance of the resulting membranes in this work exhibited high CO_2 permeance and relatively high permselectivity for CO_2 separation from CH_4 or N_2 gas. It shows great potentially practical applicability in CO_2 separation and capture from natural gas and exhaust gases from power plants and chemical industries if permselectivity of such a membrane prepared with the two-step method further improved

References

[1] C. Song, Global challenges and strategies for control, conversion and utilization of CO_2 for sustainable development involving energy, catalysis, adsorption and chemical processing, Catalysis Today, 115 (2006) 2-32.

[2] E.W. Ping, R. Zhou, H.H. Funke, J.L. Falconer, R.D. Noble, Seeded-gel synthesis of SAPO-34 single channel and monolith membranes, for CO_2/CH_4 separations, Journal of Membrane Science, 415 (2012) 770-775.

[3] Y. Zhang, J. Sunarso, S. Liu, R. Wang, Current status and development of membranes for CO_2/CH_4 separation: a review, International Journal of Greenhouse Gas Control, 12 (2013) 84-107.

[4] L. Li, T. Wang, Q. Liu, Y. Cao, J. Qiu, A high CO_2 permselective mesoporous silica/carbon composite membrane for CO_2 separation, Carbon, 50 (2012) 5186-5195.

[5] A.M. Hillock, S.J. Miller, W.J. Koros, Crosslinked mixed matrix membranes for the purification of natural gas: effects of sieve surface modification, Journal of Membrane Science, 314 (2008) 193-199.

[6] I.C. Omole, R.T. Adams, S.J. Miller, W.J. Koros, Effects of CO_2 on a high performance hollow-fiber membrane for natural gas purification, Industrial and Engineering Chemistry Research, 49 (2010) 4887-4896.

[7] Y. Cui, H. Kita, K. Okamoto, Preparation and gas separation properties of zeolite T membrane, Chemical Communications, (2003) 2154-2155.

[8] Y. Cui, H. Kita, K. Okamoto, Preparation and gas separation performance of zeolite T membrane, Journal of Materials Chemistry, 14 (2004) 924-932.

[9] J. Bengoa, S. Marchetti, N. Gallegos, A. Alvarez, M. Cagnoli, A. Yeramian, Stacking faults effects on shape selectivity of offretite, Industrial and Engineering Chemistry Research, 36 (1997) 83-87.

[10] Q. Jiang, J. Rentschler, G. Sethia, S. Weinman, R. Perrone, K. Liu, Synthesis of T-type zeolite nanoparticles for the separation of CO_2/N_2 and CO_2/CH_4 by adsorption process, Chemical Engineering Journal, 230 (2013) 380-388.

[11] Q. Li, D. Creaser, J. Sterte, The nucleation period for TPA-silicalite-1

crystallization determined by a two-stage varying-temperature synthesis, Microporous and Mesoporous Materials, 31 (1999) 141-150.

[12] C. Kong, J. Lu, J. Yang, J. Wang, Preparation of silicalite-1 membranes on stainless steel supports by a two-stage varying-temperature in situ synthesis, Journal of Membrane Science, 285 (2006) 258-264.

[13] Y. Li, X. Zhang, J. Wang, Preparation for ZSM-5 membranes by a two-stage varying-temperature synthesis, Separation and Purification Technology, 25 (2001) 459-466.

[14] R. Zhou, F. Zhang, N. Hu, X. Chen, H. Kita, Fast preparation of high-performance zeolite T membranes in fluoride media, Chemistry Letters, 40 (2011) 1383-1385.

[15] X. ZHANG, S. Xin, Q. Lingfang, D. Minzheng, H. Na, Z. Rongfei, C. Xiangshu, Synthesis and pervaporation performance of highly reproducible zeolite T membranes from clear solutions, Chinese Journal of Catalysis, 34 (2013) 542-547.

[16] S.D. Kim, S.H. Noh, J.W. Park, W.J. Kim, Organic-free synthesis of ZSM-5 with narrow crystal size distribution using two-step temperature process, Microporous and Mesoporous Materials, 92 (2006) 181-188.

[17] M. Mirfendereski, M. Sadrzadeh, T. Mohammadi, Effect of synthesis parameters on single gas permeation through T-type zeolite membranes, International Journal of Greenhouse Gas Control, 2 (2008) 531-538.

[18] S. Mirfendereski, T. Mazaheri, M. Sadrzadeh, T. Mohammadi, CO_2 and CH_4 permeation through T-type zeolite membranes: effect of synthesis parameters and feed pressure, Separation and Purification Technology, 61 (2008) 317-323.

[19] R. Zhou, L. Hu, Y. Zhang, N. Hu, X. Chen, X. Lin, H. Kita, Synthesis of oriented zeolite T membranes from clear solutions and their pervaporation properties, Microporous and Mesoporous Materials, 174 (2013) 81-89.

[20] M. Mehdipourghazi, A. Moheb, H. Kazemian, Incorporation of boron into nano-size MFI zeolite structure using a novel microwave-assisted two-stage varying temperatures hydrothermal synthesis, Microporous and Mesoporous Materials, 136 (2010) 18-24.

[21] S. Yang, N. Evmiridis, Synthesis and characterization of an offretite/erionite type zeolite, Microporous Materials, 6 (1996) 19-26.

[22] M.D. Rad, S. Fatemi, S.M. Mirfendereski, Development of T type zeolite for separation of CO_2 from CH_4 in adsorption processes, Chemical Engineering Research and Design, 90 (2012) 1687-1695.

[23] Q. Jiang, J. Rentschler, G. Sethia, S. Weinman, R. Perrone, K. Liu, Synthesis of T-type zeolite nanoparticles for the separation of CO_2/N_2 and CO_2/CH_4 by adsorption process, Chemical Engineering Journal, 230 (2013) 380-388.

Chapter 5 Effects of synthesis parameters on properties of silicalite-1 zeolite membranes

5.1 Introduction

Membrane technology is an indispensible way to realize a lot of separation processes because its low cost and energy use [1]. Compared to polymeric membranes, zeolites have proper pore size and good shape selectivity. Zeolite membranes show good thermal stability and chemical endurance. Therefore, the field of zeolite membranes has been studied as an intense research in applications of liquid separation, gas separation, chemical synthesis and sensor device [1, 2].

Hydrogen is very clean and efficient energy. During the storage, such as in methylcyclohexane-toluene-hydrogen system, H_2 is always accompanied with some organic molecules such as toluene and methylcyclohexane [3]. Thus, it is an emergent task to separate H_2 from the mixtures. Many zeolite membranes have been used for H_2 separations, such as NaA type [4], SAPO-34 type [5], sodalite type [6], SSZ-13 type [7], and MFI type [8-11].

Pure silica MFI zeolite membranes with 5.6×5.3 nm straight channels vertical (b-oriented) to the porous support have demonstrated very promising separations of H_2 (0.28 nm) [12] /toluene (0.59 nm) [13] mixture [14]. In this work, silicalite-1 (Al free MFI) membranes were prepared in the presence of fluoride. As a mineralizing agent, F^- can induce larger crystal particles [15] so that fewer crystals will penetrate into support channels. So far, few reports are about applying MFI membranes prepared in fluoride medium to gas permeation [14, 16, 17]. Herein, effects of synthesis parameters on morphology of silicalite-1 membranes prepared with F^- were investigated, such as synthesis time, synthesis temperature, silica source, seed crystal size and supports. Moreover, the as-synthesized silicalite-1 membranes were used to single gas permeation, especially for H_2 and SF_6 (0.55 nm) [18] permeations. Effects of gas permeation conditions (measurement temperature and measurement pressure

difference) also have been discussed. Finally, long-term test was done to evaluate the performance stability of the silicalite-1 membranes.

5.2 Experimental

5.2.1 Raw materials

Colloidal silica (Ludox AS-40, HS-40, and TM-40, Aldrich), fumed silica dioxide (98%, Aerosil), tetraethyl orthosilicate (TEOS, 98%, Aldrich), tetrapropylammonium hydroxide (TPAOH, 20-25% in water, Tokyo kasei), tetrapropylammonium bromide (TPABr, 99%, Tokyo kasei), ammonium floride (NH_4F, 99.99%, Aldrich), sodium hydroxide (NaOH, 97%, Wako) and distilled water were used to prepared silicalite-1 crystals and silicalite-1 membranes.

Silicalite-1 membranes were formed on three kinds of supports. The first one is called porous α-alumina tube (symmetrical Al_2O_3, o.d. 12 mm, i.d. 9 mm and length 100 mm with a membrane area of 37.68 cm^2), with an average pore size 1.25 μm and porosity of 35.20 %. The second one is called mullite tube (o.d. 12 mm, i.d. 9 mm and length 100 mm with a membrane area of 37.68 cm^2), with an average pore size 1.33 μm and porosity of 43%. The third one is called NS-1 tube (o.d. 10 mm, i.d. 7 mm and length 100 mm with a membrane area of 31.40 cm^2), with an average pore size 0.15 μm and porosity of 35-45 %.

5.2.2 Synthesis of silicalite-1 crystals

Silicalite-1 crystals with different particle sizes were prepared. Nanometer-sized crystals were prepared without floride. The gel was prepared according to a molar composition of TEOS: TPAOH: H_2O = 1: 0.36: 20. Firstly, distilled water was added into TPAOH. After stirring the solution for 20 min, TEOS was added as a silica source. The final solution was formed after being stirred for 70 min vigorously. The crystallization was carried out in a constant temperature oven at 403 K for 48 h.

On the other hand, crystals with micrometer size were synthesized with fluoride. The corresponding molar composition is SiO_2: NaOH: TPABr: H_2O: NH_4F = 1: 0.25:

0.30: 45: 0.10. The gel was prepared according to follow steps. Firstly, TPAOH was added into distilled water under stirring. After about 20 min, NaOH was added and stirred until NaOH was dissolved. Then after adding AS-40 slowly, the solution was stirred and aged for 23 h. Finally, NH_4F was added as a floride mediate and the solution was stirred for another 1 h. The solution was then poured into a Teflon sleeve and placed in a tightly sealed stainless steel reactor and heated at 413 K for 30 h.

After crystallization, the resulting solids were then washed with water by a centrifuge. The centrifugation was kept for 30 min and the rotated speed was 3500 rp/min. To achieve a neutral, it is necessary to repeat this centrifugation a minimum of two more times. The crystals were then dried and calcined at 773 K for 15 h. The heating rate and cooling rate are 0.52 K/min. After calcination, the obtained crystals are kept in sealed bottles to be used.

5.2.3 Preparation of silicalite-1 membranes

Silicalite-1 membranes formed three kinds of supports were grown by seeding method. The synthesis solution has a molar ratio of SiO_2: TPAOH: TPABr: NH_4F: H_2O = 1: 0.20: 0.10: 0.10: 500. The tubes were cleaned with distilled water and dried at 353 K over night before use. The reaction solution was prepared as follows. Firstly, TPAOH was drop wisely added to water. After stirring for 5 min, TPABr was added. 10 min later, as silica source, silica source was added into water/template mixture under stirring. The mixture solution was then stirred for 1 h at room temperature. Herein, silicalite-1 membranes were synthesized in fluoride mediate. Thus, NH_4F was finally added to provide F^- and stirred for another 5 min. After finishing the rub coating procedure, the seeded supports were dried at 353 K for over 30 min and then put vertically into an autoclave. Silicalite-1 membranes were synthesized at (438-468) K for (2-16) h. After crystallization, the zeolite coated membranes were washed thoroughly with pure water until the pH of the washing liquid became neutral. The synthesized membranes were calcined at 773 K for 20 h to remove the organic compounds. The calcination heating and cooling rates are 0.26 K/min and 0.39 K/min, respectively. All the heat treated membranes will be treated by vacuuming in an oven

before applied to gas permeation and other characterizations.

5.2.4 Characterization

X-ray diffraction (XRD, SHIMADZU XRD-6100) with Cu-$K\alpha$ radiation was used to identify crystal structures of silicalite-1 crystals and membranes. These spectra were scanned in the range of $2\theta = 5^{o}$-45^{o} at a scanning rate of 4^{o}/min.

Scanning electron microscopy (FE-SEM, JEOL JSM 6335F) was used to observe the morphologies and thickness of obtained samples.

5.2.5 Single gas permeation measurement

The as-synthesized silicalite-1 membranes were applied to single gas permeation. The gas permeation setup has been shown by Cui et al.[19]. The membrane was fixed in a stainless steel cell with the zeolite layer facing upstream and was sealed by rubbery O-rings and stainless O-rings on both ends. The leakage flow, which came from the O-rings, is between 1.25×10^{-8} $mol^{-2}\cdot s^{-1}\cdot Pa^{-1}$ and 2.84×10^{-11} $mol^{-2}\cdot s^{-1}\cdot Pa^{-1}$ at 308 K. This leakage flow was negligible compared to the permeation flow through the zeolite membranes.

In the gas permeation equipment, a single gas (He, H_2, N_2, O_2, CO_2, CH_4 or SF_6) was fed into the module. And then the gas permeated across the membrane at (308-473) K by means of a vacuum method. Prior to gas permeation, all the membranes were evacuated for 48 h at 473 K to dehydrate from zeolite pores. Then the system was evacuated for 1 h to remove air and other impurities at the given temperature. After cutting off the upstream from the vacuum line, a single gas was introduced into the upstream side. The pressure on the permeate side was controlled at a pressure difference varied from 0.11MPa to 0.40 MPa. This pressure difference was the driving force across the membrane. The permeate pressure was measured by a pressure transducer after the downstream was cut off from the vacuum line. The ideal selectivity of (A/B) (α^{ideal} (A/B)) was the ratio of permeance of gas A and permeance of gas B. It should be noted that, because of high permeance, in case of H_2 permeation tests, permeate side was open to the air with an over pressure at the feed side, and the

flow rate going through the membrane was measured.

5.3 Results and discussion

5.3.1 Silicalite-1 crystal seed

After hydrothermal synthesis, pure silicalite-1 crystals can be obtained successfully as shown in **Figure 5-1**.

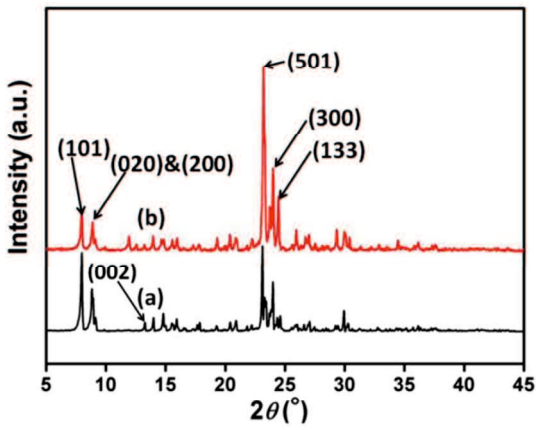

Figure 5-1 XRD patterns of MFI seeds: (a) seed with small crystal size and (b) seed with larger crystal size

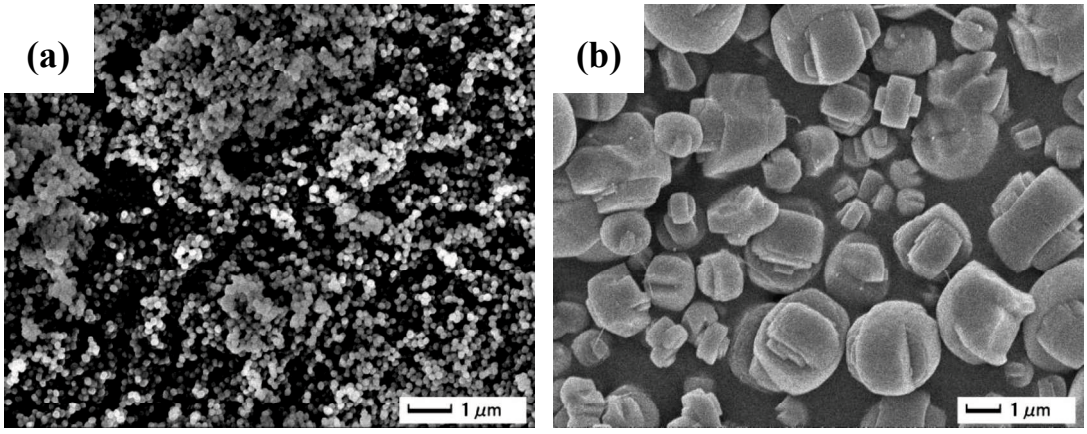

Figure 5-2 SEM images of MFI zeolite with different crystal size (a) 100-200 nm and (b) 1-2μm

For the two kinds of seed, strongly diffracted peaks can be observed at 2θ = (8-10)^{o} and (24-25)^{o}, respectively. The peaks reflect the growth direction of (101), (200)&(020), (002), (501), (300) and (133) of silicalite-1-type typical structure [20].

Moreover, SEM images of seeds are shown in **Figure 5-2**, respectively. **Figure 5-2** (a) shows randomly oriented ball-like small crystals with particle size of (1-2) μm and Figure 5-2 (b) shows twin crystals with particle size of (100-200) nm.

5.3.2 Effects of synthesis parameters on gas permeation performance of silicalite-1 zeolite membranes

5.3.2.1 Effect of silica source

Silica sources of TEOS, HS-40, AS-40, fumed SiO_2 and TM-40 were used to prepare silicalite-1 zeolite membranes on mullite supports. As XRD patterns in **Figure 5-3** shows, except typical peaks of pure silicalite-1 crystal phase and mullite support, there are no impure crystals formed on the supports. According to the XRD patterns, the peak intensities were used to calculate the ratio of $I_{(101)}/I_{(sup.)}$, where $I_{(101)}$ is the intensity of peak located at 7.95° and $I_{(sup.)}$ is the intensity of support peak located at 35.1°.

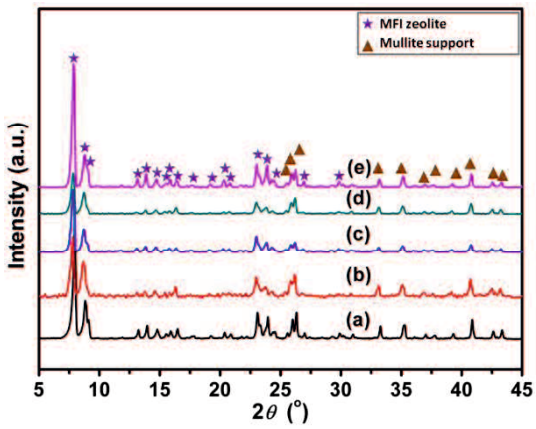

Figure 5-3 XRD patterns of membranes prepared with different silica source: (a) TEOS, (b) HS-40, (c) AS-40, (d) fumed SiO_2 and (e) TM-40.

Figure 5-4 shows that the intensity ratios of membranes prepared by HS-40 (4.8) and fumed SiO_2 (5.1) are much lower than intensity ratios of other membranes. Among the five kinds of silica sources, TM-40 can induce a silicalite-1 membrane with a highest $I_{(101)}/I_{(sup.)}$ of 11.2. The SEM images of silicalite-1 membranes prepared by different silica sources are shown in **Figure 5-5.**

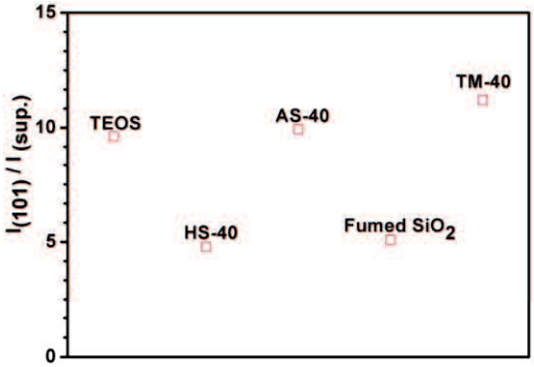

Figure 5-4 $I_{(101)}/I_{(sup.)}$ of membranes prepared using different silica sources.

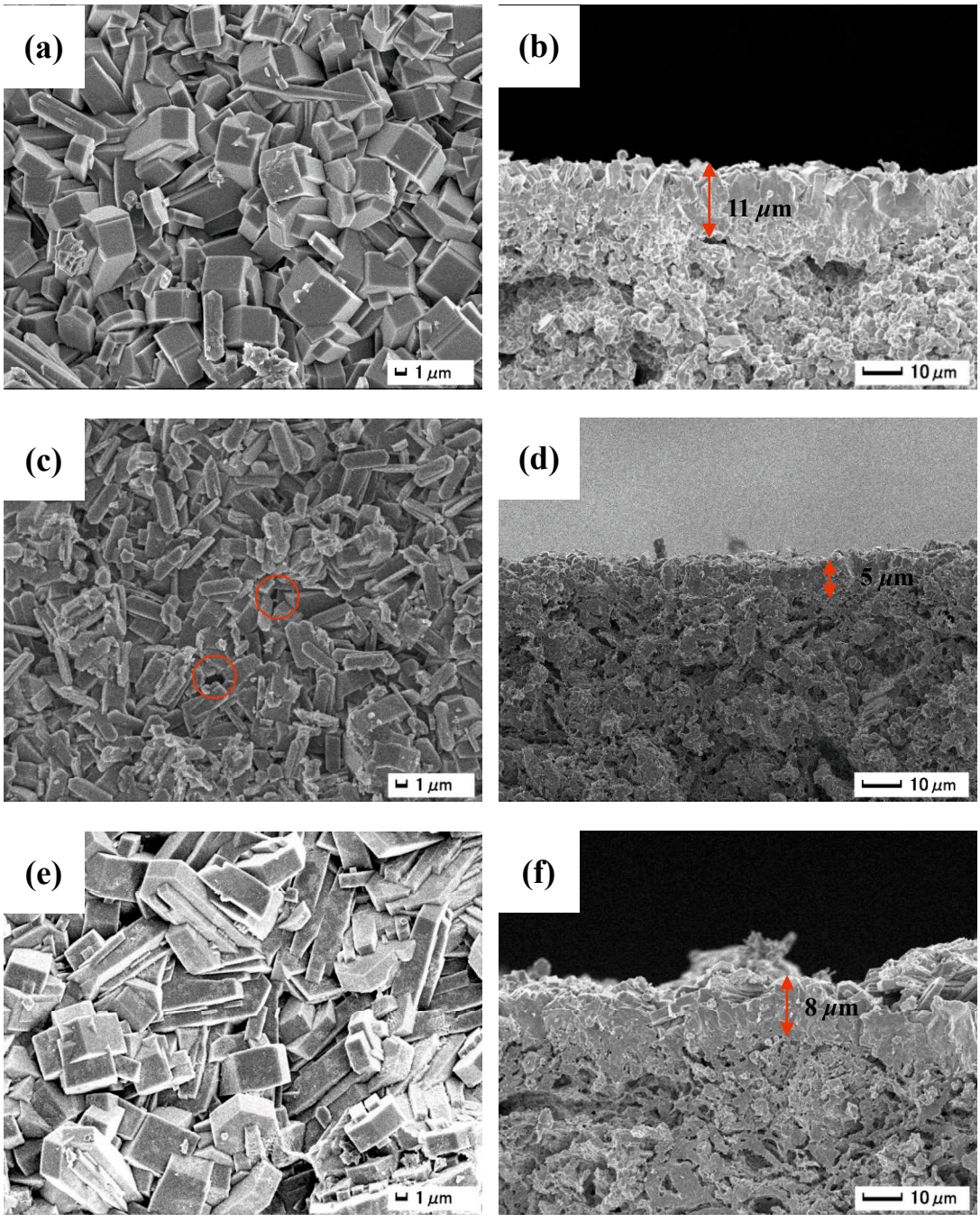

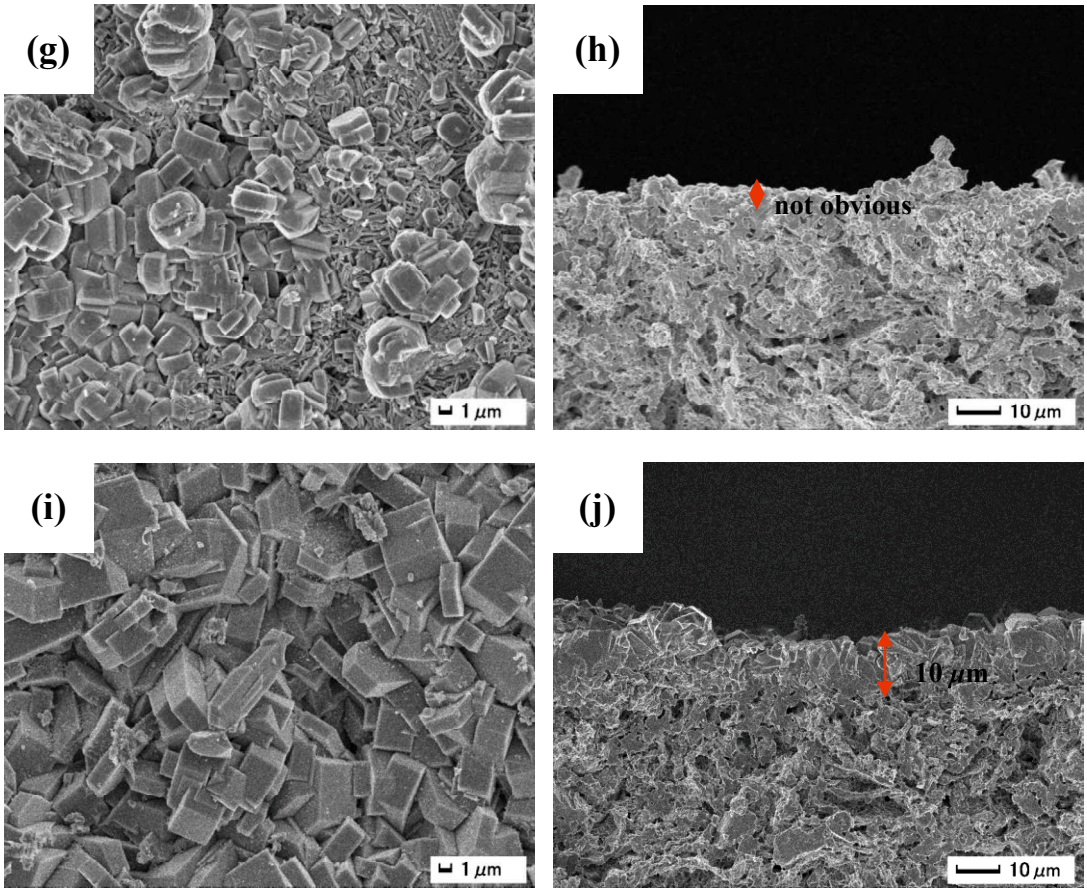

Figure 5-5 SEM images of MFI membranes prepared with different silica source: (a-b) TEOS, (c-d) HS-40, (e-f) AS-40, (g-h) fumed SiO_2 and (i-j) TM-40.

The difference of intensity ratio should be explained by membrane morphology. When HS-40 was used, thin coffin-like silicalite-1 crystals covered on the surface of support all in a mess (**Figure 5-5(c)**). Many obvious pin holes appeared and the zeolite layer was about 5 μm. When fumed SiO_2 was used, heterogeneous phase appeared. On the surface of support, both twinned inter-grown shape crystals and stick-like crystals were formed. Moreover, there is no clear continuous zeolite layer as shown by the cross sectional image of **Figure 5-5(h)**. Based on the obvious defects in silicalite-1 membranes and the relatively thin membrane thickness, support layer is easy to be detected by XRD. Therefore, it is naturally that the intensity of $I_{(101)}$ for this membrane will be weak. Besides, the membrane thicknesses of silicalite-1 membranes prepared using TEOS, AS-40 and TM-40 are about 11 μm, 8 μm, and 10 μm, respectively. Therefore, the intensity ratio increased successively.

In addition, all the membranes have been applied to H_2 and SF_6 permeations. The results have been list in the **Table 5-1**.When TEOS was used, H_2 permeance of the membrane was 9.99×10^{-7} $mol\cdot m^{-2}\cdot s^{-1}\cdot Pa^{-1}$ and the ideal selectivity of H_2/SF_6 was as high as 50.0. However, when AS-40 and TM-40 are used, silicalite-1 membranes show poor ideal selectivities of H_2/SF_6 with high H_2 permeance. **Figure 5-5 (a-b)** of silicalite-1 membrane prepared with TEOS are in accordance with the good gas permeation performance. The crystals grow compactly and the continuous membrane layer has been showed by a red double arrow. When AS-40 was used, the corresponding silicalite-1 membrane shows a very low H_2/SF_6 ideal selectivity of 7.8 and the H_2 permeance is higher than membrane prepared with TEOS. While TM-40 was used, the silicalite-1 membrane shows a high H_2 permeance of 1.68×10^{-6} $mol\cdot m^{-2}\cdot s^{-1}\cdot Pa^{-1}$ and a relatively lower ideal selectivity of 25.5 for H_2/SF_6. That results maybe because polymeric silica sources(AS-40 and TM-40) can't be dissolved completely in a diluted solution in this work which has a very low alkalinity [21] even though it seems membranes prepared with AS-40 and TM-40 show compact zeolite layers. On another hand, it is certain that silicalite-1 membranes using HS-40 and fumed SiO_2 leaked because of the poor morphology so that they can't be used in permeation process.

Table 5-1 H_2 permeation performances of MFI membranes on different supports with different silica sources (synthesis: 458 K, 14 h; measurement: 308 K, ΔP = 0.40 MPa)

No.	Support	Silica source	Permeance (10^{-8} $mol\cdot m^{-2}\cdot s^{-1}\cdot Pa^{-1}$)		Ideal selectivity
			H_2	SF_6	
SI-1	Mullite	TEOS	99.90	2.00	50.0
SI-2	Mullite	HS-40	Leak		
SI-3	Mullite	AS-40	55.90	7.20	7.8
SI-4	Mullite	Fumed SiO_2	Leak		
SI-5	Mullite	TM-40	168.00	6.60	25.5
SI-6	Sysmmetric α-Al_2O_3	TEOS	14.00	0.09	155.6
SI-7	NS-1	TEOS	65.00	0.43	151.2

5.3.2.2 Effect of synthesis temperature

As shown in **Figure 5-6**, XRD patterns of membranes synthesized at different temperatures indicate that pure silicalite-1 crystals were formed on the four supports.

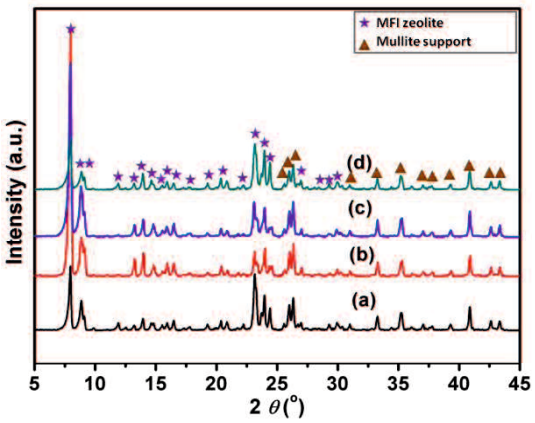

Figure 5-6 XRD patterns of membranes synthesized prepared for 14 h at (a) 438 K, (b) 448 K, (c) 458 K, and (d) 468 K.

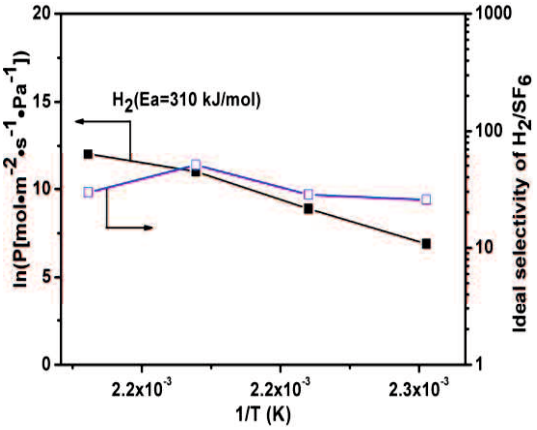

Figure 5-7 Arrhenius plot and ideal selectivity of H_2/SF_6 of MFI zeolite membranes as a function of synthesis temperature.

The apparent activated energy is shown in **Figure 5-7**. **Figure 5-8** presents SEM images of silicalite-1 membranes prepared at different temperatures. Based on the images, membrane thicknesses were judged as 8 μm, 10 μm, 11 μm and 12 μm for membranes prepared at 438 K, 448 K, 458 K and 468 K, respectively. The apparent activation energy (Ea) of H_2 permeation can be calculated to be 310 kJ/mol which is much higher than other silicalite-1 membranes [12]. Moreover, as synthesis

temperature increased α^{ideal} (H_2/SF_6) has a maximum of 50 when synthesis temperature is 458 K. However, even though the membrane layer became a little thicker at higher temperature, the H_2 permeance was not affected, instead, it increased slightly. That maybe because of some crystals formed in support pores of membranes prepared at lower temperature as marked by red circles in **Figure 5-8**.

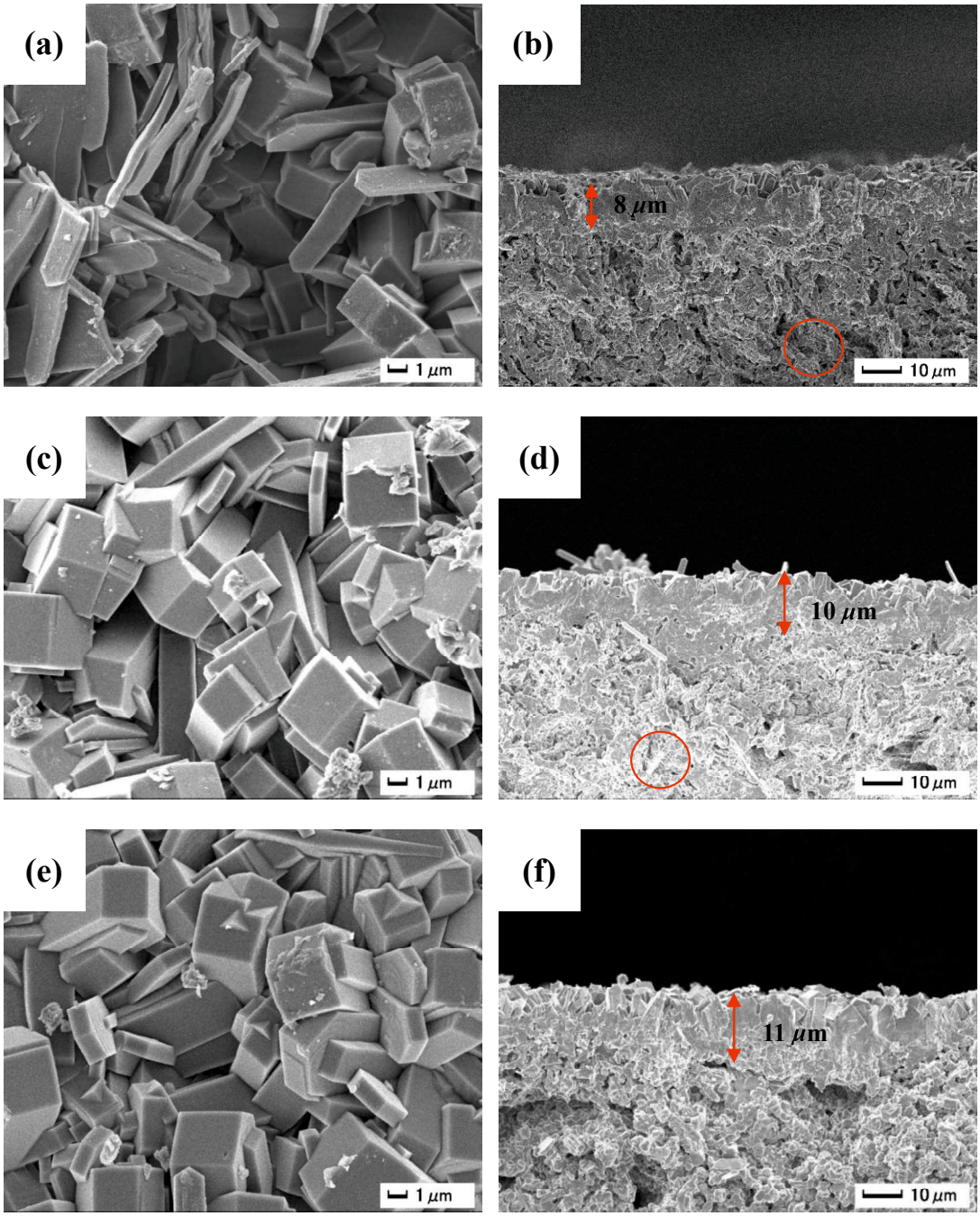

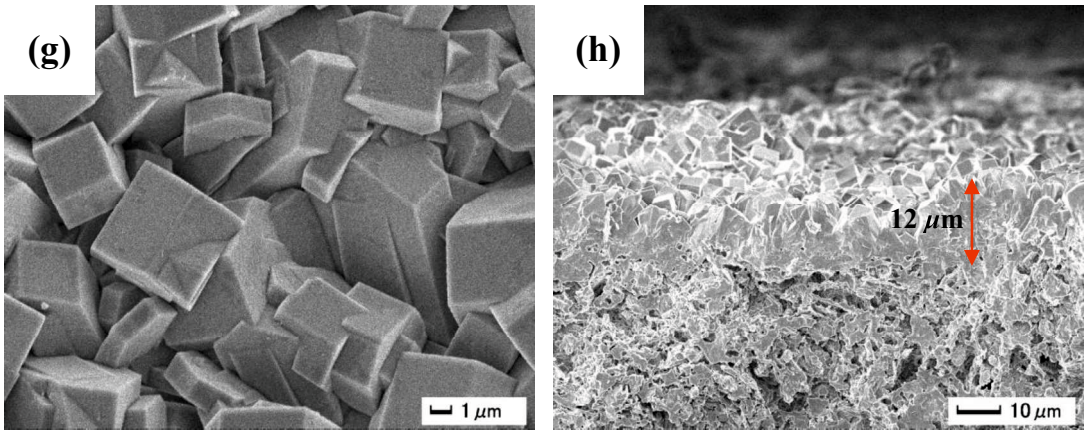

Figure 5-8 SEM images of MFI membranes prepared for 14 h at (a, b) 438 K, (c, d) 448 K, (e, f) 458 K, and (g, h) 468 K.

It is clearly that silicalite-1 crystal size is about 4-6 μm for membranes prepared at 438 K and 448 K. However, membranes prepared at 458 K and 468 K show a crystal size larger than 10 μm. It is easy to draw a conclusion that higher H_2 permeance can be obtained at higher synthesis temperature. **Figure 5-9** shows the effects of synthesis temperature on film orientation. Obviously, the predominant growth direction is that of (101) located at 2θ = 7.95 ^{o}, especially for membrane prepared at 438 K. Orientation of (200) located at 2θ = 8.9 ^{o} became stronger at higher temperature. **Figure 5-8** shows that the crystal shapes are different. Flat plates dominant the crystal shape of membrane synthesized at 438 K. As temperature increased, crystals became thicker and longer which should be due to the stronger direction of (200).

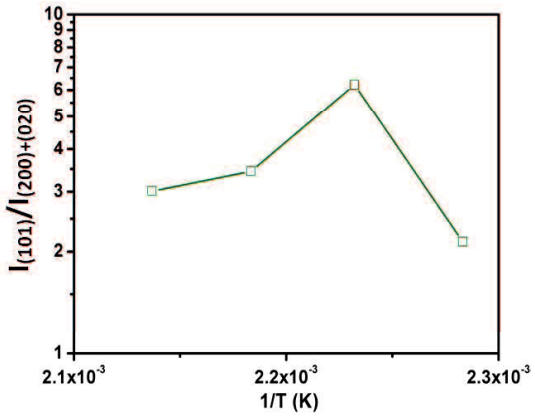

Figure 5-9 $I_{(101)}/I_{(200)\&(020)}$ of MFI zeolite membranes as a function of synthesis

temperature.

5.3.2.3 Effect of synthesis time and seeds with different crystal size

As described in **Chapter 5.3.1**, silicalite-1 crystals with particle size of (1-2) μm and (100-200) nm were obtained successfully. Herein, the two kinds of seeds were used to prepare membranes for (2-16) h. **Figure 5-10** shows that all the membranes obtained are pure silicalite-1 zeolite membranes. When larger particles were used, as **Figure 5-10 (left)** shows, typical peaks of silicalite-1 membrane prepared for 2 h are very weak especially at $2\theta = (10\text{-}25)^{o}$.

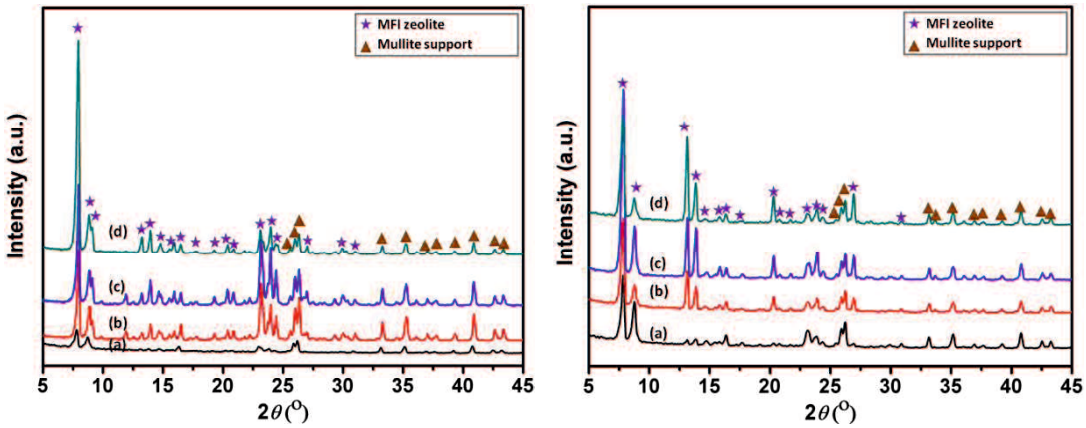

Figure 5-10 XRD patterns of membranes prepared for different periods: (a) 2 h, (b) 8 h, (c) 14 h and (d) 16 h. (left: using seed with larger particle size, right: using seed with smaller particle size.)

Herein, both the two seeds have been used to prepare silicalite-1 membranes for (2-16) h. It's easy to obtain silicalite-1 membranes without impurities. **Figure 5-10** shows they have silicalite-1 typical peaks. **Figure 5-10** indicates that synthesis time increased, twin peaks appeared at $2\theta = 8.9^{o}$ when micrometer-sized seed was used whereas twin peaks never appeared when nanometer-sized seed was used.

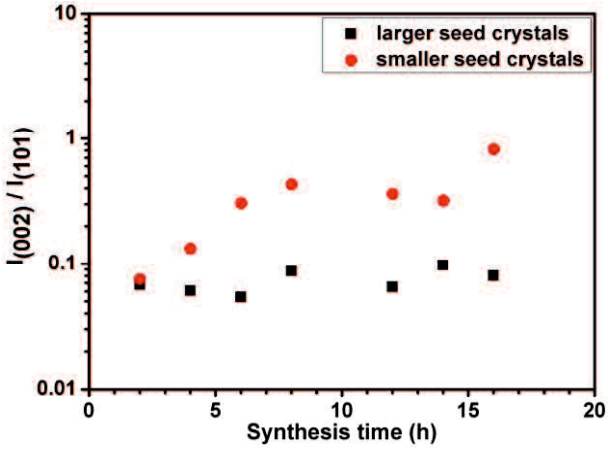

Figure 5-11 $I_{(002)}/I_{(101)}$ of MFI zeolite membranes as a function of synthesis time.

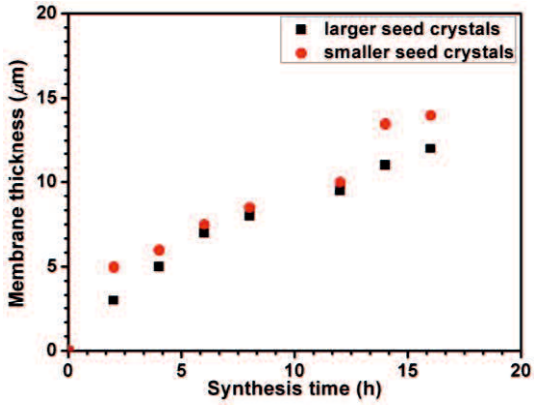

Figure 5-12 Membrane thickness as a function of synthesis time for membranes prepared using seeds with different particle sizes.

In the meantime, as shown in **Figure 5-11** and **Figure 5-12,** both of intensity ratio of $I_{(002)}/I_{(101)}$ and membrane thickness increased as synthesis time increased. The membrane thickness can be obtained from the SEM images exhibited in **Figure 5-13** and **Figure 5-14**. And the membrane layer growth rate decreased as synthesis time increased due the reduction of nutrition in solution. **Figure 5-11** indicates that the $I_{(002)}/I_{(101)}$ ratios of most membranes prepared with smaller seed are stronger than the ratios of membranes using larger seed. Moreover, **Figure 5-10** also indicates the growth of (002) orientation in silicalite-1 membranes using smaller seed crystals.

Membrane cystal morphologies in **Figure 5-13** and **Figure 5-14** are in accordance with these phenomena. When larger seed crystals were used, silicalite-1

membranes were formed by twin crystals. The crystals in membrane layer show no good uniformity. In addition, when smaller seed crystals were used, silicalite-1 memrbanes were formed by uniform flat and long coffin-like crystals, which is affected by (002) orientation. Crystals became thicker and longer for a longer time. The membrane layer is also more uniform.

Besides, as synthesis time increased from 2 h to 16 h, membranes prepared with both seeds became thicker gradually. To be noticed, membranes prepared with smaller seed crystals are thicker than membranes using larger seed crystals. The difference is because of the faster crystallization in small seed layer [22].

On the other hand, it is obvious that conspicuous pinholes have been eliminated a lot as crystallization time increased and the membrane thickness increased as well, which can be demonstrated by **Figure 5-15**. **Figure 5-15 (a)** shows that all the membranes have promising H_2 permeance higher than 5.90×10^{-7} $mol \cdot m^{-2} \cdot s^{-1} \cdot Pa^{-1}$. H_2 permeance became lower as synthesis time increased to 6 h but changed little after a longer synthesis time. SF_6 permeation also behaved similarly. **Figure 5-15 (b)** shows the α^{ideal} (H_2/SF_6) of the membranes. When synthesis time was 2 h, membrane using large seed was leak. When synthesis time increased to 4 h and 6 h, α^{ideal} (H_2/SF_6) of membranes increased, especially using smaller seed. In accordance to gas permeance behavior, α^{ideal} (H_2/SF_6) also almost kept stable after a longer crystallization period.

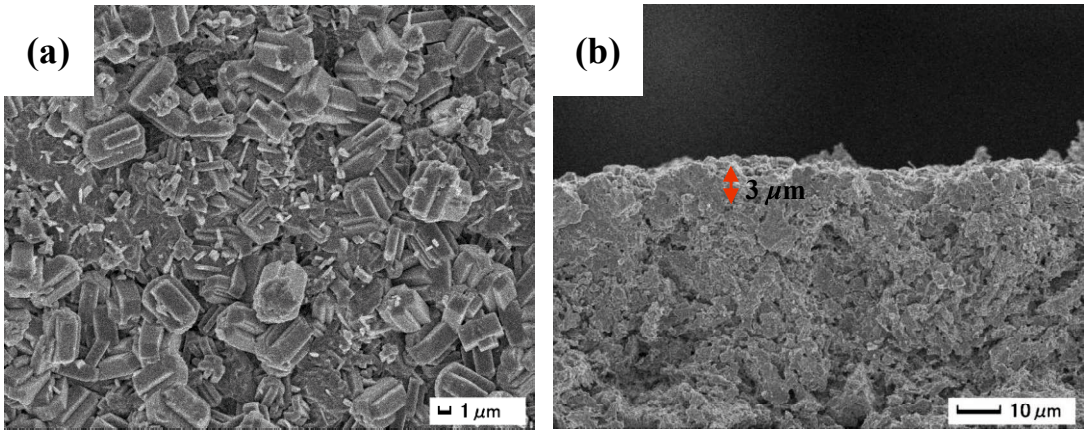

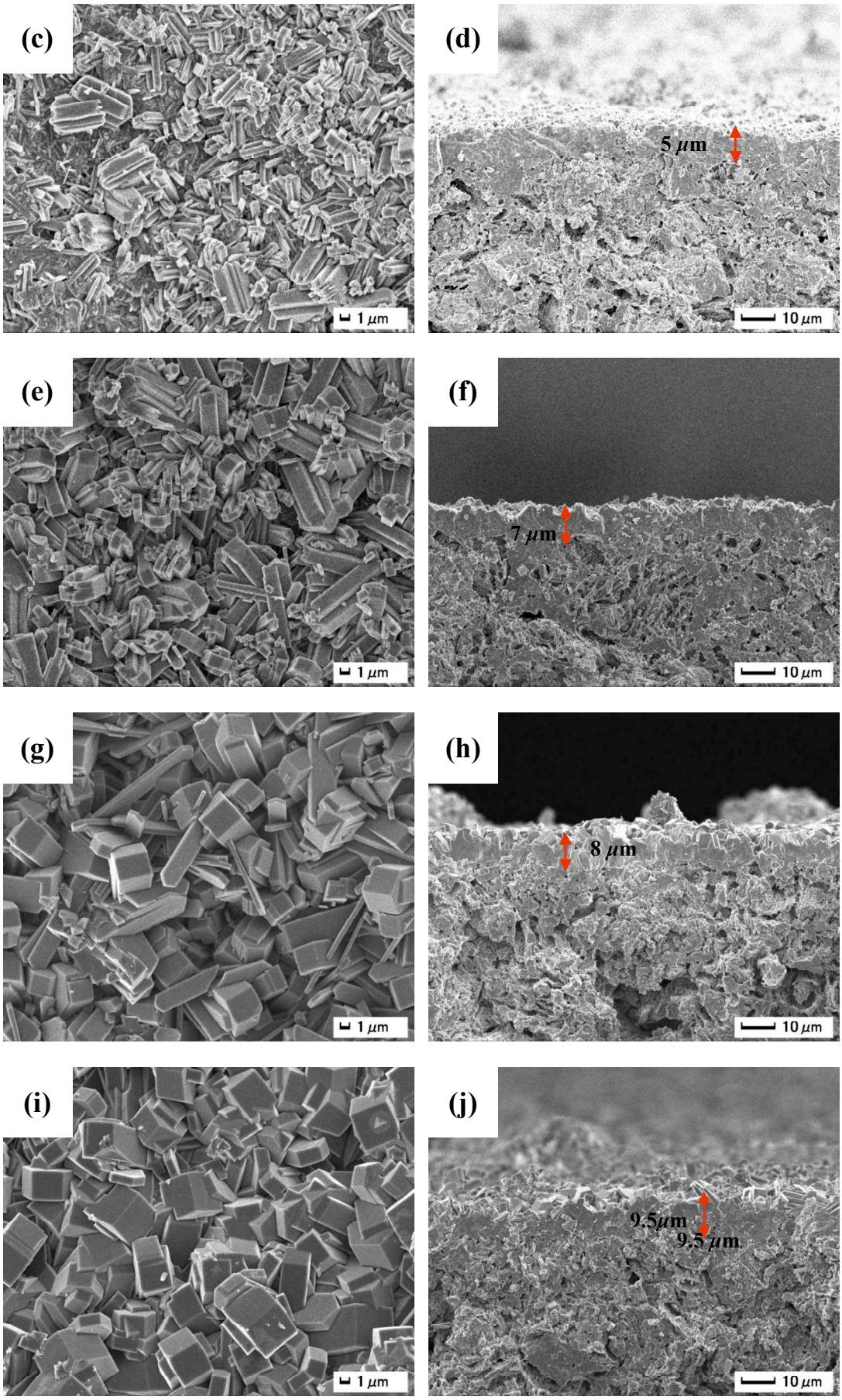
(c)
1 μm
(d)
5 μm
10 μm
(e)
1 μm
(f)
7 μm
10 μm
(g)
1 μm
(h)
8 μm
10 μm
(i)
1 μm
(j)
9.5μm
9.5 μm
10 μm

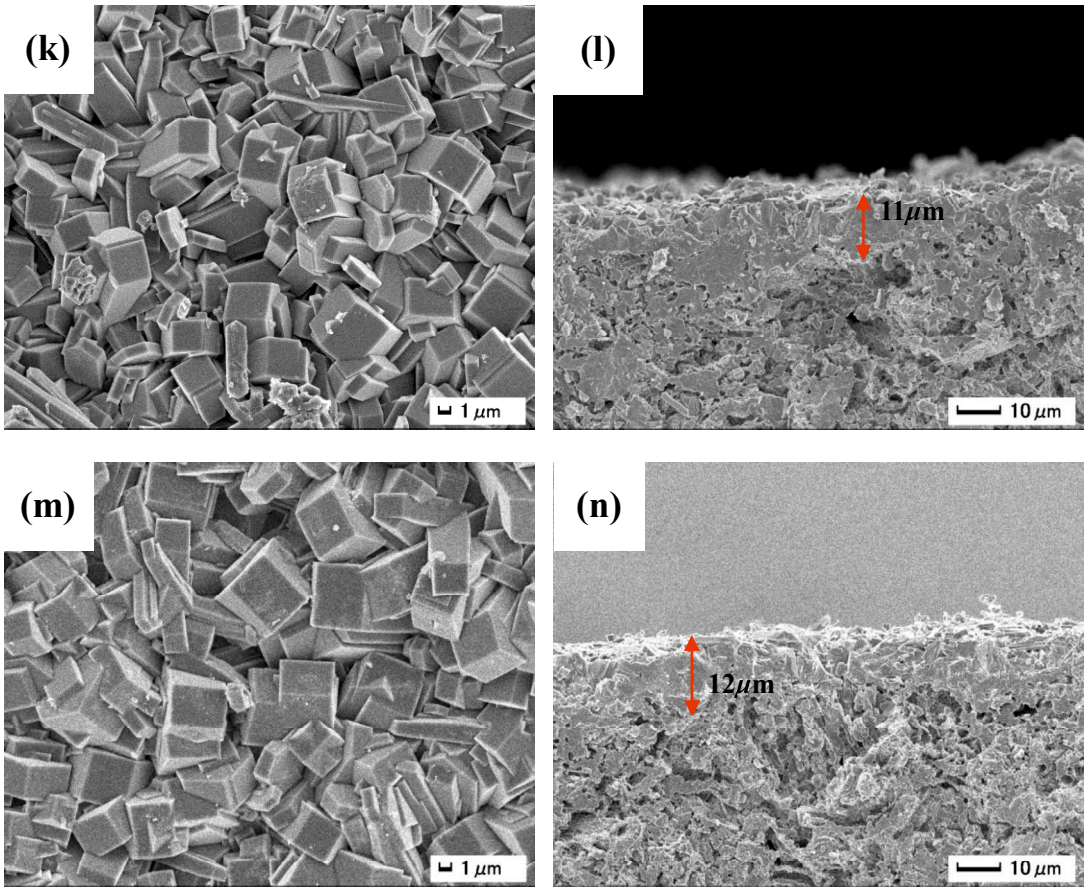

Figure 5-13 SEM images of mullite support seeded with micrometer-sized crystals and MFI membranes prepared at 458 K for (a, b) 2h, (c, d) 4h, (e, f) 6 h, (g, h) 8 h, (i, j) 12 h,(k, l) 14 h and (m, n) 16 h.

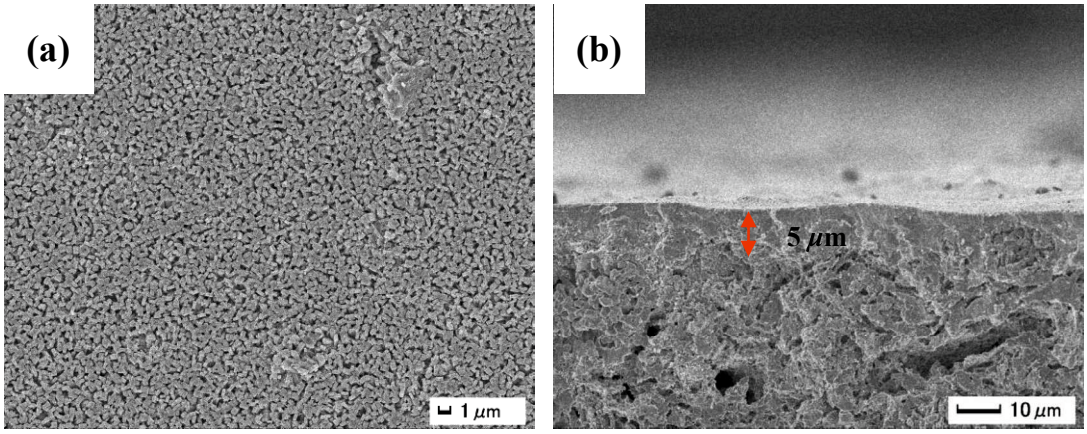

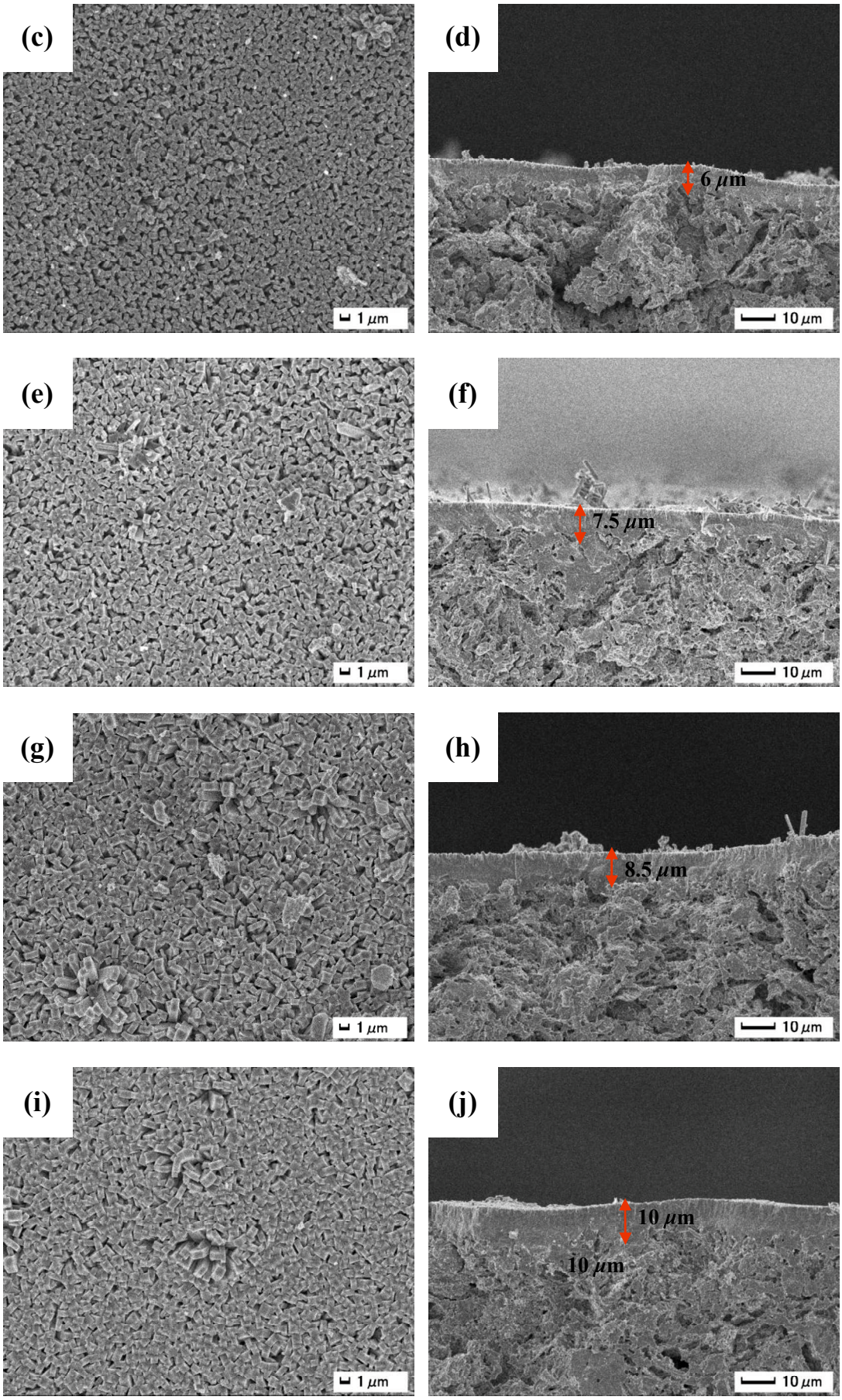
(c)
1 μm
(d)
6 μm
10 μm
(e)
1 μm
(f)
7.5 μm
10 μm
(g)
1 μm
(h)
8.5 μm
10 μm
(i)
1 μm
(j)
10 μm
10 μm
10 μm

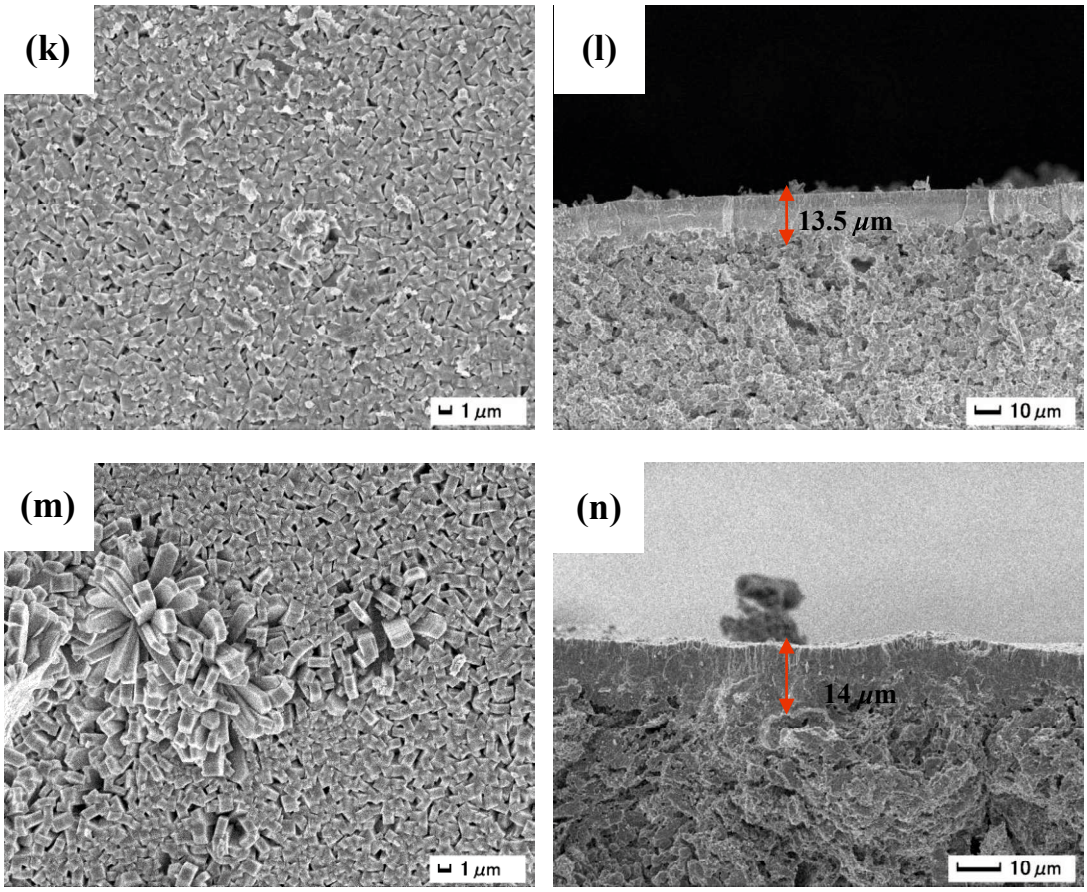

Figure 5-14 SEM images of mullite support seeded with nanometer-sized crystals and MFI membranes prepared at 458 K for (a, b) 2h, (c, d) 4h, (e, f) 6 h, (g, h) 8 h, (i, j) 12 h,(k, l) 14 h and (m, n) 16 h.

Besides, c-axis facilitates H_2 permeance of MFI membranes [23, 24]. The actual membrane thicknesses of the membranes are not very different. Therefore, it can be estimated the strong (002) orientation also made contribution to high H_2 permeances of silicalite-1 membranes prepared with smaller seed. In addition, when smaller seed was used, membranes show better α^{ideal} (H_2/SF_6), which should be due to the compactness of silicalite-1 membranes. Seeded smaller supports always have fewer gaps between crsytals, which favors of crystal growth on supports.

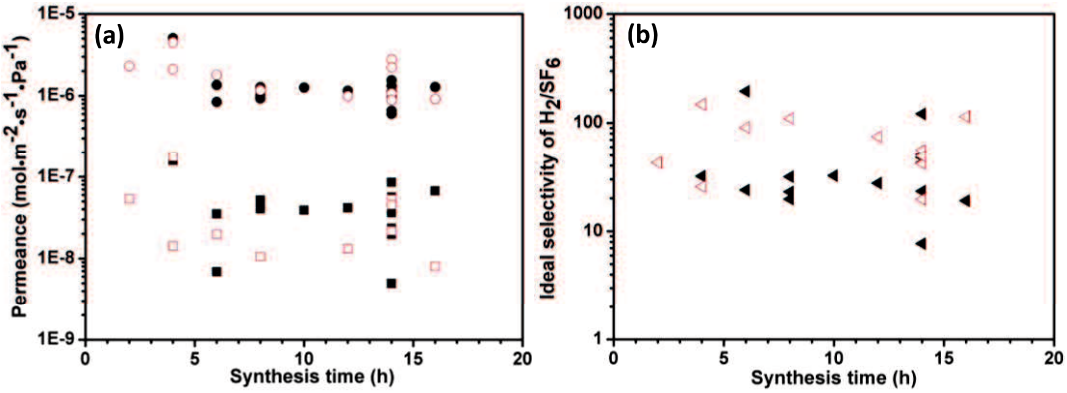

Figure 5-15 (a) H_2 and SF_6 single gas permeance and (b) ideal selectivities of H_2/SF_6 as a function of synthesis time for silicalite-1 membranes prepared with seeds with different particle sizes. (Closed symbols: using larger seed crystals, open symbols: using smaller seed crystals,○ and● : H_2 permeance, □and ■: SF_6 permeance)

5.3.2.4 Effect of support

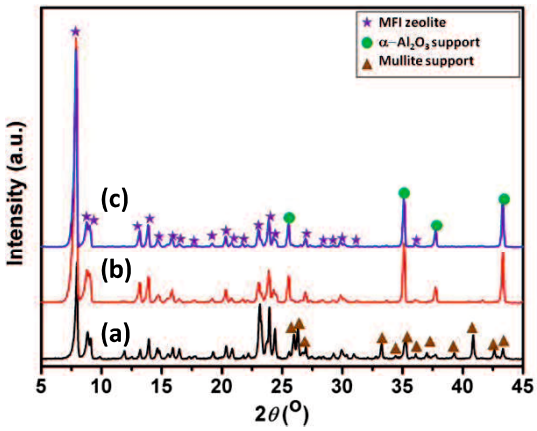

Figure 5-16 XRD patterns of silicalite-1 membranes prepared on different supports: (a) mullite, (b) symmetric α-Al_2O_3 support and (c) NS-1 support.

The XRD patterns of membranes formed on mullite support, symmetric α-Al_2O_3 support and NS-1 support have been showed in **Figure 5-16**. It indicates that it is easy to obtain pure silicalite-1 membranes with the current conditions. **Figure 5-13 (a-b)**, **Figure 5-17 (a-b)** and **Figure 5-17 (e-f)** are SEM images of seeded mullite support, symmetric α-Al_2O_3 support and NS-1 support, respectively. Many seed crystals can be seen in support pores in **Figure 5-17 (b)** so that many silicalite-1 zeolite crystals formed inside support channels as marked by red circle in **Figure 5-17(d)**.

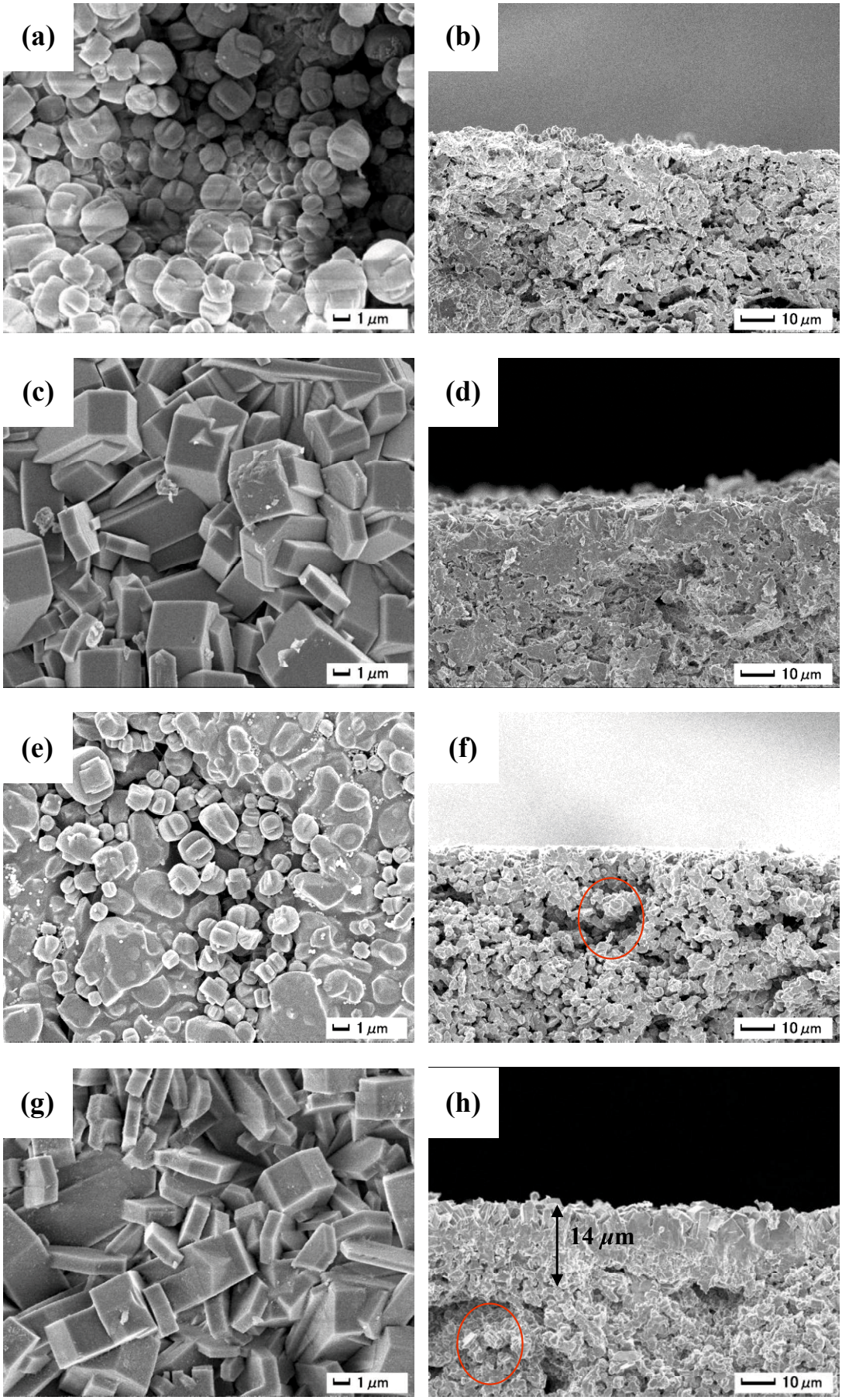
(a)
1 μm
(b)
10 μm
(c)
1 μm
(d)
10 μm
(e)
1 μm
(f)
10 μm
(g)
1 μm
(h)
14 μm
10 μm

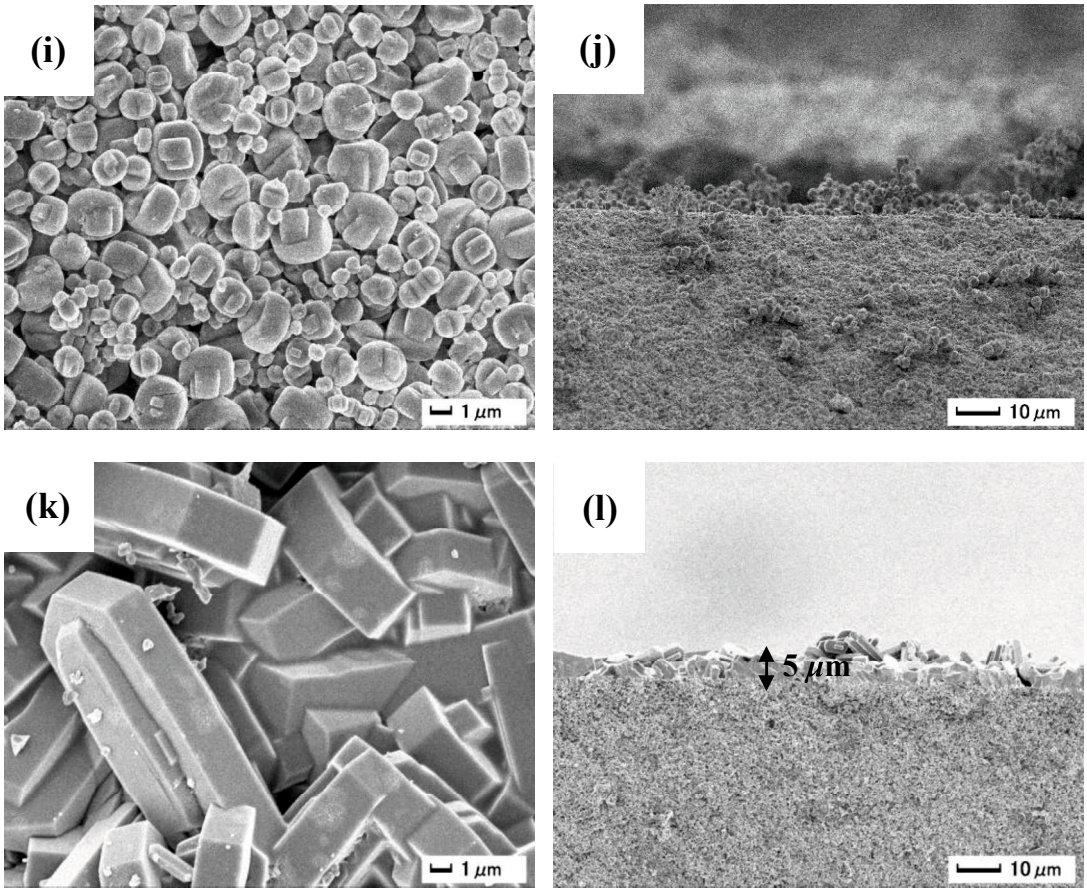

Figure 5-17 SEM images of (a-b) seeded mullite support, (c-d) silicalite-1 membrane on mullite support, (e-f) seeded α-Al_2O_3 support, (g-h) silicalite-1 membrane on α-Al_2O_3 support, (i-j) seeded NS-1support and (k-l) silicalite-1 membrane on NS-1 support, respectively.

Moreover, silicalite-1 membrane on α-Al_2O_3 is about 14 μm. However, there are no crystals penetrating into the NS-1 support pore after seeding because of the sufficient small pore size of NS-1 support as showed in **Figure 5-17 (f)**. Besides the membrane layer on NS-1 support is just about 5 μm. As **Table 5-1** shows, one silicalite-1 membrane on NS-1 support shows α^{ideal} (H_2/SF_6) and H_2 permeance of 151.2 and 6.5×10^{-7} mol·m^{-2}·s^{-1}·Pa^{-1}, respectively. Due to the thick membrane layer, H_2 permeance of silicalite-1 membrane on symmetric α-Al_2O_3 is lower, and one membrane shows H_2 permeance of 1.4×10^{-7} mol·m^{-2}·s^{-1}·Pa^{-1} and the α^{ideal} (H_2/SF_6) of 155.6. In additon, more gas permeation results of membranes on three supports using two seeds show H_2 permeation performance differently. The results can be seen in **Figure 5-18**. Smaller seed can improve membrane compactness and membranes on

mullite can show much higher H_2 permeance, which is more important for commerciallzation.

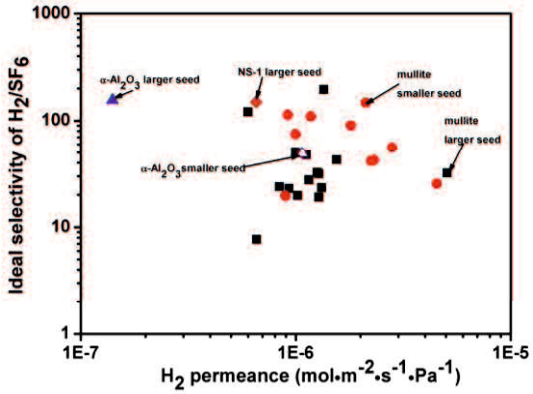

Figure 5-18 H_2 permeance of silicalite-1 membrane formed on different supports gas as a function of α^{ideal} (H_2/SF_6) (0.40 MPa, 308 K)

5.3.3 Gas permeation performance of silicalite-1 membranes on mullite support

5.3.3.1 Effect of measurement temperature

Herein, 7 kinds of single gases were used. **Figure 5-19** shows the all single gases permeation performance of the membrane as a function of gas molecular kinetic diameter at a temperature varied from 308 K to 473 K. The pressure difference was fixed on 0.40 MPa.

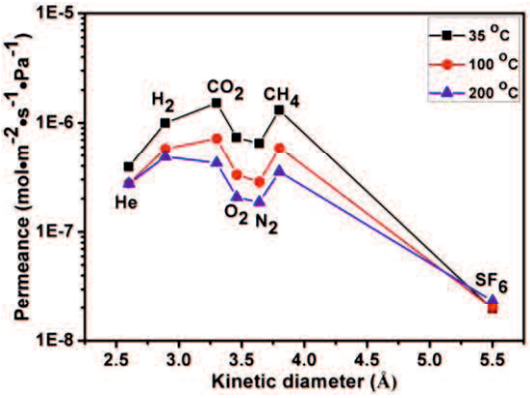

Figure 5-19 Single gas permeation performance of silicalite-1 membrane formed on mullite support as a function of molecular kinetic diameter of every single gas (ΔP = 0.40 MPa).

When the measurement temperature is low (308 K), H_2 permeance is 9.99×10^{-7} $mol\cdot m^{-2}\cdot s^{-1}\cdot Pa^{-1}$ and the α^{ideal} (H_2/SF_6) is 50.0. However, when the measurement temperature is as high as 473 K, the H_2 permeance decreased to 4.9×10^{-7} $mol\cdot m^{-2}\cdot s^{-1}\cdot Pa^{-1}$ and the α^{ideal} (H_2/SF_6) also decreased to 20.7. Moreover, other single gases also show higher permeances than the results of membrane measured at higher temperature.

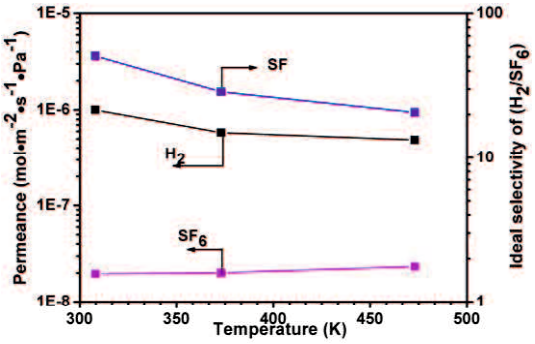

Figure 5-20 H_2 and SF_6 single gas permeation performance as a function of measurement temperature. ($\Delta P = 0.40$ MPa).

Because SF_6 moves fast at higher temperature [25] , SF_6 permeance increased from 2.0×10^{-7} $mol\cdot m^{-2}\cdot s^{-1}\cdot Pa^{-1}$ to 2.3×10^{-7} $mol\cdot m^{-2}\cdot s^{-1}\cdot Pa^{-1}$ as temperature increased as shown in **Figure 5-20**. However, H_2 permeance decreased so that permselectivity of H_2 and SF_6 decreased from 51 to 21.

5.3.3.2 Effect of measurement pressure difference

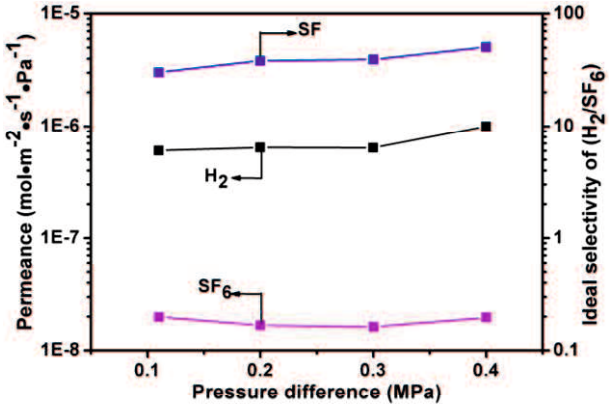

Figure 5-21 H_2 and SF_6 single gas permeation performance as a function of measurement pressure difference. (Temperature is 308 K).

Figure 5-21 shows the result of H_2 and SF_6 permeation as a function of pressure difference. Although at lower pressure difference, the gas permeation performance is better [25], both of H_2 and SF_6 permeation here didn't allow to this principle. It may be due to the effect of some inter-crystal pores.

5.3.3.3 Long-term stability

The silicalite-1 membrane on mullite was applied to a long-term stability measurement. The membrane was kept in the air at room temperature before every measurement. And before measurement, membrane was vacuumed in the module fore over 12 h.

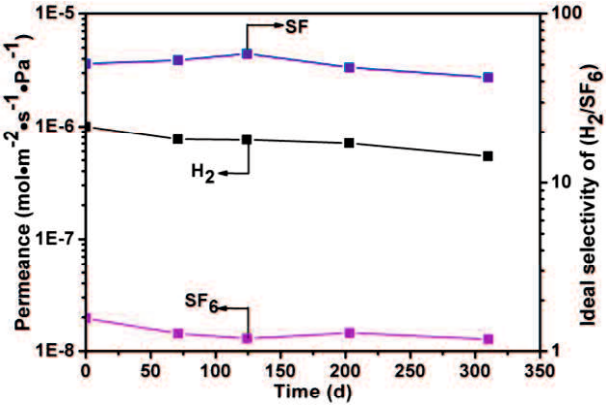

Figure 5-22 Long-term stability of H_2 and SF_6 permeation performance of silicalite-1 membrane on mullite support (308 K, ΔP = 0.40 MPa)

Figure 5-22 shows the result of H_2 and SF_6 permeation performance. When the save time was less than 203 d, H_2 permeance just reduced from 9.99×10^{-7} $mol\cdot m^{-2}\cdot s^{-1}\cdot Pa^{-1}$ to 7.05×10^{-7} $mol\cdot m^{-2}\cdot s^{-1}\cdot Pa^{-1}$. After 203 d, the silicalite-1 membrane can still show a high H_2 permeance of 5.40×10^{-7} $mol\cdot m^{-2}\cdot s^{-1}\cdot Pa^{-1}$. Besides, the α^{ideal} (H_2/SF_6) varied between 58.2 and 42.2. The results demonstrate that silicalite-1 membranes in this work have good gas permeation stability.

5.3.4 Comparison

In **Table 5-2**, H_2 and SF_6 permeances silicalite-1 membranes in this work are compared with data in papers. The measurement conditions are also list in the table.

The H_2 permeances vary from 3.05×10^{-7} mol·m^{-2}·s^{-1}·Pa^{-1} to 0.93×10^{-7} mol·m^{-2}·s^{-1}·Pa^{-1} and the SF_6 permeances vary from 4.4×10^{-8} mol·m^{-2}·s^{-1}·Pa^{-1} to 3.1×10^{-10} mol·m^{-2}·s^{-1}·Pa^{-1}. The ideal selectivity ranges from 6.7 up to 165. It is obviously that H_2 permeance of membranes in this work is comparable with H_2 permeance of most silicalite-1 membranes in papers. Compared with data in papers, both of silicalite-1 membranes formed on mullite and NS-1 supports own high H_2 permeance and ideal selectivity of H_2/SF_6. On the other hand, gas permeation measurement method seems have obvious effect on H_2 permeation performance of silicalite-1 membranes.

Table 5-2 Comparison of H_2 and SF_6 permeances and ideal selectivity for silicalite-1 membranes in this work with reported data of silicalite-1 membranes

Measurement method	Support	Measurement conditions		Permeance (10^{-8} mol·m^{-2}·s^{-1}·Pa^{-1})		α^{ideal}	F-mediate	Ref.
		ΔP (MPa)	T (K)	H_2	SF_6			
Vacuum	SSS[a]	0.20	378	9.3	0.031	300	No	[26]
Vacuum	SSS[b]	0.20	298	23.6	0.56	42.2	No	[25]
PD[a]	SSS[b]	0.10	298	43.0	0.84	51	No	[27]
PD[a]	α-Al_2O_3[c]	0.08	298	2190	130	17	No	[28]
PD[a]	SSS[c]	0.06	473	10.0	1.50	6.7	No	[29]
PD[a]	α-Al_2O_3[d]	0.12	323	256.0	4.40	58.1	No	[30]
PD[a]	α-Al_2O_3[d]	0.12	323	305.0	3.80	80.4	No	[30]
Sweep gas	α-Al_2O_3[c]	0.10	300	23.2	0.14	165	No	[31]
Sweep gas	α-Al_2O_3[c]	0.10	300	19.6	0.13	150	No	[31]
Sweep gas	YZ[e]	0.10	300	36.9	2.88	13	No	[31]
Sweep gas	YZ[e]	0.10	300	9.81	0.118	83	No	[31]
/	α-Al_2O_3[d]	0.10	323	73.6	2.57	28.6	No	[32]
/	α-Al_2O_3[d]	0.12	323	120	1.42	84.8	No	[33]
Vacuum	Mullite[f]	0.40	308	99.90	2.00	50	Yes	This work
Vacuum	α-Al_2O_3[d]	0.40	308	14.00	0.09	155.6	Yes	This work
Vacuum	NS-1[d]	0.40	308	65.00	0.43	151.2	Yes	This work

PD[a]: pressure difference method, SSS[a]: stainless steel tube, SSS[b]: stainless steel No disc,α-Al_2O_3[c] disk,α-Al_2O_3[d] tube (NS-1: asymmetric α-Al_2O_3 tube), YZ[e]: YZ-α-alumina-supported (yttria-doped zirconia) disc, Mullite[f]: Mullite tube.

5.4 Conclusions

Pure silicalite-1 membranes have been prepared at different conditons. The variation of silica sources influences the morphology of silicalite-1 membranes significantly. TEOS can induce silicalite-1 membranes with continuous membrane layer and best single gas permeation performance. Crystal shapes are different when HS-40 and fumed SiO_2 were used. It resulted in poor gas permeation performances.

Cystallization temperature affected the membrane thickness. Silicalite-1 membranes prepared at higher temperature show higher H_2 permeance.

Membranes prepared with smaller seed show stronger (002) orientation. When synthesis increased from 2 h to 6 h, H_2 permeance of membranes reduced, but membranes became denser. When the gas permeation measurement temperature is 308 K and pressure difference is 0.40 MPa, better results can be obtained.

Using mullite and NS-1 tubes, silicalite-1 membranes prepared at 185 ^{o}C for 14 h show high H_2 permeance of 9.99×10^{-7} $mol\cdot m^{-2}\cdot s^{-1}\cdot Pa^{-1}$ and 6.52×10^{-7} $mol\cdot m^{-2}\cdot s^{-1}\cdot Pa^{-1}$, respectively. And the α^{ideal} (H_2/SF_6) are 50 and 151.2, respectively. The results are comparable to data in papers. Silicalite-1 membrane in this work can show good stability for H_2 permeation.

References

[1] N.W. Ockwig, T.M. Nenoff, Membranes for hydrogen separation, Chemical Reviews, 107 (2007) 4078-4110.

[2] W.C. Wong, L.T.Y. Au, C.T. Ariso, K.L. Yeung, Effects of synthesis parameters on the zeolite membrane growth, Journal of Membrane Science, 191 (2001) 143-163.

[3] E. Newson, T. Haueter, P. Hottinger, F. Von Roth, G. Scherer, T.H. Schucan, Seasonal storage of hydrogen in stationary systems with liquid organic hydrides, International Journal of Hydrogen Energy, 23 (1998) 905-909.

[4] X. Chen, W. Yang, J. Liu, X. Xu, A. Huang, L. Lin, Synthesis of NaA zeolite membrane with high performance, Journal of Materials Science Letters, 21 (2002) 1023-1025.

[5] M. Yu, H.H. Funke, R.D. Noble, J.L. Falconer, H_2 separation using defect-free, inorganic composite membranes, Journal of the American Chemical Society, 133 (2011) 1748-1750.

[6] M.J. Vaezi, A.A. Babaluo, Effect of dehydration temperature on the H_2 separation potential of hydroxy sodalite zeolite membranes, Iranian Journal of Hydrogen & Fuel Cell, 1 (2015) 209-214.

[7] H. Kalipcilar, T.C. Bowen, R.D. Noble, J.L. Falconer, Synthesis and separation performance of SSZ-13 zeolite membranes on tubular supports, Chemistry of Materials, 14 (2002) 3458-3464.

[8] M. Hong, J.L. Falconer, R.D. Noble, Modification of zeolite membranes for H_2 separation by catalytic cracking of methyldiethoxysilane, Industrial and Engineering Chemistry Research, 44 (2005) 4035-4041.

[9] R.W. Baker, Membrane technology and applications, 3rd Edition, WILEY, 2012.

[10] M. Kanezashi, Y. Lin, Gas permeation and diffusion characteristics of MFI-type zeolite membranes at high temperatures, The Journal of Physical Chemistry C, 113 (2009) 3767-3774.

[11] H. Richter, I. Voigt, G. Fischer, P. Puhlfürß, Preparation of zeolite membranes on the inner surface of ceramic tubes and capillaries, Separation and Purification

Technology, 32 (2003) 133-138.

[12] X. Gu, Z. Tang, J. Dong, On-stream modification of MFI zeolite membranes for enhancing hydrogen separation at high temperature, Microporous and Mesoporous Materials, 111 (2008) 441-448.

[13] J. Stelzer, M. Paulus, M. Hunger, J. Weitkamp, Hydrophobic properties of all-silica zeolite beta, Microporous and Mesoporous Materials, 22 (1998) 1-8.

[14] M. Zhou, D. Korelskiy, P. Ye, M. Grahn, J. Hedlund, A uniformly oriented MFI membrane for improved CO_2 separation, Angewandte Chemie International Edition, 53 (2014) 3492-3495.

[15] X. Zhang, M. Zhu, R. Zhou, X. Chen, H. Kita, Synthesis of silicalite-1 membranes with high ethanol permeation in ultradilute solution containing fluoride, Separation and PurificationTechnology, 81 (2011) 480-484.

[16] C. Nicolas, P. M, Synthesis and characterisation of nanocomposite Ge-MFI-alumina membranes for CO_2/N_2 separation from wet flue gases, Microporous and Mesoporous Materials, 153 (2012) 254-262.

[17] H. Zhou, D. Korelskiy, E. Sjöberg, J. Hedlund, Ultrathin hydrophobic MFI membranes, Microporous and Mesoporous Materials, 192 (2014) 76-81.

[18] G. Cao, Y. Lu, L. Delattre, C.J. Brinker, G.P. López, Amorphous silica molecular sieving membranes by sol-gel processing, Advanced Materials, 8 (1996) 588-591.

[19] Y. Cui, H. Kita, K. Okamoto, Preparation and gas separation performance of zeolite T membrane, Journal of Materials Chemistry, 14 (2004) 924-932.

[20] M.M. Treacy, J.B. Higgins, Collection of simulated XRD powder patterns for zeolites fifth (5th) revised edition, Elsevier, 2007.

[21] X. Zhang, M. Zhu, R. Zhou, X. Chen, H. Kita, Synthesis of a silicalite zeolite membrane in ultradilute solution and its highly selective separation of organic/water mixtures, Industrial and Engineering Chemistry Research, 51 (2012) 11499-11508.

[22] X. Zhang, H. Liu, K.L. Yeung, Influence of seed size on the formation and microstructure of zeolite silicalite-1 membranes by seeded growth, Materials Chemistry and Physics, 96 (2006) 42-50.

[23] P.H. Nelson, M. Tsapatsis, S.M. Auerbach, Modeling permeation through

anisotropic zeolite membranes with nanoscopic defects, Journal of Membrane Science, 184 (2001) 245-255.

[24] J. O'Brien-Abraham, M. Kanezashi, Y. Lin, A comparative study on permeation and mechanical properties of random and oriented MFI-type zeolite membranes, Microporous and Mesoporous Materials, 105 (2007) 140-148.

[25] M. Noack, G. Mabande, J. Caro, G. Georgi, W. Schwieger, P. Kölsch, A. Avhale, Influence of Si/Al ratio, pre-treatment and measurement conditions on permeation properties of MFI membranes on metallic and ceramic supports, Microporous and Mesoporous Materials, 82 (2005) 147-157.

[26] M. Noack, P. Kölsch, J. Caro, M. Schneider, P. Toussaint, I. Sieber, MFI membranes of different Si/Al ratios for pervaporation and steam permeation, Microporous and Mesoporous Materials, 35 (2000) 253-265.

[27] G. Mabande, G. Pradhan, W. Schwieger, M. Hanebuth, R. Dittmeyer, T. Selvam, A. Zampieri, H. Baser, R. Herrmann, A study of silicalite-1 and Al-ZSM-5 membrane synthesis on stainless steel supports, Microporous and Mesoporous Materials, 75 (2004) 209-220.

[28] J. Hedlund, J. Sterte, M. Anthonis, A. Bons, B. Carstensen, N. Corcoran, D. Cox, H. Deckman, W. De Gijnst, P. de Moor, High-flux MFI membranes, Microporous and Mesoporous Materials, 52 (2002) 179-189.

[29] V.A. Tuan, J.L. Falconer, R.D. Noble, Isomorphous substitution of Al, Fe, B, and Ge into MFI-zeolite membranes, Microporous and Mesoporous Materials, 41 (2000) 269-280.

[30] L. Au, K. Yeung, An investigation of the relationship between microstructure and permeation properties of ZSM-5 membranes, Journal of Membrane Science, 194 (2001) 33-55.

[31] J.H. Dong, Y. Lin, M.Z.C. Hu, R.A. Peascoe, E.A. Payzant, Template-removal-associated microstructural development of porous-ceramic-supported MFI zeolite membranes, Microporous and Mesoporous Materials, 34 (2000) 241-253.

[32] Y.J. Xiao W., Wu H., Wang, J., Preparation of silicalite-1 zeolite membrane on

porous α-Al_2O_3 tube by modified secondary growth method and its characterization, Petrochemical Technology, 38 (2009) 497-503.

[33] D.M.S. C. L. Kong, J.M. Lu, J.H. Yang, J.Q. Wang, Synthesis of silicalite-1 membrane by a novel embellishing method and its gas permeance, Acta Petrolei Sinica (Peroleum Processing Section), 24 (2008) 106-111.

Chapter 6 Gas permeation performance of silicalite-1 zeolite membranes modified by 3-aminopropyltriethoxysilane

6.1 Introduction

Hydrogen is a clean fuel and used widely [1]. Before using H_2, methylcyclohexane-toluene-hydrogen system is often used to realize H_2 storage [2]. Thus, many researchers have investigated H_2 purification from larger gas molecules, such as SF_6 (0.55 nm) [3] which is a little larger than toluene (0.59 nm) [4].

K. Oda et al. obtained H_2/SF_6 permselectivity of around 10^4 and H_2 permeance of 1.3×10^{-6} $mol\cdot m^{-2}\cdot s^{-1}\cdot Pa^{-1}$ by using a amorphous silica membrane at 573 K [5]. K. Akamatsu et al. also prepared an amorphous silica membrane and obtained H_2 permeance of 1.20×10^{-6} $mol\cdot m^{-2}\cdot s^{-1}\cdot Pa^{-1}$ and the permselectivity of H_2/SF_6 was as high as 15000 [6]. On the other hand, R. D. Noble et al. measured silicalite-1zeolite membranes at 298 K and the permselectivity of H_2/SF_6 was 136 [7]. M. Noack et al. prepared silicalite-1 membranes on stainless steel discs and they obtained H_2 permeance and H_2/SF_6 permselectivity of 2.36×10^{-7} $mol\cdot m^{-2}\cdot s^{-1}\cdot Pa^{-1}$ and 42.2, respectively. Q.Y. Zhao et al. reported their MFI membrane has a H_2 permeance and permselectivity of H_2/SF_6 of 1.64×10^{-6} $mol\cdot m^{-2}\cdot s^{-1}\cdot Pa^{-1}$ and 71, respectively [7].

So far, many modification ways have been used to improve compactness of zeolite membranes. B-ZSM-5 and SAPO-34 membranes were silylated by the catalytic cracking deposition (CCD) of methydiethoxysilane [8]. DDR membranes have been modified by chemical vapor deposition (CVD) [9]. And H_2/CO_2 permselectivity was improved from 2.6 to 32.7 at 823 K. Silicalite-1 membranes were modified by surface modification which calcined TEOS in pores. $H_2/n\text{-}C_4H_{10}$ permselectivity increased a lot [10]. After modifying supports with 3-aminopropyltriethoxysilane (APTES), separation factors of H_2/CH_4, H_2/N_2, H_2/O_2 and H_2/CO_2 of LTA membranes were improved significantly [11]. The H_2 permeance can be as high as 3.0×10^{-7} $mol\cdot m^{-2}\cdot s^{-1}\cdot Pa^{-1}$. Moreover, by treating supports

with APTES, FAU membranes showed H_2 permeance and separation factor of H_2/CO_2 of 4.0×10^{-7} mol·m^{-2}·s^{-1}·Pa^{-1} and 6.5, respectively [12]. Silicalite-1 membranes also have ever been prepared on APTES modified supports. N_2 permeance was reduced effectively [13].

In this work, as-synthesized silicalite-1 membrane surface was modified with APTES to reduce existing defects. It is an easy way to improve permselectivity of H_2 other gases. Effects of different measurement conditions were investigated. The gas permeation performances of unmodified and modified silicalite-1 membranes were compared in detail.

6.2 Experimental

6.2.1 Raw materials

Tetraethyl orthosilicate (TEOS, 98%, Aldrich), tetrapropylammonium hydroxide (TPAOH, 20-25% in water, Tokyo kasei), tetrapropylammonium bromide (TPABr, 99%, Tokyo kasei), ammonium floride (NH_4F, 99.99%, Aldrich), sodium hydroxide (NaOH, 97%, Wako) and distilled water were used to prepare silicalite-1 crystals and silicalite-1 membranes.

Silicalite-1 membranes were formed on NS-1 support. NS-1 tube (o.d. 10 mm, i.d. 7 mm and length 100 mm with a membrane area of 31.40 cm^2) has an average pore size 0.15 μm and porosity of 35-45 %.

6.2.2 Membrane preparation

The synthesis process of silicalite-1 seed has been described in detail in **Chapter 5**. The synthesis solution for membranes has a molar ratio of SiO_2: TPAOH: TPABr: NH_4F: H_2O = 1: 0.20: 0.10: 0.10: 500. The tubes were cleaned with distilled water and dried at 353 K over night before use. The reaction solution was prepared as follows. Firstly, TPAOH was drop wisely added to water. After stirring for 5 min, TPABr was added. 10 min later, as silica source, TEOS was added into water/template mixture under stirring. In this work, silicalite-1 membranes were synthesized in

fluoride mediate.After stiiring for 1 h, NH_4F was finally added to provide F^-. After the rub coated with micrometer sized crystals, supports were dried at 353 K for over 30 min and then put vertically into an autoclave. Silicalite-1 membranes were synthesized at 458 K for 14 h. After crystallization, the membranes were washed thoroughly until neutral. The synthesized membranes were calcined at 773 K for 20 h to remove the organic compounds. The calcination heating and cooling rates are 0.26 K/min and 0.39 K/min, respectively.

6.2.3 Membrane modification

As-synthesized silicalite-1 membrane was treated with APTES (0.6 mM in 10 mL toluene) at 383 K for 3 h under influx, leading to APTES monolayer deposited on the membrane surface. The mechanism was shown in **Figure 6-1**. **Figure 6-1(a)** shows the ideal modification between APTES and crystal surface. **Figure 6-2(b)** shows the reaction between APTES and APTES, which can fabricate a net topology on membrane layer in this work. The modification setup is shown in **Figure 6-2**. After modification, the membrane was washed with toluene to remove the successive APTES.

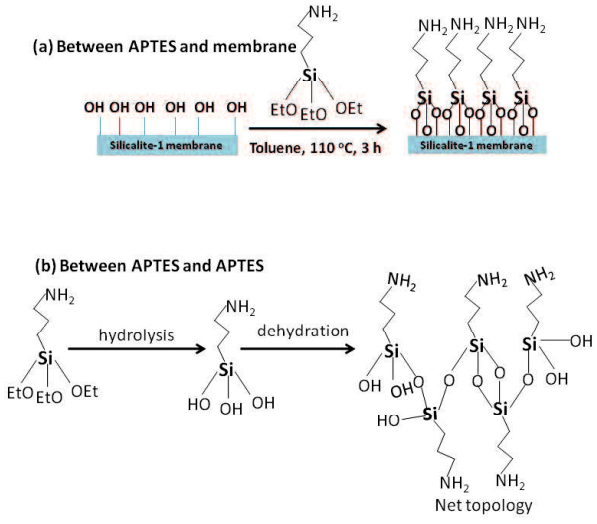

Figure 6-1 Schematic diagram for modification of silicalite-1 membrane by using 3-aminopropyltriethoxysilane (APTES): (a) APTES reacts with surface silanol group of silicalite-1 crystal and (b) APTES react with surface silanol group of APTES

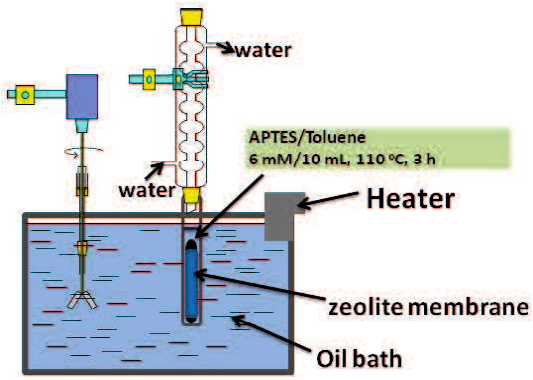

Figure 6-2 Setup of modification process.

6.2.4 Characterization

X-ray diffraction (XRD, SHIMADZU XRD-6100) with Cu-$K\alpha$ radiation was used to identify crystal structures of silicalite-1 crystals and membranes. These spectra were scanned in the range of 2θ = 5-45^{o} at a scanning rate of 4^{o}/min.

Scanning electron microscopy (FE-SEM, JEOL JSM 6335F) was used to observe the morphologies and thickness of obtained samples.

6.2.5 Single gas permeation

The as-synthesized silicalite-1 membranes were applied to single gas permeation. The gas permeation setup has been shown by Cui et al. [14]. The process is the same as described in **Chapter 5.2.5**.

6.2.6 Nanopermporometry

The process is the same as described in **Chapter 3.2.5.2.**

6.3 Results and discussion

6.3.1 Reproducibility of single gas permeation performance of silicalite-1 membranes

Four silicalite-1 membranes have been prepared on NS-1 supports and the performances have been shown in **Table 6-1**. Three membranes have promising H_2 permeance and ideal selecitivity of H_2/SF_6. However, one membrane (S-4) shows a highest H_2 permeance but a poor ideal selecitivity of H_2/SF_6. As **Chapter 5** described,

there is almost no crystal formed inside NS-1 support and the membrane layer is thin. Therefore, we attempted to apply that membrane to modification using APTES to reduce pinholes as shown in **Figure 6-2**. Modified membrane was also applied to gas permeation.

Table 6-1 Reproducibility of single gas permeation performance of silicalite-1 membranes on NS-1 supports (308 K, ΔP = 0.40 MPa)

No.	Permeance (10^{-8} mol·m^{-2}·s^{-1}·Pa^{-1})		α^{ideal}
	H_2	SF_6	
SI-7	65.20	0.43	151.6
SI-8	52.40	0.67	78.2
SI-9	151.00	2.28	66.2
SI-10	200.00	7.43	26.9

6.3.2 Morphologies of silicalite-1 membrane before and after modification.

Figure 6-4(a-b) shows the typical SEM images of silicalite-1 zeolite membrane before modification. The SEM images indicate that the silicalite-1 zeolite membrane with a thickness of about 4.5 μm is made of coffin-like silicalite-1 crystals and the crystal size is about 10 μm. Some small pinholes can be found easily as marked by red circles in **Figure 6-4(a)**.

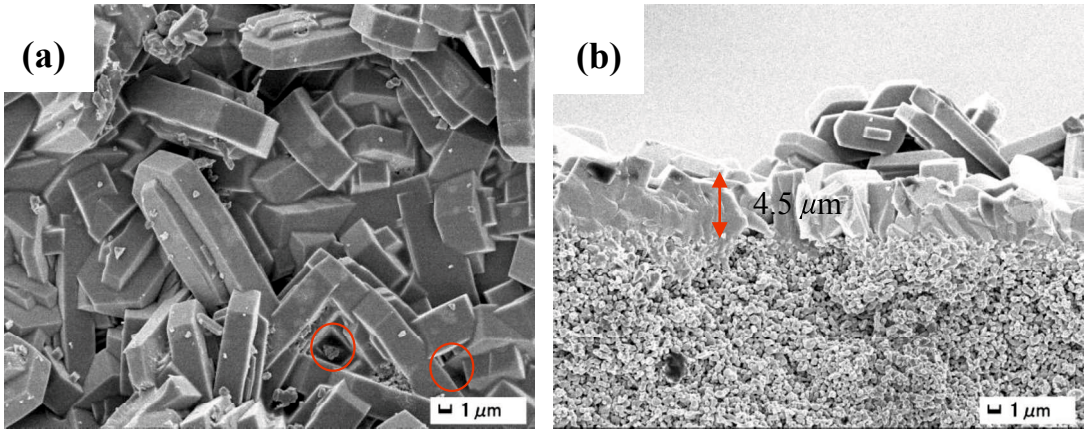

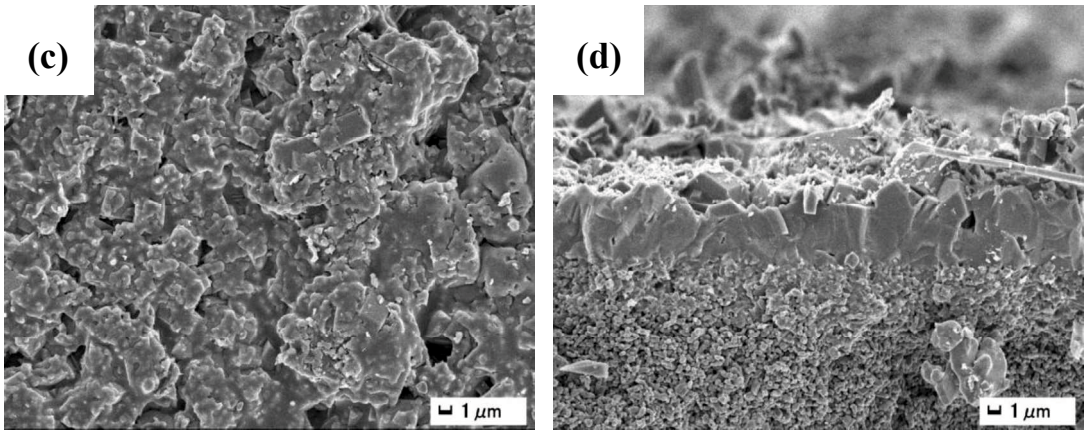

Figure 6-4 Typical SEM images of the MFI zeolite membrane: (a-b) before modification and (c-d) after modification.

A. Huang et al. have found that "the ethoxy groups of APTES react with surface hydroxy groups of the support" [11]. In this work, APTES was used to react with the surface hydroxyl groups of silicalite-1 zeolite crystals so that a net-like layer can be formed on the surface of the membrane. **Figure 6-4(c-d)** shows the SEM images of the modified silicalite-1 membrane. **Figure 6-4(c)** indicates an amorphous layer is covering over the zeolite. **Figure 6-4(d)** shows no changes in the area of cross section. **Figure 6**-5 shows that there is no obvious diversification in the case of XRD pattern after modification.

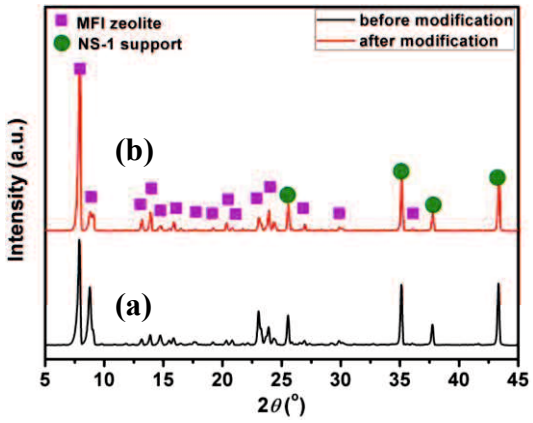

Figure 6-5 XRD patterns of the MFI zeolite membrane: (a) before modification and (b) after modification.

6.3.3 Single gas permeation performance of silicalite-1 membranes

6.3.3.1 All single gases permeation performance under different temperatures

Single gases were measured (He, H_2, CO_2, O_2, N_2, CH_4 and SF_6) at (308~473) K under 0.10 MPa. **Figure 6-6** presents the results for modified membrane at the three selected temperatures in comparison with the results obtained before modification.

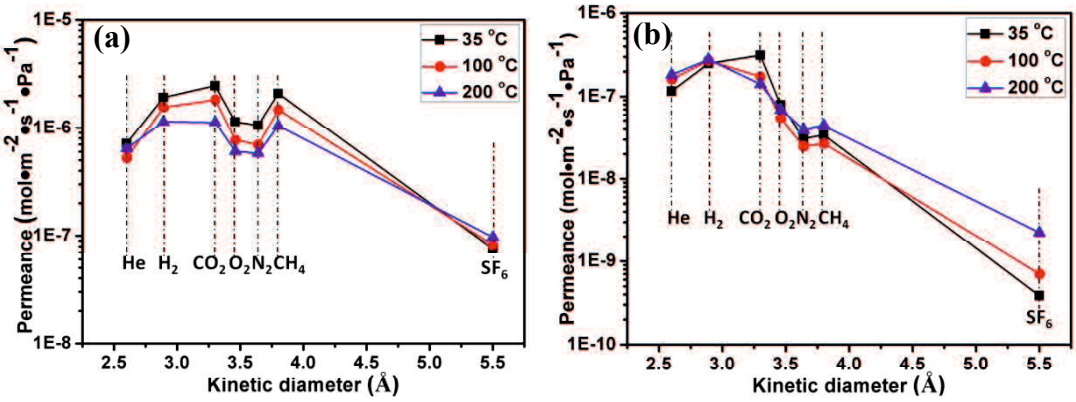

Figure 6-6 Single gas permeance as function of molecular kinetic diameter in the MFI zeolite membrane (a) before and (b) after modification. ($\Delta P = 0.40$ MPa)

Unmodified membrane shows poor permselectivity below the Knudsen factors for H_2 over the other gases except for SF_6 under the temperature arrange. The modification caused an obvious decrease in permeance for all the gas molecules, especially for O_2, N_2, CH_4 and SF_6 whose permeances decreased more than 90% of the previous results.

It was also observed that, the permselectivity for H_2 and He of the modified silicalite-1 membrane behaved oppositely. Before modification, H_2 has larger permeance than He. “Because the dominant Knudsen diffusion mechanism by which the lighter H_2 has greater diffusivity”. [15]. Thus, He decreased less than H_2 although He permeance was still lower than H_2 permeance, and the ideal selectivity of He/H_2 became close to Knudsen diffusion. When the pressure difference was 0.10 MPa and the temperature was 308 K, α^{ideal} (He/H_2) increased from 0.37 to 0.47 and the Knudsen diffusion coefficient was 0.71.

Even though both of CO_2 and H_2 permeances reduced, the α^{ideal} (H_2/CO_2) was the same, and it is 0.8. "The carbon dioxide adsorption capacity was dramatically in creased by the modification" [16].

6.3.3.2 The relationship of the change between H_2 and He permeation

The energy production by nuclear reactions is a very popular research topic in recent decades. Tritium recovery is an important task among the researches [17]. The obtained permeances of H_2 and He and the α^{ideal} (H_2/He) were presented in **Figure 6-7** and **Figure 6-8**, respectively. H_2 still permeates more after modification. Before modification. The α^{ideal} (H_2/He) decreased from 2.7 to 1.8 when temperature increased from 308 K to 473 K. Meanwhile, for the modified membrane, the α^{ideal} (H_2/He) increased from 1.7 to 2.4 at the same conditions. The appearing of small peaks of H_2 and He permeance revealed the competition between the adsorption and translation diffusion as temperature increased [18]. In terms of the effect of pressure difference on H_2 and He permeation performance, **Figure 6-8** shows the changes. For the unmodified silicalite-1 zeolite membrane, both of H_2 and He permeance increased slightly, but the α^{ideal} (H_2/He) decreased a little from 2.7 to 2.4. After modification, the He permance become consistent with H_2 permeance.

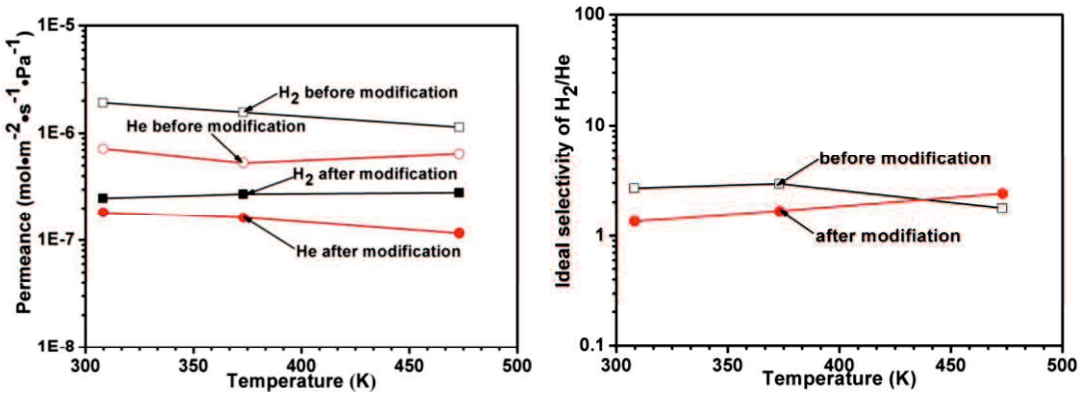

Figure 6-7 Comparison of the relationship between H_2 and He permeation performance in a function of temperature through the MFI zeolite membrane before and after modification (ΔP = 0.11 MPa).

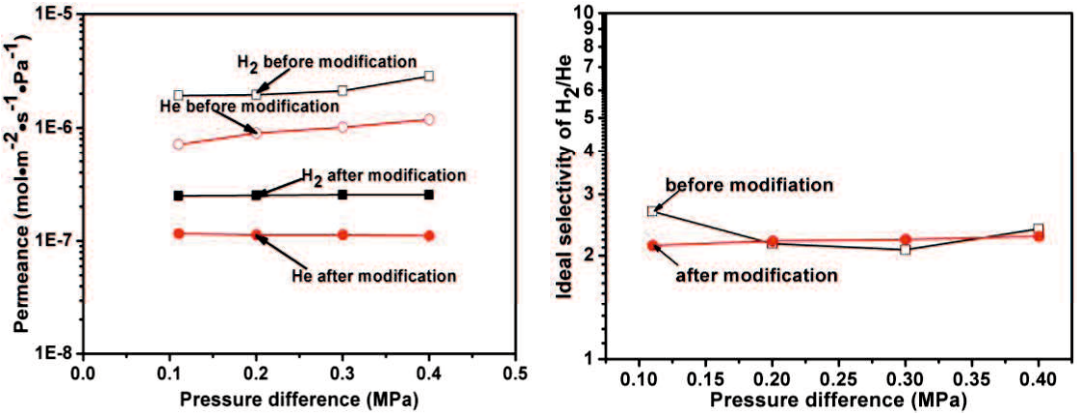

Figure 6-8 Comparison of the relationship between H_2 and He permeation performance in a function of pressure difference through the MFI zeolite membrane before and after modification (T = 308 K).

6.3.3.3 The relationship of the change between H_2 and N_2 permeation

As Figure 6-9 shows, before modification, both of H_2 and N_2 permeances decreased as temperature increased, which is similar as reported by Alshebani et. al. [19]. However, results for modified membrane are very different. N_2 permeance decreased a lot. There are turning points at 373 K for both of permeance and α^{ideal} (H_2/N_2). Based on modification, N_2 permeance decreased a lot so that the α^{ideal} (H_2/N_2) increased to values higher than Knudsen diffusion coefficient 3.7. Moreover, α^{ideal} (H_2/N_2) varied from 7.2 to 10.9.

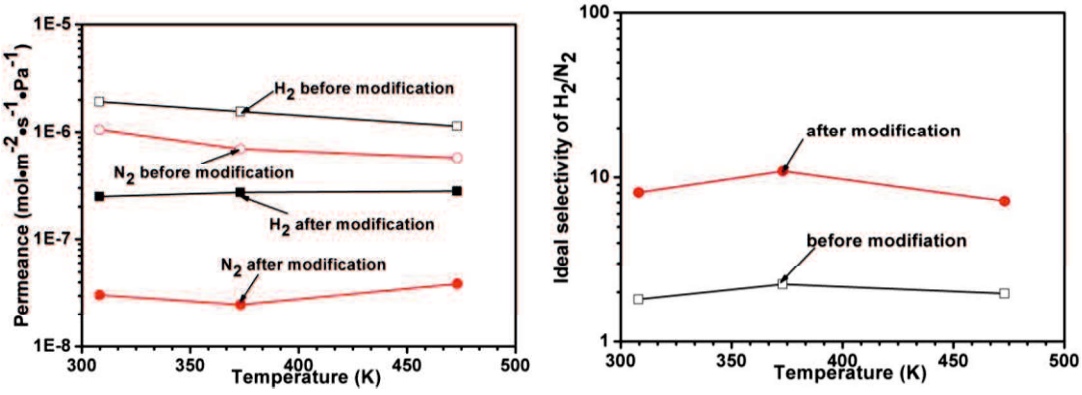

Figure 6-9 Comparison of the relationship between H_2 and N_2 permeation performance in a function of temperature through the MFI zeolite membrane before and after modification (ΔP = 0.11 MPa).

As pressure difference changed, **Figure 6-10** shows no obvious effect on N_2 permeance. After modification, α^{ideal} (H_2/N_2) increased to 4 times and varied slightly from 8.1 to 9.1. However, the unmodified silicalite-1 membrane has α^{ideal} (H_2/N_2) changing from 1.7 to 2.0.

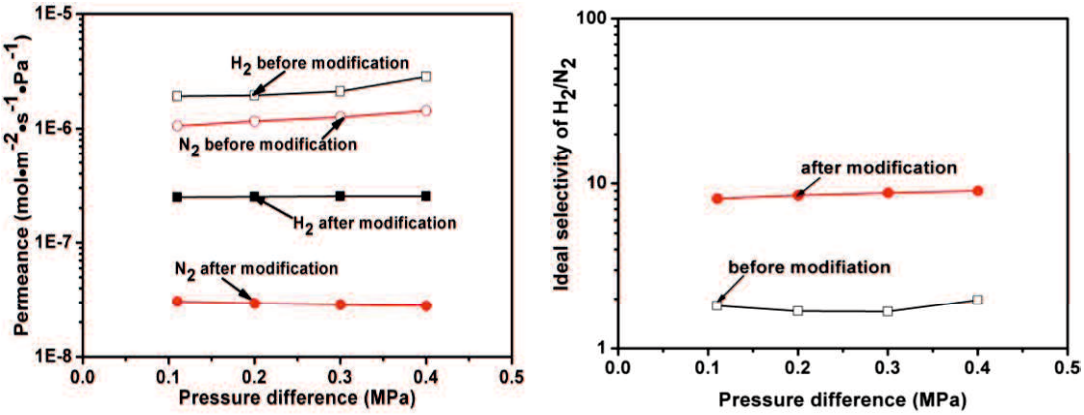

Figure 6-10 Comparison of the relationship between H_2 and N_2 permeation performance in a function of pressure difference through the MFI zeolite membrane before and after modification (T = 308 K).

6.3.3.4 The relationship of the change between H_2 and CH_4 permeation

It is a meaningful task to separate the H_2 and CH_4 in coal gas. **Figure 6-11 and Figure 6-12** shows the effects of temperature and pressure difference. Before modification, H_2 and CH_4 permeance of the silicalite-1 zeolite membrane decreased sharply. "Although H_2 is the smallest molecule because the adsorption of CO_2 and CH_4 is stronger than that of H_2, especially at low temperatures" [20], the CH_4 pemeance is similar as H_2 permeance. To be noted, the α^{ideal} (H_2/CH_4) is just 0.91, which means the CH_4 permeance is higher than H_2 permeance.

After modification, both of H_2 and CH_4 permeance decreased. Because of the reducing permeation pore size in membrane, CH_4 behaved much poor permeation ability so that the α^{ideal} (H_2/CH_4) increased to higher than Knudsen diffusion coefficient (2.8) and varied from 6.4 to 10.1. Besides, there is a common phenomenon of the α^{ideal} (H_2/CH_4) as temperature changed. That is there is a slight max with temperature.

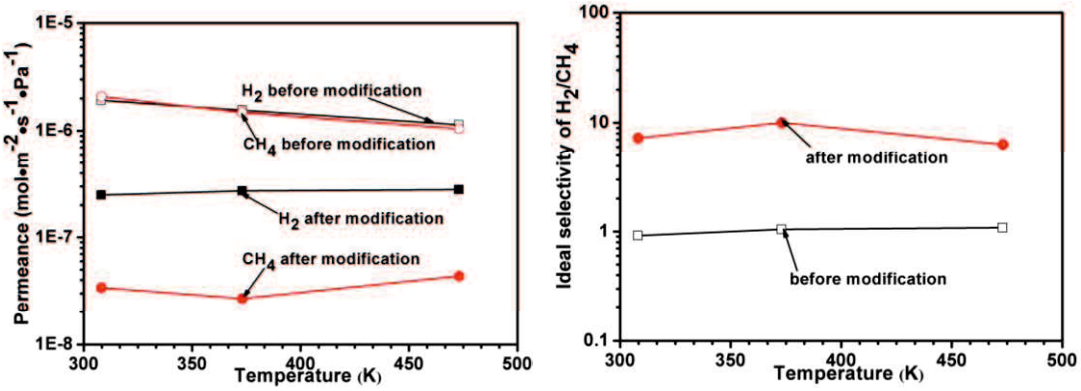

Figure 6-11 Comparison of the relationship between H_2 and CH_4 permeation performance in a function of temperature through the MFI zeolite membrane before and after modification (ΔP = 0.11 MPa).

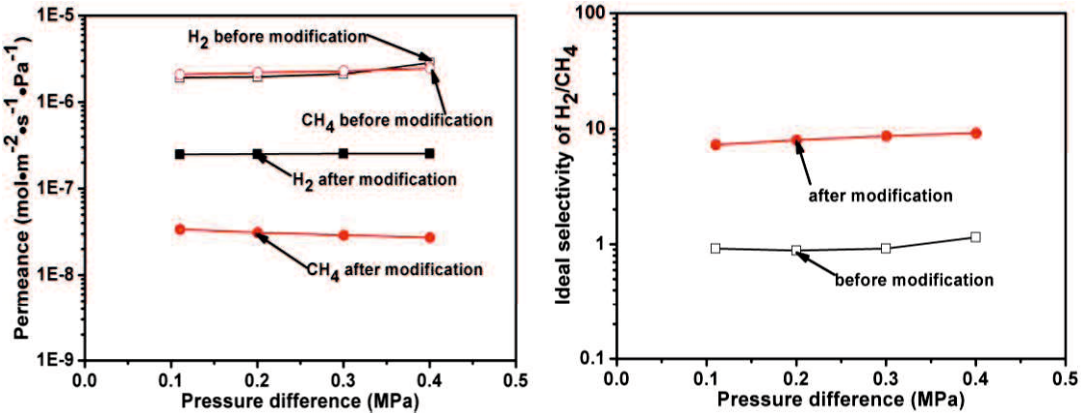

Figure 6-12 Comparison of the relationship between H_2 and CH_4 permeation performance in a function of pressure difference through the MFI zeolite membrane before and after modification (T = 308 K).

As can be seen in **Figure 6-12**, CH_4 permeance of modified silicalite-1 membrane decreased a little with increasing pressure difference, which is consistent with the results discovered by J. C. Poshustaand et al. [21]. In addition, α^{ideal} (H_2/CH_4) increased from 7.3 to 9.2 as pressure difference increased.

6.3.3.5 The relationship of the change between H_2 and CO_2 permeation

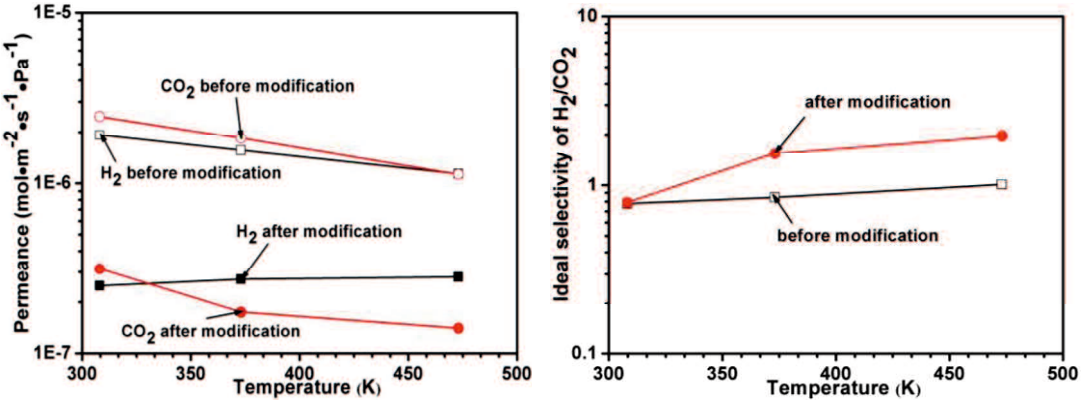

Figure 6-13 Comparison of the relationship between H_2 and CO_2 permeation performance in a function of temperature through the MFI zeolite membrane before and after modification (ΔP = 0.11 MPa).

The comparison of CO_2 and H_2 permeance in **Figure 6-13** indicates that CO_2 permeance is higher than H_2 because CO_2 has stronger adsorption than H_2 in silicalite-1 crystals [20]. But the $\alpha^{ideal}(H_2/CO_2)$ increased little because of the weaker adsorption ability of CO_2. However, CO_2 permeance decreased more after modification. Thus, α^{ideal} (H_2/CO_2) just increased from 0.8 to 1.3 as temperature increased. **Figure 6-14** shows single gas (CO_2 or H_2) permeation under varying pressure difference at 308 K.

The H_2 permeance is not affected by pressure difference because "H_2 permeance is modelled assuming surface diffusion in the Henry regime in the zeolite pores" [22]. In contrast to the H_2 permeance, the CO_2 permeance decreased obviously as the pressure difference increased. Gas saturation in zeolite may be the reason for CO_2 permeance decrease. Saturation happened at both the feed side and permeate, which leads to a low concentration gradient in the zeolite and a low driving force. Despite the small change of CO_2 and H_2 permeance, the $\alpha^{ideal}(H_2/CO_2)$ increased a little after modification.

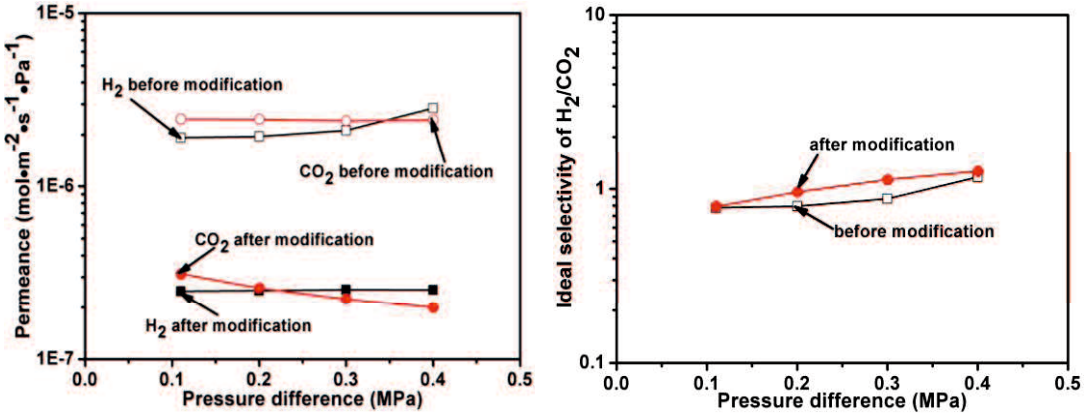

Figure 6-14 Comparison of the relationship between H_2 and CO_2 permeation performance in a function of pressure difference through the MFI zeolite membrane before and after modification (T = 308 K).

6.3.3.6 The relationship of the change between H_2 and SF_6 permeation

In this work, the H_2 and SF_6 permeations were measured on the silicalite-1 membrane before and after modification at 308 K, 373 K and 473 K with a pressure difference of 0.11 MPa. Mobility of both H_2 and SF_6 will increase as temperature increase especially for SF_6 with larger molecular size [23]. It is clearly that $\alpha^{ideal}(H_2/SF_6)$ is higher at lower temperature for membrane before and after modification as shown in **Figure 6-15**. After modification, $\alpha^{ideal}(H_2/SF_6)$ decreased significantly from 647 to 124 as temperature increased from 308 K to 473 K. Meanwhile, H_2 permeance decreased from 1.9×10^{-6} $mol\cdot m^{-2}\cdot s^{-1}\cdot Pa^{-1}$ to 2.5×10^{-7} $mol\cdot m^{-2}\cdot s^{-1}\cdot Pa^{-1}$ at 308 K. In this work, vacuum method was used for gas permeation. The feed side and permeate side volumes are known precisely. Therefore, the single gas permeances is determined by increasing pressure in a known permeate side volume [24].

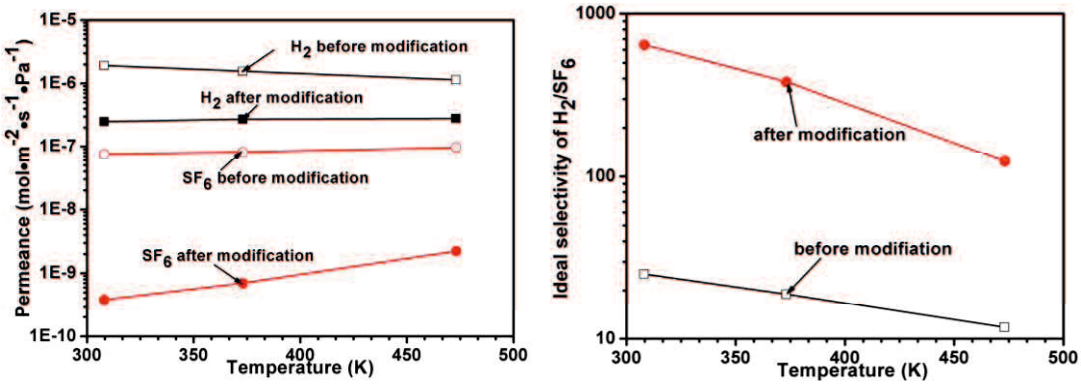

Figure 6-15 Comparison of the relationship between H_2 and SF_6 permeation performance in a function of temperature through the MFI zeolite membrane before and after modification (ΔP = 0.11 MPa).

Figure 6-16 shows the single gas permeance as a function of pressure difference. All of the gas permeances increased as pressure difference increased. α^{ideal} (H_2/SF_6) for modified membrane decreased from 647 to 609 under higher pressure difference. E. R. Geus et al. demonstrated that for microporous membranes such as zeolite membranes, the interplay of adsorption and diffusion effects play a very important role in permeation behavior [25] as described by the Maxwell-Stefan equations for both single component and mixture permeation [26-28]. Under higher pressure difference, gas permeance decreased because of limite pore volume and lower driving force, which verifies the change of H_2 and SF_6 permeance in this work [23].

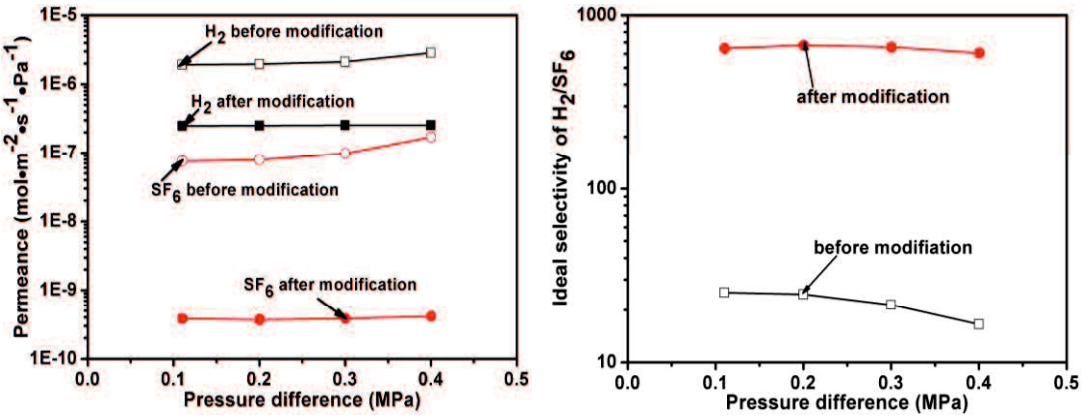

Figure 6-16 Comparison of the relationship between H_2 and SF_6 permeation performance in a function of pressure difference through the MFI zeolite membrane before and after modification (T = 308 K).

6.3.3.7 The relationship of the change between CO_2 and CH_4 permeation

Methane is commonly used as a fuel, especially for heating. However, CO_2 always accompanies with natural gas. The existence of CO_2 will do harm to methane ultilization, but also to the transportation equipments [29]. Therefore, we used the silicalite-1 membrane for CO_2 and CH_4 permeation in this work. As **Figure 6-17** shows, due to the stronger CO_2 and CH_4 adsorptions than H_2 in silicalite-1 crystals, the unmodified silicalite-1 membrane shows a little lower α^{ideal} (CO_2/CH_4) (1.2) than α^{ideal}(CO_2/H_2) (1.3) at 308 K with a pressure difference of 0.11 MPa. However, the modified membrane shows a much higher α^{ideal} (CO_2/CH_4) of 9.2 at the same gas permeation conditions while the α^{ideal} (CO_2/H_2) is still 1.3. This α^{ideal} (CO_2/CH_4) is much higher than Knudsen diffusion coefficient of 0.6, which should own to the modification. In addition, both CO_2 and CH_4 permeance decreased over the investigated arrange (308-473 K). CO_2 and CH_4 permeances of modified silicalite-1 membrane varied from 3.1×10^{-7} mol·m^{-2}·s^{-1}·Pa^{-1} to 1.4×10^{-7} mol·m^{-2}·s^{-1}·Pa^{-1} and from 3.4×10^{-8} mol·m^{-2}·s^{-1}·Pa^{-1} to 2.7×10^{-8} mol·m^{-2}·s^{-1}·Pa^{-1}, respectively.

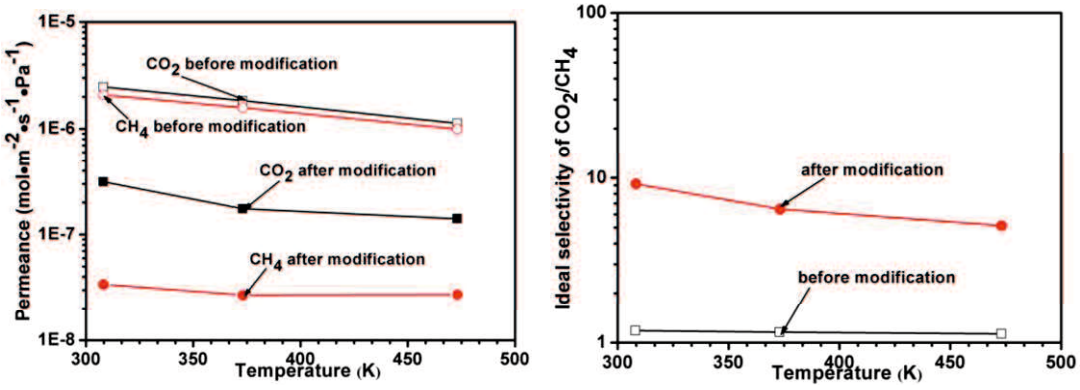

Figure 6-17 Comparison of the relationship between CO_2 and CH_4 permeation performance in a function of temperature through the MFI zeolite membrane before and after modification (ΔP=0.11 MPa).

Figure 6-18 shows results as a function of pressure difference at 308 K. Both CO_2 and CH_4 permeance decreased with increasing pressure difference. The results are in a good agreement with results reported by W. J. W. Bakker et al. [30], A. J. Burggraaf et al [31]. and W. D. Zhu et al [32]. The α^{ideal} (CO_2/CH_4) of modified

silicalite-1 membrane decreased from 9.2 to 7.3 with an increase in feed pressure at 308 K. Meanwhile, the α^{ideal} (CO_2/CH_4) of unmodified silicalite-1 membrane decreased from 1.2 to 1.0.

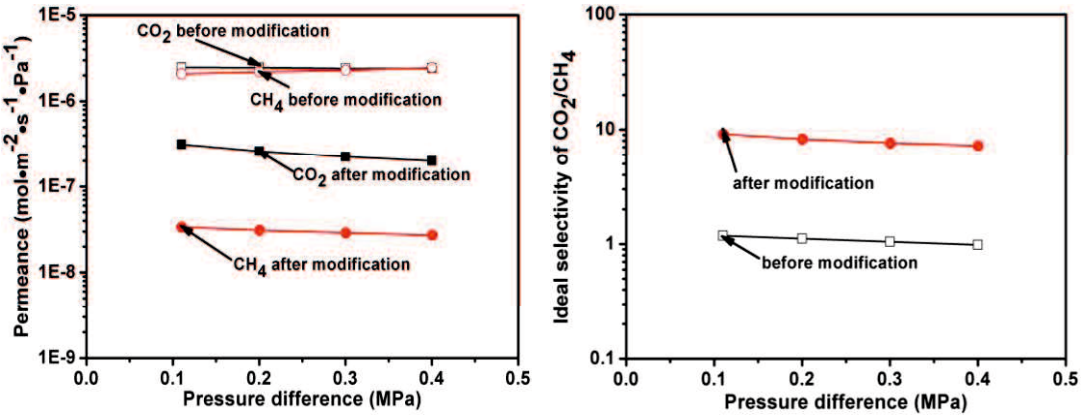

Figure 6-18 Comparison of the relationship between CO_2 and CH_4 permeation performance in a function of pressure difference through the MFI zeolite membrane before and after modification (T = 308 K).

6.3.3.8 The relationship of the change between CO_2 and N_2 permeation

Figure 6-19 and **Figure 6-20** show the results of modified and unmodified silicalite-1 membranes depended on temperature and pressure difference using CO_2 and N_2.

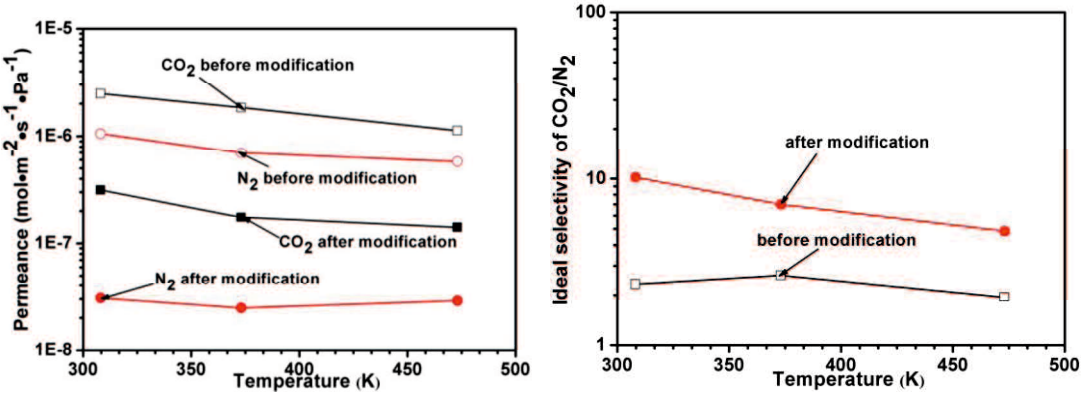

Figure 6-19 Comparison of the relationship between CO_2 and N_2 permeation performance in a function of temperature through the MFI zeolite membrane before and after modification (ΔP = 0.11 MPa).

When the temperature was 308 K and pressure difference was 0.11 MPa, CO_2 permeance decreased from 2.5×10^{-6} $mol\cdot m^{-2}\cdot s^{-1}\cdot Pa^{-1}$ 3.1×10^{-7} $mol\cdot m^{-2}\cdot s^{-1}\cdot Pa^{-1}$, and N_2 permeance decreased from 1.1×10^{-6} $mol\cdot m^{-2}\cdot s^{-1}\cdot Pa^{-1}$ to 3.1×10^{-8} $mol\cdot m^{-2}\cdot s^{-1}\cdot Pa^{-1}$, respectively. The $\alpha^{ideal}(CO_2/N_2)$ also has a maximum with a lower pressure difference at lower temperature. For the unmodified silicalite-1 membrane, CO_2 and N_2 permeance didn't go in an obvious opposite directions as pressure difference increased at low temperature of 308 K, which was mentioned by K. Makrodimitris et al. [33]. In that report, they simulated "silicalite as a perfect, fully siliceous crystalsilicalite crystal" [33]. But the unmodified membrane here should have inter-crystal pores which may lead to a different result. After modification, the membrane shows a higher α^{ideal} (CO_2/N_2) of 10.23 which is only 2.33 before modification, which is due to the modification.

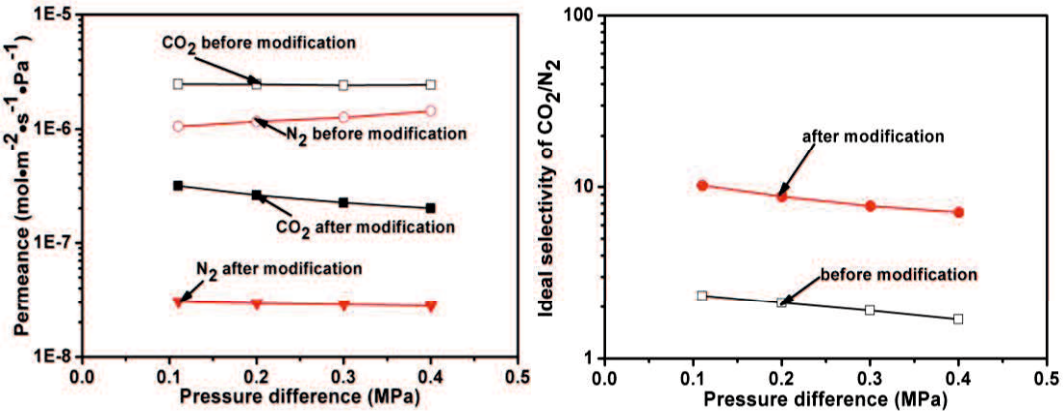

Figure 6-20 Comparison of the relationship between CO_2 and N_2 permeation performance in a function of pressure difference through the MFI zeolite membrane before and after modification (T = 308 K).

6.3.4 Stability of the modified silicalite-1 membrane

Long-term stability of H_2 and SF_6 permeation performances of modified membrane has been discussed and exhibited in **Figure 6-21**. H_2 and SF_6 single permeations were measured at 308 K with a pressure difference of 0.11 MPa. The modified membrane shows a stable H_2 permeance and SF_6 permeance for a period as long as 120 h. During the test, H_2 permeance varied around 2.5×10^{-7} $mol\cdot m^{-2}\cdot s^{-1}\cdot Pa^{-1}$ while the $\alpha^{ideal}(H_2/SF_6)$ varied around 635. It can be concluded that after modification,

silicalite-1 membrane has a good long-term stability for H_2 permeance as well as high α^{ideal} (H_2/SF_6). Compared to data in **Table 5-2** in **Chapter 5**, α^{ideal} (H_2/SF_6) of silicalite-1 membrane here are relatively high.

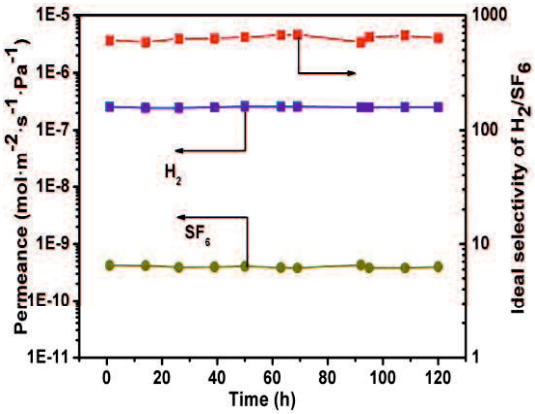

Figure 6-21 Long-term stability of H_2 and SF_6 permeation performance through modified MFI membrane within 120 h.

6.3.5 Nanopermporometry results of the silicalite-1 membrane

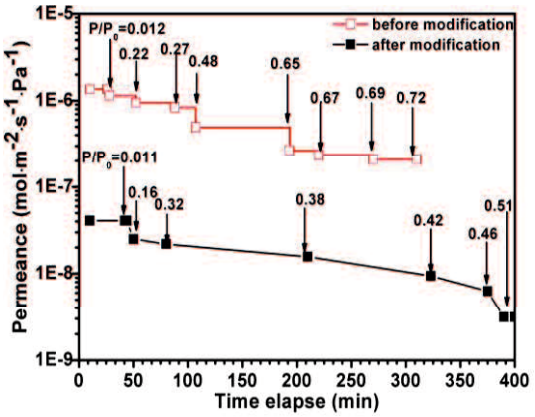

Figure 6-22 Time course for N_2 permeance for MFI membrane before and after modification. (H_2O, 308 K)

Figure 6-22 shows the time course of N_2 permeance of silicalite-1 membrane before and after modification at 308 K. The permeance of N_2 in the dry state was kept for a period to check the steady state. After the N_2 permeance became a constant value, water was introduced into the feed side. P/P_s increased from 0.11 to 0.51 and even

0.72 according to the time indicated by arrows in the figure. After increasing the vapor pressure, the N_2 permeance decreased gradually and reached a steady value. The N_2 permeance of unmodified silicalite-1 membrane reached a constant earlier than value of modified membrane because of the high permeance. On contrast, the N_2 permeance of modified silicalite-1 membrane decreased a lot and kept constant with a lower water concentration. It is the water blocking effect of N_2 permeation decreased N_2 permeance [34]. But modified membrane haver smaller permeation pores decreased by net toplogy layer, which made N_2 permeance decreased more quickly.

6.4 Conclusions

By using modification with APTES, defects in membrane layer were eliminated significantly. The nanopermporometry result indicated that silicalite-1 membrane has a better quality after modification. The modification process had dramatic effects on the single gas permeation performance of silicalite-1 membrane. The modification increased ideal selecitivity of H_2/SF_6 from 26.9 to 647. Meanwhile, H_2 permeance is 2.5×10^{-7} $mol\cdot m^{-2}\cdot s^{-1}\cdot Pa^{-1}$ which is comparable to data of silicalite-1 membranes in papers. Moreover, the ideal selectivities of H_2/N_2, H_2/CH_4, CO_2/CH_4, and CO_2/N_2 also increased to higher than the corresponding Knudsen diffusion factors. The modified silicalite-1 membrane shows stable H_2 permeation ability.

References

[1] S. Hosseinzadeh Hejazi, A. Avila, T. Kuznicki, A. Weizhu, S. Kuznicki, Characterization of natural zeolite membranes for H_2/CO_2 separations by single gas permeation, Industrial and Engineering Chemistry Research, 50 (2011) 12717-12726.

[2] E. Newson, T. Haueter, P. Hottinger, F. Von Roth, G. Scherer, T.H. Schucan, Seasonal storage of hydrogen in stationary systems with liquid organic hydrides, International Journal of Hydrogen Energy, 23 (1998) 905-909.

[3] G. Cao, Y. Lu, L. Delattre, C.J. Brinker, G.P. López, Amorphous silica molecular sieving membranes by sol-gel processing, Advanced Materials, 8 (1996) 588-591.

[4] J. Stelzer, M. Paulus, M. Hunger, J. Weitkamp, Hydrophobic properties of all-silica zeolite beta, Microporous and Mesoporous Materials, 22 (1998) 1-8.

[5] K. Oda, K. Akamatsu, T. Sugawara, R. Kikuchi, A. Segawa, S. Nakao, Dehydrogenation of methylcyclohexane to produce high-purity hydrogen using membrane reactors with amorphous silica membranes, Industrial and Engineering Chemistry Research, 49 (2010) 11287-11293.

[6] K. Akamatsu, Y. Ohta, T. Sugawara, T. Hattori, S. Nakao, Production of hydrogen by dehydrogenation of cyclohexane in high-pressure (1-8 atm) membrane reactors using amorphous silica membranes with controlled pore sizes, Industrial and Engineering Chemistry Research, 47 (2008) 9842-9847.

[7] R.D. Noble, J.L. Falconer, Silicalite-1 zeolite composite membranes, Catalysis Today, 25 (1995) 209-212.

[8] M. Hong, J.L. Falconer, R.D. Noble, Modification of zeolite membranes for H_2 separation by catalytic cracking of methyldiethoxysilane, Industrial and Engineering Chemistry Research, 44 (2005) 4035-4041.

[9] Z. Zheng, A.S. Hall, V.V. Guliants, Synthesis, characterization and modification of DDR membranes grown on α-alumina supports, Journal of Materials Science, 43 (2008) 2499-2502.

[10] K. Kusakabe, F. Shibao, G. Zhao, K. Sotowa, K. Watanabe, T. Saito, Surface modification of silica membranes in a tubular-type module, Journal of Membrane

Science, 215 (2003) 321-326.

[11] A. Huang, F. Liang, F. Steinbach, J. Caro, Preparation and separation properties of LTA membranes by using 3-aminopropyltriethoxysilane as covalent linker, Journal of Membrane Science, 350 (2010) 5-9.

[12] A. Huang, N. Wang, J. Caro, Seeding-free synthesis of dense zeolite FAU membranes on 3-aminopropyltriethoxysilane-functionalized alumina supports, Journal of Membrane Science, 389 (2012) 272-279.

[13] M.K. Naskar, D. Kundu, M. Chatterjee, Silicalite-1 zeolite membranes on unmodified and modified surfaces of ceramic supports: A comparative study, Bulletin of Materials Science, 32 (2009) 537-541.

[14] Y. Cui, H. Kita, K. Okamoto, Preparation and gas separation performance of zeolite T membrane, Journal of Materials Chemistry, 14 (2004) 924-932.

[15] Z. Tang, J. Dong, T.M. Nenoff, Internal surface modification of MFI-type zeolite membranes for high selectivity and high flux for hydrogen, Langmuir, 25 (2009) 4848-4852.

[16] J. Lindmark, J. Hedlund, Modification of MFI membranes with amine groups for enhanced CO_2 selectivity, Journal of Materials Chemistry, 20 (2010) 2219-2225.

[17] M. Simplício, M.D. Afonso, O. Borisevich, X. Lefebvre, D. Demange, Permeation of single gases and binary mixtures of hydrogen and helium through a MFI zeolite hollow fibres membrane for application in nuclear fusion, Separation and Purification Technology, 122 (2014) 199-205.

[18] C. Algieri, P. Bernardo, G. Golemme, G. Barbieri, E. Drioli, Permeation properties of a thin silicalite-1 (MFI) membrane, Journal of Membrane Science, 222 (2003) 181-190.

[19] A. Alshebani, M. PeraTitus, E. Landrivon, T. Schiestel, S. Miachon, J. Dalmon, Nanocomposite MFI-Ceramic hollow fibres: Prospects for CO_2 separation, Microporous and Mesoporous Materials, 115 (2008) 197-205.

[20] M. Hong, R.D. Noble, J.L. Falconer, Highly selective H_2 separation zeolite membranes for coal gasification membrane reactor applications, in, Technical Report, University of Colorado, 2004.

[21] J.C. Poshusta, R.D. Noble, J.L. Falconer, Temperature and pressure effects on CO_2 and CH_4 permeation through MFI zeolite membranes, Journal of Membrane Science, 160 (1999) 115-125.

[22] E. Sjöberg, Zeolite membranes for effective production of biofuels, (2012).

[23] M. Noack, G. Mabande, J. Caro, G. Georgi, W. Schwieger, P. Kölsch, A. Avhale, Influence of Si/Al ratio, pre-treatment and measurement conditions on permeation properties of MFI membranes on metallic and ceramic supports, Microporous and Mesoporous Materials, 82 (2005) 147-157.

[24] M. Noack, P. Kölsch, R. Schäfer, P. Toussaint, I. Sieber, J. Caro, Preparation of MFI membranes of enlarged area with high reproducibility, Microporous and Mesoporous Materials, 49 (2001) 25-37.

[25] E.R. Geus, H. van Bekkum, W.J. Bakker, J.A. Moulijn, High-temperature stainless steel supported zeolite (MFI) membranes: preparation, module construction, and permeation experiments, Microporous Materials, 1 (1993) 131-147.

[26] F. Kapteijn, W.J. Bakker, G. Zheng, J.A. Moulijn, Temperature-and occupancy-dependent diffusion of n-butane through a silicalite-1 membrane, Microporous Materials, 3 (1994) 227-234.

[27] F. Kapteijn, W.J. Bakker, G. Zheng, J. Poppe, J.A. Moulijn, Permeation and separation of light hydrocarbons through a silicalite-1 membrane: Application of the generalized Maxwell-Stefan equations, The Chemical Engineering Journal and The Biochemical Engineering Journal, 57 (1995) 145-153.

[28] R. Krishna, L. Van den Broeke, The Maxwell-Stefan description of mass transport across zeolite membranes, The Chemical Engineering Journal and The Biochemical Engineering Journal, 57 (1995) 155-162.

[29] V.V. Guliants, A.J. Huth, J.M. Stueve, A molecular dynamics and grand canonical Monte Carlo study of silicalite-1 as a membrane material for energy-related gas separations, Journal of Porous Materials, 20 (2013) 235-247.

[30] W.J. Bakker, L.J. Van Den Broeke, F. Kapteijn, J.A. Moulijn, Temperature dependence of one-component permeation through a silicalite-1 membrane, AIChE Journal, 43 (1997) 2203-2214.

[31] A. Burggraaf, Z. Vroon, K. Keizer, H. Verweij, Permeation of single gases in thin zeolite MFI membranes, Journal of Membrane Science, 144 (1998) 77-86.

[32] W. Zhu, P. Hrabanek, L. Gora, F. Kapteijn, J.A. Moulijn, Role of adsorption in the permeation of CH_4 and CO_2 through a silicalite-1 membrane, Industrial and Engineering Chemistry Research, 45 (2006) 767-776.

[33] K. Makrodimitris, G.K. Papadopoulos, D.N. Theodorou, Prediction of permeation properties of CO_2 and N_2 through silicalite via molecular simulations, The Journal of Physical Chemistry B, 105 (2001) 777-788.

[34] T. Tsuru, T. Hino, T. Yoshioka, M. Asaeda, Permporometry characterization of microporous ceramic membranes, Journal of Membrane Science, 186 (2001) 257-265.

Chapter 7 Conclusions and future works

7.1 Conclusions

In this dissertation, we explored the synthesis and permeation applications of zeolite membranes. SOD membranes were prepared by secondary growth by seeded with uniform and small sodalite crystals. T-type zeolite membranes are prepared with two-step varying-temperature hydrothermal synthesis process. The effects of conditions on the first and second steps were discussed in detail, such as synthesis time and synthesis temperature. The preparation and permeation performance of silicalite-1 have been discussed.

Our first objective in this regard was to demonstrate the ability to control microstructure of sodalite membranes. As seed for sodalite membranes, preparation of sodalite crystals were discussed and optimized in **Chapter 2**. The issue for ethanol dewatering was addressed in **Chapter 3**. Dense sodalite membrane with thin layer was formed on α-Al_2O_3 support by seeding method. The thickness of the sodalite membrane was affected by water concentration in precursor. The crystallinity and compactness of sodalite membranes are determined by both synthesis time and synthesis temperature. Lower temperature result in impure sodalite membranes and longer synthesis time leads to appearance of ANA crystal phase. Also, pervaporation operator conditions were controlled to evaluate water selectivity of sodalite membranes. Lower temperature is favor of higher PV performance. And the membrane showed stable permeation state in both of ethanol/water and iso-propanol/water mixtures for 10-20 h at 75 ^{o}C.

As shown in **Chapter 4**, the second objective of this study is to develop a new synthesis method named “two-step varying-temperature hydrothermal synthesis process” to improve CO_2 separation performance of T-type zeolite membranes. Compared with the conventional synthesis method at a constant temperature, the two-step method is more effective in synthesizing a thin and continuous membrane in

a short time under optimum synthesis conditions. During the two-step method, a lower temperature favored nucleation, while a higher crystallization temperature promoted crystallization, thus improving zeolite T crystal growth and membrane separation properties.

The third objective of this research (**Chapter 5**) was to study the effect of synthesis condition on permeation performances of H_2 and other single gases through silicalite-1 membranes and using modification to improve membrane performance. By using different silica sources, silicalite-1 membrane showed very different morphology and single gas permeation behavior. Silicalite-1 membranes using smaller particles showed stronger (002) orientation.

To further improve the performance of silicalite-1 membrane, modification with APTES was applied to a silicalite-1 membrane in **Chapter 6**. After modification, ideal selectivity of H_2/SF_6 increased dramatically and H_2 permeance decreased.

7.2 Future works

(1) Silica sodalite is a good H_2 storage material because of its high H_2 adsorption capacity. If very stable sodalite can be prepared, it will be very promising to apply sodalite membranes in H_2 separation. Moreover, all-silica (or high silica) sodalite has strong hydrophobicity, good stability and proper pore structure for H_2 permeation. It is worth to explore all-silica (or high silica) sodalite membranes for H_2 separation. Non-aqueous systems such as ethylene glycol and tetramethylammonium can be considered as precursor solvents.

(2) Seed crystal size has an obvious effect on morphology and gas permeation performance of silicalite-1 membranes. If the composition of precursor solution can be changed systematicly, it is possible to analyze the effect of crystal size with more controllable microstructure and obtain more promising H_2 permeation performance.

(3) Other modification ways can be used for silicalite-1 membranes. For example, deposite a SiO_2 amophous layer on membrane surface by sol-gel methods.

List of publications

1. Xiaoliang Zhang, ***Lingfang Qiu***, Xiangshu Chen, Hidetoshi Kita, "Preparation of Zeolite T Membranes by a Two-step Temperature Process for CO_2 Separation", *Industrial & Engineering Chemistry Research*, **2013**, 52(46), 16364-16374

2. ***Lingfang Qiu***, Izumi Kumakiri, Kazuhiro Tanaka, Hidetoshi Kita, "Dehydration performance of sodalite membranes prepared by secondary growth method", *Membrane*, **2015**, 40(6), 349-354

3. Izumi Kumakiri, ***Lingfang Qiu***, Bo Liu, Kazuhiro Tanaka, Hidetoshi Kita, Takashi Saito, and Ryoichi Nishida, "Application of MFI zeolite membrane prepared with fluoride ions to hydrogen/toluene separation", *Journal of Chemical Engineering of Japan*, **2016** (Accepted).

4. ***Lingfang Qiu***, Izumi Kumakiri, Kazuhiro Tanaka, Xiangshu Chen, Hidetoshi Kita, "Effects of seed crystal size on properties of silicalite-1 zeolite membranes synthesized in a fluoride containing medium", (Submitted).

Acknowledgements

I wish to express special thanks to my supervisor Professor Hidetoshi Kita for his guidance and support throughout the course of my research. Without his guidance and careful instruction, this dissertation can't be finished. I appreciate his kind supports not only on my research but also on my daily life. I admire his academic ability.

I also would like to thank to other two teachers in my lab. One is Associate Professor Kazuhiro Tanaka, he instructed me about analyzing academic publications and taught me to use some device in lab. One is Associate Professor Izumi Kumakiri, she always has attractive smile. She often asked me about my research situation, gave me much valuable advice and instructed me about paper writing. It's necessary to mention that the cakes she made were really very delicious. All in all, their valuable comments and suggestions have been considered seriously so that better scientific work can be presented in this dissertation, and their kind made me study in Kita group more comfortably. Moreover, Dr. Tomoko Koga taught me to use many instruments and often talked with me about daily life like a sister.

Next I want to thank Prof. Xiangshu Chen. He was my supervisor when I was a master student in China. Thank him for introducing me to study in Yamaguchi University. I'm very lucky to study and live in Japan for 3 years.

I also thank all the students (Mr Yamashita, Masuda, Yoshino, Hayashi, Liu, and Ms Wu and so on) in Kita group for their help, advice, and collaborations. In particular, Japanese students taught me a lot of Japanese. In addition, thank all staffs in dean's office. They helped me a lot about course collection, applications of tuition fee exemption and scholarships so that I can finish my doctoral course successfully.

Finally, I'd like to give my deepest appreciation to my parents for their encouragement and support throughout my life. I really feel very grateful of meeting so many kind persons in my life.

Qiu Lingfang